Quantitative Analyse von T-Zell Stimulation und Costimulation durch zelluläre Mikrosysteme

Quantitative Analysis of T Cell Stimulation and Costimulation using Cellular Microsystems

DISSERTATION

Der Fakultät für Chemie und Pharmazie der Eberhard-Karls-Universität Tübingen zur Erlangung des Grades eines Doktors der Naturwissenschaften

2006

vorgelegt von

Karsten Köhler

Tag der mündlichen Prüfung : 3. August 2006

Dekan: Prof. Dr. Stefan Laufer

1. Berichterstatter: Prof. Dr. Hans-Georg Rammensee

2. Berichterstatter: PD Dr. Roland Brock

Die vorliegende Arbeit wurde unter Betreuung von Herrn Prof. Dr. Hans-Georg Rammensee unter Co-Betreuung und Anleitung von Herrn PD Dr. Roland Brock am Interfakultären Institut für Zellbiologie der Universität Tübingen in der Zeit von September 2002 bis April 2006 durchgeführt. Ihnen beiden danke ich sehr herzlich für das fortgesetzte Interesse an meiner Arbeit, exzellenten Arbeitsbedingungen und Arbeitsatmosphäre sowie das mir entgegengebrachte Vertrauen.

Danksagungen

Herzlich bedanken möchte ich mich bei allen Kollegen aus den Gruppen von PD Dr. R. Brock und Prof. Dr. G. Jung.

Bei meinen Laborkollegen Dr. Thomas André, Yi-Da Chung, Falk Duchardt, Dr. Martin Elbs, Nadja Fischer, Dr. Rainer Fischer, Alexander Ganser, Antje Hoff, Hans-Jörg Hufnagel, Wilfred Hummel, Dr. Oliver Mader, Dr. Mariola Fotin-Mleczek, Günter Roth, Ivo Ruttekolk, Michael Sinzinger, Oda Stoevesandt, Dr. Söhnke Voss, Susanne Vollmer und Susann Wolf möchte ich mich für die jederzeit angenehme und heitere Atmosphäre am Arbeitsplatz danken.

Hierbei möchte ich Thomas André für seine Einführung in den Nanospotter, und für seine große Hilfsbereitschaft nicht nur in Computer-Fragen danken. Antje Hoff danke ich für ihre Einführung in die Zellkultur und in die zellbasierten Experimente sowie in die Laserscanning-Mikroskopie. Rainer Fischer danke ich für seine Einführung in die Peptidchemie und -analytik.

Bei Günter Roth, Prof. Dr. Karl-Heinz Wiesmüller und Prof. Dieter Kern für die Zusammenarbeit in dem interessanten Projekt zur Stimulation von Zellen mit mikrostrukturierten Oberflächen.

Dr. Bernd Möhrle, Jan Jaehrling, Nina Schweizer und Prof. Dr. G. Gauglitz danke ich für die spannende und erfolgreiche Kooperation im Bereich der zellulären RifS.

Dr. Ludger Grosse-Hovest, Prof. Dr. Gundram Jung, für die immer wieder anregende Kooperation zur Untersuchung der Effekte stimulatorischer Antikörper

Dr. Anne-Marie Lellouch, Dr. Hans Rogl und Prof. Dr. Bernard Malissen vom CNRS-INSERM für die erfolgreiche Kooperation und die Generierung der GFP-T-Zell-Linien, sowie der Bereitstellung on Antikörpern. Ausserdem danke ich Prof. Dr. Carl Figdor, Dr. Christian Freund, Dr. Ben Joosten, PD Dr. Reiner Lammers, Dr. Patrick Pankert und Dr. Aukje Zimmerman, für Antikörper. Dr. Claus Belka für Zell-Linien und Prof. Dr. Stefan Laufer für chemische Inhibitoren

Ich bedanke mich bei Nicole Sessler für Peptidsynthesen, Dr. Tobias Seyberth für Hilfe bei der HPLC und Prof. Dr. Stefan Stevanović bedanke ich mich für die Möglichkeit zur Durchführung von MALDI-TOF Messungen

Stefan Welte danke ich für seine immer wieder in Anspruch genommene Hilfsbereitschaft.

Ursula Becker-Sanzenbacher, Lisa Neumann und Heiderose Neu möchte ich für ihre Unterstützung in Sachen der Organisation und Verwaltung danken.

Regina Bohnert danke ich für die professionelle Programmierung von Makros für die Bildanalyse.

Den Praktikanten Henrik Grabner, Laura Zöllner, Jan Niederländer, Anja Schindler für ihre Hilfe bei der Etablierung der zellulären Stimulationsprotokolle.

Franziska Löwenstein danke für das Spülen und Autoklavieren von sehr vieler von mir benutzter Gefäße und Georg Tiedemann für das Bringen von vielen Paketen.

Bedanken möchte ich mich bei Prof. Dr. H.-G. Rammensee für seine Betreuung der Doktorarbeit, sowie der Leitung des Graduiertenkolleg 794 „Zelluläre Mechanismen Immunassoziierter Prozesse“, und den Koordinatorinnen Valerie Bahr, Regine Grund und Dr. Bettina Weiss für die langjährige Unterstützung.

Adrian Schröder, Christan Spieth, Jochen Supper, Prof. Dr. Zell danke ich für die anregende Kooperation im Bereich der Bioinformatik.

Für die Benutzung der Mikroarray-Scanner bedanken wir uns bei Georg Otto (MPI Tübingen) und Michael Hartmann (NMI Tübingen)

Für die Finanzierung der Projekte im Namen dieser Arbeit bedanken wir uns sehr bei der Volkswagen-Stiftung (I/77472). Der Deutschen Gesellschaft für Signaltransduktion (STS) and der Europäischen Kommission danke ich für Reisestipendien.

Ausserdem bedanke ich mich bei denen, bei denen ich vergessen habe, mich zu bedanken.

Abbreviations

Ab	antibody
Ac	Acetyl
ACN	Acetonitril
AcOH	Acetic Acid
Ahx	6-aminohexanoic acid
APC	antigen-presenting cell
BSA	bovine serum albumin
DIPEA	N,N' diisopropylethylamine
DMF	N,N' dimethyl-formamide
DMSO	dimethylsulfoxide
DMEM	Dulbecco's Modified Eagle's Medium
EDTA	ethylenediaminetetraacetic acid
FCS	fetal calf serum
FITC	fluorescein isothiocyanate
Fmoc	N-(9-fluorenyl)methoxycarbonyl
GOPTS	3-(glycidyloxypropyl)trimethoxysilane
GSK-3	glycogen synthase kinase-3
HBS	HEPES-buffered saline
HEPES	N-(2-hydroxyethyl)piperazine-N'(2-ethanesulfonic acid)
HOBt	1-hydroxybenzotriazol
HPLC	high-performance liquid chromatography
ITAM/ITIM	immunoreceptor tyrosine-based activation/inhibition motif
λ	wavelength
LAT	linker of activation in T cells
LSM	confocal laser scanning microscope
M	molar
MALDI	matrix-assisted laser desorption ionisation
MeOH	methanol
MHC	major histocompatibility complex
NFAT	nuclear factor of activation in T cells
PBS	phosphate-buffered saline
PDMS	polydimethylsiloxane
PDZ	PSD 95/Disk Large/ZO-1-like domain
PFA	para-formaldehyde
PH	pleckstrin homology domain
PI3K	phosphatidylinositol-3'-kinase
PKC	protein kinase C
PLC	phospholipase C
polyP	poly-proline motif
PTB	phosphotyrosine binding domain
PTK	protein tyrosine kinase
pY	phosphotyrosine (motif)
RIfS	reflectometric interference spectroscopy
RT	room temperature
SFK	Src-family kinase
SH2/SH3	Src-homology domain 2/3
SHP	SH2-domain-containing phosphotyrosine phosphatase
SMAC	supramolecular activation complex
TCR	T cell receptor

TFA	trifluoroacetic acid
TPBS	PBS + 0.05% Tween-20
Tris	tris(hydroxymethyl)aminomethane
YFP	yellow fluorescent protein
ZAP-70	zeta-associated protein of 70 kDa

Amino acids are abbreviated using the one-letter codes suggested by IUPAC-IUB .

Preface and contents of this thesis

In the immune system and especially in the immune surveillance exerted by T lymphocytes cell-cell contacts play a key role: The principal mode of T cell activation occurs by interactions of the T cell receptors (TCR) with pathogen-associated peptides presented by major histocompatibility molecules (MHC) on a target cell [2]. The activation of a T cell is highly regulated, depending on the affinity of the interaction of the TCR with the MHC-peptide combination, the density of specific MHC-peptide combination on the cell surface, the differentiation and activation state of the T cell and on the participation of costimuli [3]. The past years have provided a wealth of information on the membrane-associated and cytoplasmic proteins in T cells and target cells that are involved in these interactions. Now, the events leading to cell-cell contact formation and T cell activation need to be analyzed in detail with respect to signal intensity and kinetics. Due to the significance of extracellular stimuli in health and disease there is a keen interest in the development of analytical techniques that enable the quantitative analysis of cellular interactions and the underlying molecular processes and to enable the systematic integration of these individual events into signalling networks.

Binding of T cell receptors (TCR) to agonistic MHC-peptide complexes initiates a cascade of signalling events central to the execution of the adaptive immune response [4]. A contact between T cell and antigen presenting cell characterized by a distinct array of surface proteins at the interface has been termed the ‘immunological synapse’ [5]. Upon TCR engagement the Src-family kinase LCK, a kinase recruited by CD4 or CD8 and associated with the immature immunological synapse, phosphorylates tyrosines of the immunoreceptor tyrosine-based activation motifs (ITAMs) within the TCR/CD3 complex, forming sites for the recruitment of the tyrosine kinase ZAP-70 within the first seconds of T cell activation [6]. Activation of ZAP-70 leads to the propagation of the signal via multiple pathways that culminate in gene expression and the cytoskeletal rearrangements stabilizing cellular contacts. Concomitant with the redistribution of transmembrane molecules, proteins involved in cell adhesion and intracellular signalling as well as actin and associated proteins are concentrated at the contact site. In addition to the TCR stimulation, engagement of coreceptors, most prominently CD28, is necessary for full T cell activation, leading to cell proliferation and cytokine expression.
In the context of this thesis, the events of T cell contact formation and activation were analyzed from the cell-morphological perspective and the protein interaction perspective applying microscopic and microstructural methods. First, the formation of the immunological

synapse and its pharmacological susceptibility to chemical inhibitors over time was analyzed morphologically (Chapter 3 of this thesis). In order investigate the role of LCK in the maintenance of T cell contacts, we analyzed the time-dependent localization of a ZAP-70-YFP fusion protein and its sensitivity to disturbances by kinase inhibitors as readouts for changes in activities that impact the activation of TCR-dependent complexes. As a strong and well-defined model system for the MHC/peptide stimulus, we stimulated T cells on CD3-functionalized surfaces, a stimulus able to recapitulate essential events of T cell activation [7]. For the analysis of the time-dependence of TCR engagement on LCK activity and formation of signalling-active multiprotein complexes, we added PP2, a specific inhibitor of Src family kinases to the cells at various stages after TCR engagement. We showed that the maintenance of signalling contacts and clusters in early stages of contact formation, up to about 5 min of TCR engagement, is sensitive to LCK inhibition, in contrast to later time points.

After the evaluation of the time-dependence of effects of signalling inhibitors on T cell activation, it was our goal to evaluate the dependence of the inhibitor effects on cells exposed to a variety of stimuli. For this purpose, we sought to develop a strategy by which the interplay of different signalling pathways in generating a cellular response could be applied systematically to the testing of low molecular weight inhibitors (Chapter 4). The method of T cell stimulation by stimulatory antibodies was extended to a format allowing parallel testing of both stimuli and stimulation conditions. For this experiment, we spotted stimulatory antibody microarrays of antibodies against CD3 and the CD28 costimulatory molecule in different intensities and exposed Jurkat cells in combination with T cell signalling inhibitors to this stimulus. As readouts for activation, we analyzed cell spreading, the clustering and phosphorylation of signalling proteins, and the translocation of the transcription factor NFAT using fluorescence microscopy followed by automated, quantitative image analysis. We found remarkable differences in the response profiles of inhibitors with overlapping target profiles, illustrating the potential of the approach in a functional profiling of drug candidates, and providing new information on the specificity of these compounds.

The combination of imaging-based readouts for cell activation with micropatterned stimuli offers a new perspective for the analysis of T cell activation taking into account geometrical stimulus parameters in the subcellular range (Chapter 5). This approach adresses the influence of spatially distinct stimuli and of the stimulus size on T cell activation. In order to spatially separate the stimuli applied to a single cell, stimulatory antibodies were transferred to a glass

surface in a microstructured format. Using immunofluorescent staining and image analysis, we analyzed the interplay of the TCR/CD3 stimulus and CD28 costimulus for the local and global activation states of the cell.

Next, the time-dependent morphological changes in T cell contact formation were analyzed using a label-free biophysical method, Reflectometric Interference Spectroscopy (RIfS) (Chapter 6)[8;9]. To our knowledge, the application of RIfS for monitoring the contact of T cells with stimulatory antibody surfaces represents the first application of a label-free optical spectroscopy technique for the analysis of activation-dependent cellular interactions. The different spreading morphologies of Jurkat cells perfused over anti-CD3- and anti-CD28-functionalized surfaces correlated with differences in the slope and amplitude of the RIfS curve. Imaging-based quantification of cell spreading and actin polymerization correlated with RIfS results and yielded the morphological basis for the observed differences. In a parallelizable format, RIfS should also allow the application for the screening of compounds that interfere with APC/T cell contact formation in a flow system.

The biochemical aspect of the microstructured approach to T cell signalling addressed in this thesis analyzes the interactions between proteins on a molecular scale (Chapter 7). Since the early steps in T cell activation-dependent signalling are also mediated by numerous protein-protein interactions via different domains, a focus in our group is the analysis of protein-protein interactions in this context. A systematic understanding of these signal transduction processes requires the development of methods for the parallel analysis of the protein-protein interactions involved. Fluorescence correlation spectroscopy allows the quantitative analysis of the binding constants of single interactions [10] and allows the screening and characterization of interaction inhibitors. In complementation to this method which enables the quantitative analysis of protein-protein interaction in solution, our group established an approach based on microarrayed peptides representative of specific protein-derived binding motifs, which interact with proteins from cell lysates and hence offers the possibility to analyze dozens of interactions under tens of conditions in one experiment. Here, the interplay of stimulatory and costimulatory signals concerning T cell signalling was analyzed on a protein-protein interaction scale. The peptide array method enables the qualitative analysis of the constituents of multiprotein complexes. Moreover, it also enables the quantitative analysis of stimulation-dependent changes in protein interactions, depending on stimuli, kinetics and inhibitors. Taken together, the methods applied here allow the observation of the features of T cell

signalling on different levels in a parallel format. Moreover, by obtaining quantitative data of activation parameters they are applicable for the screening of inhibitors and gene effects of T cell activation.

1 Introduction

1.1 TCR-proximal signalling components

The adaptive immune response is centrally controlled by T lymphocytes, or T cells, a subset of lymphocytes characterized by their development in the **t**hymus and the expression of heterodimeric receptors that are associated with the CD3 complex. These membrane-expressed receptors, the T cell receptor (TCR)/CD3 complex, consist of highly variable αβ (clonotypic) or γδ chains in a noncovalent complex with the invariant CD3γ, δ and ε subunits and the dimeric CD3ζ chains. T cells continuously circulate in the blood and lymphatic system, and engage in transient contacts with other cells mediated by interactions of their TCRs with major histocompatibility molecule (MHC)/peptide combinations on the target cells [2]. MHC molecules are highly polymorphic membrane glycoproteins involved in the presentation of peptide antigens. MHC class I molecules, expressed in different quantities by nearly all cell types, are involved in the presentation of peptides generated by the cytosolic pathways to T cells expressing the CD8 coreceptor (CD8 T cells, precursors of cytotoxic T cells). Cytotoxic T cells mediate the destruction of cells that present fragments of intracellular pathogens, such as proteins involved in viral infection, or malignant transformation. MHC class I molecules consist of 2 subunits, the transmembraneous, highly polymorphic α chain (MW 43 kDa), which forms the peptide-binding cleft, and the conserved β2 microglobulin chain (MW 12 kDa). MHC class II molecules are expressed by "professional antigen presenting cells", such as dendritic cells and B cells (lymphocytes characterized by their development in the **b**one marrow). MHC class II molecules are composed of two transmembrane glycoprotein chains (α 34 kDa, β 29 kDa), which together form the peptide-presenting cleft. Peptides that are generated by protein degradation in intracellular vesicles are presented by MHC class II to T helper cells, which express the CD4 coreceptor. T helper cells are involved in the orchestration of the immune responses characterized by the activation of macrophages and the "humoral" response characterized by secretion of antibodies by B cells. MHC restriction characterizes the effect that a T cell clone can only recognize a peptide antigen if bound to a particular MHC molecule.

Activation of a T cell by contact with an agonistic MHC/peptide complex is mediated via the activation of protein tyrosine kinases (PTKs) that associate with phosphorylated motifs the invariant units of the T cell receptor (TCR)/CD3 complex and the coreceptors CD4 or CD8. Activating signals are transduced from the extracellular moiety of the TCR via the immunoreceptor tyrosine-based activatory motifs (ITAMs) of the CD3 -γ, -δ, -ε (one ITAM each) and the ζ chains (three ITAMs). The consensus sequence of an ITAM is defined by the sequence $YXX(L/I)X_{6-8}YXX(L/I)$. The two tyrosine residues within each ITAM are subject to phosphorylation by the Src family kinases LCK and/or Fyn.

The leukocyte-specific protein tyrosine kinase (LCK) is an acylated enzyme of the Src kinases family (SFK), which is localized in glycolipid membrane microdomains (GEMs), also known as lipid rafts. Lipid rafts are membrane microdomains with about 70 nm diameter that contain an enhanced concentration of unsaturated phospholipids, cholesterol and sphingolipids [11]. The extent of ITAM phosphorylation correlates to the TCR interaction intensity with the peptide/MHC complex. In unstimulated cells, the ITAM phosphorylation by SFK is neutralized by the excess of the activity of various tyrosine phosphatases [12]. One model for the activation of T cell by APC contact assumes that TCR triggering can shift this balance towards phosphorylation by excluding phosphatases from or recruiting kinases towards the contact site. For example, CD45, a transmembrane phosphatase that deactivates LCK by dephosphorylating pY394, contains a large extracellular cellular domain. This domain excludes CD45 from the much narrower cleft between T cell and APC generated by TCR and/or CD28 engagement [13;14] in which the TCR extends only about 7-10 nm from the cell surface. On the other hand, the kinase LCK is recruited towards the TCR/MHC contact site by engagement of the CD4/CD8 coreceptors [15]. Also, LCK activity is regulated negatively by Csk- mediated phosphorylation on tyrosine 505, which leads to intramolecular SH2 binding and to the covering of the active site of LCK [16]. Together, the recruitment of CD4/CD8 towards and of CD45 away from the TCR shifts the balance of kinase-phosphatase activity towards phosphorylation of the ITAM domains upon TCR engagement, which peaks already after about 30 seconds of TCR engagement [17].

The Syk-family ζ-associated protein of 70 kDa (ZAP-70) PTK is a central enzyme in TCR dependent signal transduction. ZAP-70 is recruited to dual-phosphorylated ITAMs via its tandem SH2 domains with very high affinity [18], and then phosphorylated within its activation loop by LCK and ZAP-70 itself [19]. A further site of ZAP-70 regulation is the interdomain tyrosine residue 319, which is involved in the recruitment of the SH2 domain of the SFK LCK, resulting in augmentation or ZAP-70 activity [20]. In contrast, ZAP-70 is negatively regulated by phosphorylation of Tyr 292, which forms a site for Cbl recruitment [21]. ZAP-70 catalyzes the tyrosine phosphorylation of various downstream effector proteins, among them the transmembrane adapter linker of activation in T cells (LAT) [22]. Also, the SH2-domain containing leukocyte phosphoprotein of 76 kDa (SLP-76), and the inhibitory adapter Gab2, which are involved in the scaffolding of different downstream signalling complexes are discussed as ZAP-70 substrates [23;24]

1.2 Adapter proteins in T cell activation

The TCR-dependent activation pathway is mediated to a large extent by adapter proteins. In most cases lacking enzymatic activity themselves, adapters possess binding sites or modules that directly or indirectly mediate the binding of proteins to other proteins, and thus form the scaffold for signalling complexes (reviewed in [25]). The most important domains involved in T cell signalling are src-homology domains 2 (SH2) and phosphotyrosine binding (PTB) domains that both recognize phosphotyrosine motifs, SH3 domains recognizing polyproline motifs (polyP), PDZ domains (recognizing hydrophobic motifs at the C-terminus), WW domains (recognizing proline-rich regions and also phosphoserine motifs), and pleckstrine homology (PH) domains that interact with membrane lipids. LAT is an example for a scaffold protein that does not contain domains interacting with recognition motifs, but provides motifs for the recognition by the SH2 domains of other proteins.

Table 1.1: Selection of binding motif subtypes for protein domains; X defines a relative independence of domain binding from the amino acid at that position, pY represents a phosphorylated tyrosine residue, and COOH a free carboxy-terminus.

Domain	Name	Binding Motif
PDZ	**P**SD 95/**D**isk Large/**Z**O-1-like	X(S/T)X(V/I/L)-COOH
PTB	**P**hospho **T**yrosine **B**inding	D(N/D)XpY
SH2	**S**rc **H**omology **2**	**GRB2-like**:pYXNX **ITAM (tandem SH2):** pYXXLX_{6-8}pYXXL **SFK-like:** pY(Q/D/E/V/A/I/L)(D/E/N/P/Y/H/I)(I/P/V/G/A/H/S) **SHP/PLC-like:** pY(I/V)X(V/I/L/P)
SH3	**S**rc **H**omology 3	**Type I:** (R/K/Y)XXPXXP **Type II:** PXXPX(K/R) **Atypical I:** (P/V)XXP **Atypical II:** KPXX(Q/K) **Atypical, Hbp-type:** PX(V/I)(D/N)RXXKP **Atypical, EVH-type:** (E/D)FPPPPXDEE
WH1	**W**ASP **H**omology 1	ES(R/K)(F/Y)(Y/S/T)FH(P/S)(I/V)(E/S)D

LAT (linker for activation in T cells) is a transmembrane adapter protein expressed in T cells, which is palmitoylated on two juxtamembrane cysteine residues, mediating its recruitment into glycolipid-enriched microdomains and thus into the proximity of critical signalling molecules. LAT is phosphorylated by ZAP-70/Syk-family PTKs within the first 15 s of the TCR crosslinking and rapidly dephosphorylated after 5 min [17]. Certain phosphotyrosine residues of LAT form binding sites for different SH2 domains of several proteins. The phosporylated tyrosine residue of LAT 132 constitutes the centre of a SH2 binding motif of the SHP/PLCγ type (see table 1.1) and has been reported to directly interact with PLCγ; LAT pY226 represents a Grb2 and SFK type binding motif with reported interactions with Grb2 and Gads, while LAT phosphotyrosine 191 represents a consensus motif for the SH2 domains of SHP/PLCγ, SFK and Grb2 and has been reported to interact *in vivo* with Gads, Grb2 and phosphatidylinositol 3-kinase (PI3K) [22;26;27]. Containing other binding motifs such as SH3 domains, those proteins are in turn involved in the indirect recruitment of further molecules to the LAT-scaffolded complex. Secondary associations with Grb2 or Gads binding proteins may also facilitate the interaction of LAT with other proteins, such as PLCγ1 [26].

SLP-76 is a cytosolic adapter protein with an amino-terminal region containing regulatory tyrosine phosphorylation sites, a central proline-rich region and a carboxy-terminal SH2 domain [28]. SLP-76 is subject to phosphorylation by SFK and Syk kinases, with the amino-terminal phosphotyrosines described to be bound by the SH2 domains of Vav and Nck [29], and the carboxy-terminal phosphotyrosines to be bound by Fyb [30]. By recruiting Itk kinases, SLP-76 is involved in the activation of PLCγ [31]. Also, SLP-76 constitutively binds to Gads via its SH3 domain and thus indirectly binds to LAT [32].The trimolecular SLP76-Vav-Nck complex is involved in Pak recruitment, actin recruitment and NFAT activation [29].

Grb2 is an adapter protein containing two SH3 domains and one Grb-type SH2 domain. Grb2 has been reported to bind to the TCR ITAMs indirectly by binding the adapter Shc, which in turn binds via its SH2 domains to pYs of the ITAM [33]. The Grb2/Shc complex has been described to mediate the recruitment and activation of the Ras guanine nucleotide exchange factor SOS, leading to Ras activation [34]. GADS (Grb2-related adaptor downstream of Shc, also known as Grap-2) is an adapter protein which shows high homology to Grb2, but additionally contains a proline-rich sequence between its SH2- and its carboxy-terminal SH3 domain. While the C-terminal SH3 domain of GADS constitutively binds a proline-rich domain of SLP-76 [35], the SH2-domain binds to LAT. The tetrameric LAT centered complex including SLP-76, GADS and PLCγ1 is known as the LAT signalosome [36]. It forms a scaffold for the recruitment of other linker proteins, such as Vav, Gab2 and Fyb [37], which can further expand the scaffold. Also, GADS contains a cleavage site for caspases. Upon caspase activation, induced e.g. by TCR or Fas stimulation, the disintegrated GADS fragments may function as competitive inhibitors for GADS [38].

Fyb (also known as ADAP and SLAP-130), is a cytosolic adapter protein containing a proline-rich region and a SH3 domain (binding sites for SKAP-55), phosphotyrosine motifs (binding sites for Fyn and SLP-76) and an Ena/VASP homology domain (binding sites for Ena/VASP proteins) [39]. Via recruitment of the SKAP-55 protein, Fyb is a possible linker from T cell activation to the activation of integrins.

Nck is a cytosolic adapter protein consisting of three SH3 domains and one SH2 domain, which binds to an SFK type consensus sequence pYDE(P/D/V) [40]. The three distinct SH3 domains each have characteristic binding specificities. While all three SH3 domains associate with Cbl [41], the third SH3 domain associates with WASP [42], and the second one with SOS and PAK [43]. PAK is a serine/threonine kinase involved in the regulation of JNK and p38 kinase signalling [44]. Also, Nck has been described to bind via its N-terminal SH3 domains to the proline-rich regions of the TCRε complexes, which are supposedly exposed upon TCR crosslinking [45].

1.3 Negative regulation of the early steps in TCR signalling

As a counterbalance to the activating components, the extent and/or duration of T cell stimulation is regulated by inhibiting signalling components. As antagonists to the protein kinase activities in T cell signalling, phosphotyrosine phosphatases (PTPases) play a key role, particularly the SH2 domain-containing PTPases SHP1 and SHP2 (also known as SHPTP1 and 2). In analogy to the recruitment of PTKs to the ITAMs of the TCR, SHP1 is recruited to the contact site by different inhibitory receptors containing ITIMs (immunoreceptor tyrosine-based inhibition motifs), where SHP1 directly dephosphorylates its SFK and Syk antagonists. In contrast, depending on its recruitment mediated by adapter proteins, SHP2 can both act as a positive or negative regulator of T cell signalling. Also, SHP2 has been reported to dephosphorylate and inactivate CD3ζ [46], depending on Gab2 activity [47]. Different types of adapters are involved in the recruitment of SHPs, among them membrane-associated ones, like SIT and LAX, and cytoplasmic adapters like SLAP-2, Cbl, Grap2 and Gab2.

Kinases can be involved in negative signalling as well. Csk is a negative regulatory tyrosine kinase catalyzing the inhibitory phosphorylation of LCK. In the resting cell, Csk is associated with the transmembrane protein Cbp/PAG and localized in lipid rafts [48]. TCR stimulation induces the dephosphorylation of Cbp, followed by the dissociation of Csk and thus the activation of LCK [16]. A c-terminal VTRL/ITRL motive of Cbp/PAG also interacts with a PDZ domain of ezrin-radixin-moesin binding protein EBP50, which limits lipid raft aggregation by anchoring lipid rafts to the cytoskeleton [49]. TCR stimulation abrogates the interaction between Cbp/PAG and EBP50, a possible

mechanism for the induction of lipid raft coalescence.

Cbl is an adapter protein containing, among other domains, one atypical phosphotyrosin binding domain (also known as PTB domain), proline- and pY- rich motifs and an ubiquitin-ligase domain. Cbl is tyrosine-phosphorylated upon engagement of several receptors, including the TCR and acts as a negative regulator of tyrosine-kinase signalling pathways [50]. Via its PTB domain, Cbl is recruited to the pY292 of ZAP-70 and thereby a ternary inhibitory complex between ZAP-70, Cbl and CD3ζ is formed [51]. Together with the Src-like adapter protein SLAP-2, Cbl may be involved in the ubiquitinylation, internalization, and degradation of CD3ζ and ZAP-70 [52].

Gab2 is a member of the Gab (Grb2-associated binder) adapter proteins, consisting of a pleckstrin homology (PH) domain, phosphotyrosine-motifs for SH2 binding, and the PxxxR sequence, which forms an atypical binding motif for the SH3 domains of Gads and Grb2 [53], and also occurs on SLP-76. Phosphorylated by ZAP-70 [54], pY 614 of Gab2 forms a binding site for the SH2-domain-containing phosphatase 2 (SHP2). SHP2 is believed to dephosphorylate and thus inactivate positive signalling molecules when located to the LAT signalling complex by Gab2 [50] via Grb2 or GADS.

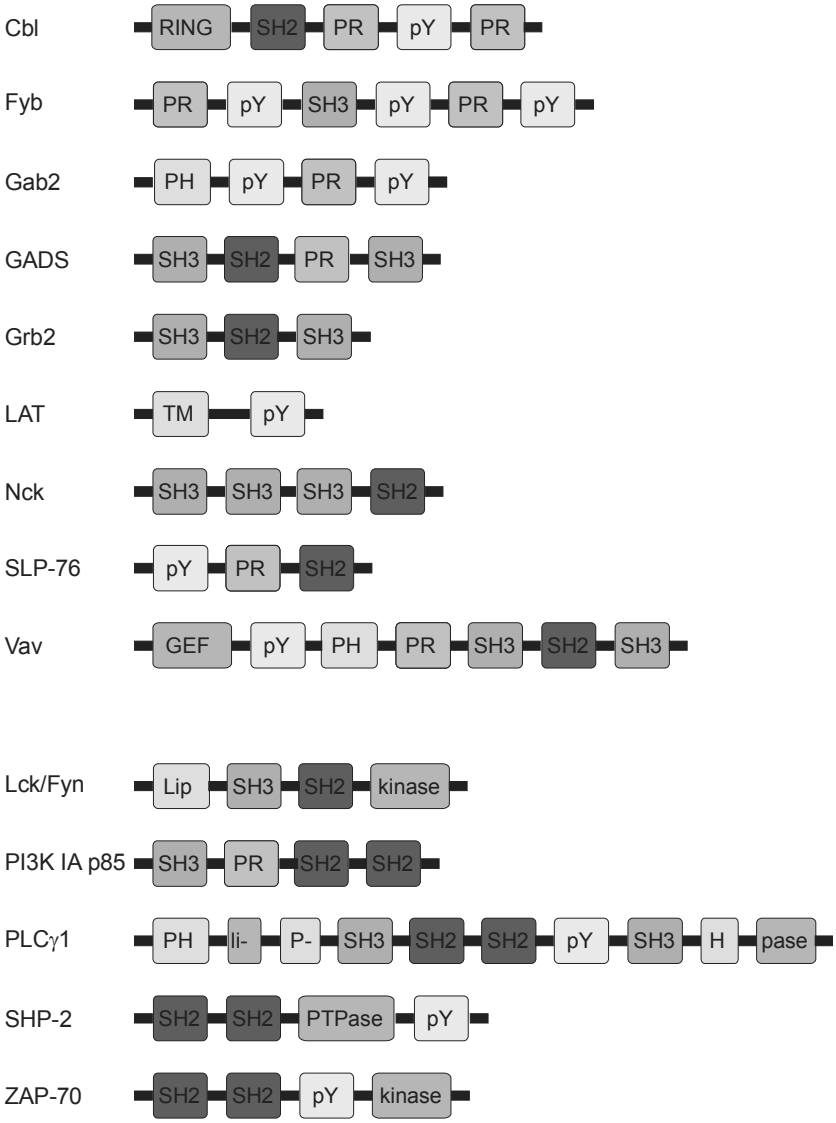

Figure 1.1 Simplified overview of the structure of some proteins involved in TCR dependent complex formation. (GEF = guanine nucleotide exchange factor ; Lip = acylation; PH = pleckstrin homology domain; PR = polyP motif; pY = phosphotyrosine motif ; PTPase = phosphatase; TM = transmembrane region; li-pase = discontinuous lipase domain)

1.4 Lipid- and calcium-associated signals in T cell signalling

Phosphoinositide-3-kinases (PI3K) are an enzyme family involved in various pathways, with the class IA PI3K activated by tyrosine-kinase-associated receptors like the TCR. Class IA PI3Ks are heterodimeric enzymes containing of a regulatory subunit (p85) and a catalytic subunit (p110), each in various isoforms. In T cells, Class I PI3K are recruited by to membrane-associated molecules by interacting with phosphotyrosines in YXXM, such as in CD28 [55] and the T cell receptor interacting molecule TRIM, and also

in the adapter proteins in the Gab family. Upon binding the pYXXM motifs with its SH2 domains and association with the membrane, PI3K phosphorylates the membrane lipid phosphatidylinositol-(4,5)-bisphosphate (PIP2) on the D3-position of its inositol ring to generate phosphatidylinositol-(3,4,5)-trisphosphate (PIP3) on the inner leaflet of the plasma membrane. PIP3 is selectively bound by various intracellular proteins via their pleckstrin PH domains, prominently among them the serine/threonine kinase Akt/PKB [56]. One main substrate of Akt is the glycogen-synthase kinase-3 (GSK-3), a kinase which is in its active state in resting cells, and inactivated by serine phosphorylation [57]. Additionally to modulating glycogen metabolism, activated GSK-3 mediates the nuclear export of the nuclear factor of activated T cells.

TCR engagement induces the activation of three members of the Tec/Btk kinase family: Inducible T cell kinase (Itk), Tec, and Rlk, of which the former two are also activated by CD28 stimulation. Like Akt, Itk and Tec are also recruited to the membrane by interactions of their amino-terminal pleckstrin-homology domains with products of PI3K [58], and by association of their SH2 and SH3 domains with SLP-76 [31;59]. Tec family kinases are subsequently activated by SFK-mediated tyrosine phosphorylation [60]. Also, the activity of Tec kinases is positively regulated by Vav, involving PI3K dependent and –independent mechanisms [61].

Phospholipase C γ1 (PLCγ1) is a lipase containing two SH2 domains and one SH3 domain. One feature of PLCγ1 activation is initiated by the recruitment to phosphorylated LAT-mediated and thus to its lipid substrate in the membrane. On the other hand, PLCγ1 activity is dependent on a Itk-dependent stimulatory phosphorylation on tyrosine 783, [17]. Itk itself is recruited to the SLP-76 molecule in the LAT signalosome, which, in concert with the PIP3 in the lipid rafts exposes the activation loop tyrosine to phosphorylation by LCK [32]. Upon activation, PLCγ1 catalyzes the hydrolysis of the lipid phosphatidyl-inositol-4,5-bisphosphate (PIP2) to the second messenger molecules inositol-1,4,5-trisphosphate (IP3) and diacylglycerol (DAG). IP3 releases calcium from intracellular stores and the extracellular space. Cytoplasmic calcium activates various proteins, among them protein kinase C (PKC), of which PKCθ is the most prominent effector in lymphocytes, and the serine/threonine phosphatase calcineurin (see below). PKCθ is a PKC isoform which is expressed in lymphoid tissue with the exception of B cells, and can

be alternatively activated independently from the calcium signal [62]. Upon TCR engagement, PKCθ is recruited to the lipid rafts, where it interacts with LCK and is phosphorylated [63]. The protein remains associated in the immunological synapse throughout the later stages of contact formation. Activated PKCθ then phosphorylates RasGRP, leading to the activation of the Ras/Raf/Erk pathway [64]. PKCθ signalling is critical for the induction of IL-2-expression, via the transcription factors AP1 (a dimer of Fos and Jun) and NFκB, possibly via Akt or MAP3K[65].

1.5 Cytoskeletal effects and G proteins

The products of PI3K activity also recruit a PH-containing group of proteins that are known as guanine nucleotide exchange factors (GEFs) for Rho GTPases like Rac, Rho, Cdc42. Additionally to regulating lymphocyte proliferation and differentiation, Rho GTPases are responsible for the initiation of the formation of different cytoskeletal patterns: RhoA regulates actin stress fiber formation, Rac1 lamellapodia and focal contact formation, and Cdc42 microspikes and filopodia, but consecutively also induce Rac- and Rho-mediated responses [66]. The complex of Cdc42 with its effector WASP has been reported to be involved in actin nucleation via the Arp2/3 complex [67] and T cell polarization towards the APC. The WASP-interacting protein (WIP) mediates the Arp 2/3 mediated actin polymerization by interacting with actin and profilin [68].

The Vav family proteins are involved in various signalling pathways acting as cytoplasmic guanine nucleotide exchange factors (GEFs) for Rho family GTPases and exerting additional functions as an adapter protein. In TCR signalling, Vav1 is required for the initiation of a calcium flux by activating of Tec family kinases and thus indirectly of PLCγ [69]. Also, Vav seems to be involved in the stabilization of the LAT signalosome [70]. After WASP is recruited towards the cell-cell contact by Nck [71], Vav activates WASP, which in turn binds and activates the actin nucleation comples Arp2/3. Also, Vav inactivates the actin-crosslinking ezrin/radixin/moesin proteins, and thus enables actin remodelling [72]. Vav seems also to be involved in actin reorganization via Rac-1 [73]. Also, Rac-1 induces the activation of the transcription factor AP1, which is a Fos/Jun/Dimer, which is mediated via JNK and MEKK [74].

1.6 Costimuli

In addition to the activation of the TCR by a peptide/MHC complex, the ligation of costimulatory molecules is required for an effective immune response. The glycoprotein CD28 is the most effective and best characterized costimulatory receptor on T cells, and binds to the membrane proteins CD80 and CD86, expressed by activated antigen-presenting cells. TCR crosslinking on a naïve cell in the absence of a CD28 costimulus results in either apoptosis or anergy.

Signalling induced by CD28 triggering is thought to be mediated by components that are also involved in CD28 TCR-dependent signalling [75]. Like the TCR, CD28 lacks an intrinsic kinase activity, and contains tyrosine residues in its intracellular tail, that are phosphorylated by kinases like SFK [76]. Also, CD28 crosslinking is described to induce the activation of Tec kinases [77] which catalyze the phosphorylation of intracellular tyrosine residues in YMNM motifs. Phosphorylation of the pY173 of CD28 results in recruitment of SH2-containing proteins such as PI3K, GADS and Grb2 [55;78]. The co-activation of the PI3K pathway by CD28 has been described to be necessary for the induction of IL-2 expression [79]. Like the TCR-downstream pathway, the activation of the PI3K/Akt pathway leads to NFκB activation via PKCθ [80] and enhancement of NFAT nuclear import via GSK-3 inhibition [81]. In contrast to the TCR, CD28 does not recruit ZAP-70 and does not initiate the formation of a LAT/SLP-76 complex [75].

On regarding the effect of CD3 and CD28 signals for the integration of an immunological response, CD28 is required for the production of IL-2 by T helper cells via the so-called CD28 response element, which includes NFAT and AP1 [82], and also stabilizes the mRNA of IL-2 [83]. CD28 was shown to sustain general tyrosine phosphorylation associated with TCR-induced aggregation of GEMs [84], and enhances the activation of the PLCγ1-signal [77]. By recruiting the structural component Vav, CD28 might enhance the stability of the signalosome and thus lower the threshold for the induction of cell activation with low TCR occupancy [75]. The enhanced stability of T cell/APC contacts by engagement of coreceptors may also be involved in maintaining immunological synapse stability. Also, CD28 has been reported to mediate the PI3K/Akt dependent inactivation of glycogen-synthase-kinase 3 (GSK-3) [79]. With most signalling

molecules in CD28 dependent signalling also playing a role in CD3-dependent signalling, it is still under dispute whether CD28 engagement only quantitatively enhances CD3-dependent signalling or activates qualitatively different signalling activities.

1.7 Transcription factors in T cell signalling

T cells express the calcium-regulated NFAT proteins NFAT1 (also known as NFATc2), NFAT2 (=NFATc1), and NFAT4 (=NFATc3). NFATs are activated by dephosphorylation of their regulatory domains mediated by the serine/threonine phosphatase calcineurin [85]. Calcineurin is activated by a complex of the regulatory protein calmodulin together with the increase of the intracellular free calcium [86]. Upon activation, NFAT enters the nucleus and acts a transcriptional regulator for, the expression of different cytokines such as IL-2, IL-6 and TNFα [82]. In a resting cell, nuclear NFAT is subject to phosphorylation by different kinases, like GSK-3 [87], casein kinase 1 [88], p38 [89] and Jun N-terminal kinase [90], which induce the nuclear export of NFAT. GSK-3 is inactivated by a serine phosphorylation mediated by Akt [80], which thus indirectly augments NFAT translocation and gene expression.

Nuclear factor-κB (NFκB) is a family of transcription factors involved in the gene expression associated with immune, inflammatory and apoptotic responses (reviewed in [91] Following different stimuli, the IκB kinase (IKK) phosphorylates the inhibitor of κB (IκB), which is subsequently degraded via the ubiquitin-pathway. For the initiation of IKK activation, the PKCθ-mediated recruitment of the proteins Carma1 and Bcl10 to the immunological synapse is under discussion, followed by a Bcl10 and MALT1-initiated activation of the IKK complex [92]. The free NFκB translocates to the nucleus and activates the transcription of a large number of target genes, among them genes encoding cytokines (e.g. IL-2; IL-8, TNFα), immunoreceptors, transcription factors and regulators of apoptosis.

1.8 The immunological synapse

The stable contact between a T cell and an antigen-presenting cell is characterized by the ordered formation of supermolecular activation complexes (SMAC) at the contact site, and also known as the immunological synapse. Contact formation depends on the recognition of MHC/peptide complexes by matching TCR receptors. The first step, T cell polarization before cell-cell contact formation, is still mediated by indirect interactions, for example by chemokines [93]. This step is followed by initial adhesion, in which non-antigen-specific adhesion molecules like LFA-1 interacting with ICAM and CD2 interacting with CD58 are the central contact molecules and localize to the centre of the contact area. The next intermediate step, in which the first, but not spatially restrained TCR/MHC recognitions are occurring, is termed the "immature" immunological synapse. The interaction of MHC/peptide complexes and TCRs are stabilized and sustained by means of the cytoskeleton. Also, the activities of the early kinases such as LCK and ZAP-70 in the first 2-5 minutes of receptor engagement are associated with the "immature synapse" [6]. After about 10 minutes after T cell/APC contact, the ordered and stable "mature immunological synapse" is formed by an active reorganization of surface molecules and cytoskeletal rearrangements. Here, a central cluster of T cell, CD28 and CD2 molecules (cSMAC) is surrounded by a ring of adhesion molecules (pSMAC), the CD11/CD18 integrins, and LFA-1 [94;95]. Though protein phosphorylation already peaks at about the 2 minute time point, enhanced protein phosphorylation in signalling clusters is still detectable in the "mature immunological synapse".

1.9 Chemical biology

The term "Chemical biology" defines a field at the interface between chemistry and biology in which chemicals are used to manipulate biological systems. The subfield "Chemical genetics" [96] characterizes an approach in which small molecule effectors generated or purified by chemical approaches are used to directly affect the functions of gene products. In contrast to the traditional genetics approach in which genes encoding the proteins are affected, the inhibitors can be applied in real time [97;98]. The small molecule effectors are often supplied from large chemical libraries, and the phenotypic,

cell- or organism-based screening for inhibitor effects is usually done similar to genetic screens. Inhibitor-based analyses allow the analysis of dose-response functions, the combination of inhibitors, and the testing in different cell lines. The specificity of the inhibitors is a field of concern. For some inhibitors, a specificity comparable to a gene knockout has been described [96]. An advantage difficult to achieve by gene knockouts or knockdowns is the applicability of chemical inhibitors at closely defined time points.

Methods for the analysis of a cellular response are essential both for the analysis of the functions of a gene product and of the effects of pharmaceuticals interfering with this gene product. A phenotype-based testing of a chemical is able to give information about the functional effect of this component in the complex system of the whole cell. Fluorescence microscopy allows the detection of a number of different parameters, like protein phosphorylation, but also even more complex morphological parameters such as cell attachment and spreading, cytoskeletal reorganization and protein translocation. An often used approach of phenotype-based screening leads to an active compound, the identification of the target of that compound and from there, to the gene product and its functional involvement. Due to the high number of different parameter information obtainable by image-based screening, this method is also referred to as “high content screening” [99]. In the conventional manner, the microscopy-based testing of chemicals is time consuming, expensive, and, most importantly, limited to a small number of substances to be tested at a time. With the growing coverage of gene and chemical libraries to be tested, the parallelization of cellular assay system is an important task. This task involves the miniaturization of assay conditions, and the establishment of methods for quantitative analysis of the results. For the cellular testing of drugs, the parallelization applying multiwell systems (e.g. in microtiter plates) is a widely used method. In this manner, the group of Tim Mitchison screened a library of 16,000 compounds in 384-well plates for different complex parameters such as wound healing, and cytoskeletal reorganization using automated microscopy [100].

1.10 Cellular microarrays

In its natural environment, a cell is exposed to a high number of external stimuli. For the analysis of the effects of surface stimuli on the activation state of a cell, the immobilization of cell-interacting substrate by microspotting is able to add another degree of complexity to cellular systems. For the manufacturing of the array, either cells or cell-interacting substrates are immobilized. In this case, the use of stimuli immobilized in a miniaturized format in microarrays allows the additional testing of the effects of chemicals for a multitude of different surface stimuli using only a small number of cells.

Arrays of immobilized cells in parallel have been employed for the phenotype-based screening of the functions of a library of gene products [101]. On the other hand, a high number inhibitors has been immobilized by embedding in biodegradable polymers [102]. As T cells interact with a high number of different stimuli in the context of the immune system, the testing of the effects of various stimuli, including combinations of stimuli, represents an important task. Microarrays of immobilized antibodies against CD antigens that induce cell attachment have been used for the parallel analysis of surface antigens in leukemias [103]. In recent years, microarrays of stimuli, such as immobilized peptide/MHC complexes have been applied to cellular systems. Soen et al. immobilized different MHC/Peptide-complexes and analyzed the interaction with different antigen-specific T cells concerning contact formation and calcium influx as early readouts [104]. Stone et al. have quantified the stimulation-dependent secretion of cytokines using co-immobilizing capture antibodies. Also, another late readout, the display of CD3 and CD69 antigens was analyzed, thereby monitoring readouts in the range of several hours after TCR engagement [105].

Due to the different structural properties of proteins, an effective and reproducible substrate for protein immobilization is needed for the fabrication of protein microarrays. The firm attachment of the protein to its immobilization surface and the maintenance of the native structure of the protein have to be ensured. Since in experiments involving the stimulation of cells the reproducibility of the stimulation intensity concerning is essential both that within one spot and that on an array it is also necessary to provide a homogenous surface for protein immobilization.

2. Contributions to other projects

In the context of the research interest in the group of PD Dr. Roland Brock, one focus was the development of molecules selectively interfering into protein-protein interactions in a living system, and the analysis of these effects on the cellular level. Using peptides as interactors, our research involved the design of peptides corresponding to recognition motifs as well as the transport of these peptides to their place of effect. This task includes the analysis of the cellular import mechanisms and the intracellular processing of these cell-penetrating peptides.

Fischer, R., Köhler, K., Fotin-Mleczek, M., Brock, R. (2004): A stepwise dissection of the intracellular fate of cationic cell-penetrating peptides. J. Biol. Chem. 26; 279(13):12625-35

The author of this thesis participated in the establishment and measurement of the effects of inhibitors of the pathways of proteasomal and lysosomal proteolysis on the import efficiency and import mechanism of cell-penetrating peptides.

Stoevesandt, O., Köhler, K., Fischer, R., Johnston, I., Brock, R. (2005): One-step detection of protein complexes in microliters of cell lysate. Nature Methods 2 (11): 833-835.

In this paper, the tetrameric multiprotein complex called the “LAT signalosome” was selectively disrupted by peptides corresponding to protein-protein interaction motifs (see also part 7.3.4 of this thesis), and the effect monitored on by fluorescence- (cross-) correlation spectroscopy. The author of this thesis synthesized and purified the bisphosphorylated peptides used in this study.

3. Chemical genetics when timing is critical: A pharmacological concept for the maturation of T cell contacts

3.1 Summary

Cellular signal transduction proceeds through a complex network of molecular interactions and enzymatic activities. The timing of these molecular events is critical for the propagation of a signal and the generation of specific cellular response. Here we introduce the combination of high resolution confocal microscopy with the application of small molecule inhibitors at various stages of signal transduction in T cells to define the timing of signalling events. Inhibitors of Src-family tyrosine kinases and actin reorganization were employed to dissect the role of the lymphocyte-specific tyrosine kinase LCK in the formation and maintenance of T cell receptor/CD3-dependent T cell contacts. Anti-CD3-coated coverslips served as a highly defined stimulus. The kinetics of the recruitment of the yellow-fluorescent protein-tagged signalling protein ZAP-70 was detected by high resolution confocal microscopy. The analyses revealed that at 5 min after receptor engagement LCK activity was required for maintenance of contacts. In contrast, after 20 min of receptor engagement, the contacts were LCK-independent. The relevance of the timing of inhibitor application provides a pharmacological concept for the maturation of T cell-substrate contacts.

This section has been adapted from:

Köhler, K., Lellouch, A.C., Vollmer, S., Hoff, A., Peters, L., Rogl, H., Malissen, B., Stoevesandt, O., Brock, R. (2005): Chemical genetics when timing is critical: A pharmacological concept for the maturation of T cell contacts. *Chembiochem* 6(1):152-61

For this paper, the generation of the fusion protein cell line was performed by Dr. Anne-Marie C. Lellouch. Susanne Vollmer and Lasse Peters were involved in the establishment of the cellular readout system. Antje Hoff, Susanne Vollmer and Dr. Hans Rogl performed a part of microscopical analysis, and Oda Stoevesandt a part of the biochemical experiments. The work was supervised by PD Dr. Roland Brock and Prof. Dr. Bernard Malissen. The figures were prepared by the author unless indicated otherwise.

3.2 Introduction

The interaction of a T lymphocyte with an antigen presenting cell (APC) is a primary example for a regulation of an intercellular interaction. The past years have provided a wealth of information on the molecules in the plasma membrane and inside the T cells and target cells that participate in and modulate these interactions. Now, the timing and contribution of individual molecular events to contact formation and generation and execution of a T cell response needs to be addressed in detail.

Binding of T cell receptors (TCR) to agonistic peptide-major histocompatibility complex (MHC) complexes initiates a cascade of signalling events central to the execution of the adaptive immune response [106]. Upon TCR engagement the Src-family kinase (SFK) LCK phosphorylates tyrosines of the immunoreceptor tyrosine-based activation motifs (ITAMs) within the TCR/CD3 complex [107]. The cytoplasmic Syk family tyrosine kinase ZAP-70 is recruited to the TCR/CD3 complex by binding to the phosphorylated CD3ζ ITAMs. Activation of ZAP-70 leads to the progagation of the signal via multiple pathways that culminate in gene expression and the formation of a highly ordered supramolecular structure at the interface of the T lymphocyte and the APC, the 'immunological synapse' [94]. Formation of the immunological synapse occurs through the rearrangement of transmembrane molecules in the T cell-APC contact [108]. Concomitant with the redistribution of transmembrane molecules, factors involved in cell adhesion and intracellular signalling as well as microfilaments and associated proteins are concentrated at the contact site.

Given the prominence of the redistribution of membrane proteins, to this end, research on the immunological synapse has been based on T cell-APC contacts or on model systems in which the APC was replaced by lipid bilayers incorporating membrane proteins [94]; experimental approaches that allow for the lateral diffusion of membrane proteins. As a consequence synapse maturation has been associated with the morphological reorganization of the T cell-APC contact. Limited information exists on the individual contributions of signalling molecules to the transformation of the contact from a premature early stage into a mature late stage.

In order to focus the analysis of contact maturation on the role of signalling activities, we selected anti-CD3 antibody-coated coverslips as a well defined stimulus for the activation of T cells [109]. In contrast to stimuli provided by APCs or lipid bilayers,

surface-coated anti-CD3 antibodies are immobile, precluding the rearrangement of transmembrane receptors by lateral diffusion as a mechanism for contact maturation. As a consequence, stimulation of T cells with immobilized antibodies eliminates one level of complexity in the analysis of CD3-dependent signalling events. Coverslips coated with anti-CD3ε antibodies reproduce major events of T cell receptor-dependent signalling and enable the analysis of the recruitment of signalling molecules to the CD3 complex by high-resolution confocal microscopy [7].

We applied a chemical genetics approach to investigate the role of LCK in the maintenance of T cell contacts at various stages after engagment of receptors [97;98] . Previously, it has been shown that active LCK is associated with the immature immunological synapse [6]. However, cells lacking this kinase fail to establish stable contacts with anti-CD3-coated coverslips. Therefore, application of small molecule inhibitors after contact formation is the only way to analyse the functional role of LCK activity at later stages of signalling.

T cell hybridoma cells stably expressing a YFP-fusion of ZAP-70 alone or in combination with a CD3ζ-cyan fluorescent protein (CFP) fusion protein were exposed to anti-CD3 coated coverslips and inhibitors were added at different time points before and after formation of contacts. ZAP-70 is recruited into the TCR signalling complexes within the first minutes of T cell activation and remains associated with the synapse through the early stages of immunological synapse formation [6]. We therefore expected ZAP-70 localization to be a sensitive readout for any changes in activities that have impact on the engagement and activation of CD3 complexes.

3.3 Results

We intended to elucidate the functional role of signalling active LCK in the early stages of CD3 engagement. Moreover, using anti-CD3 antibody-coated coverslips as a stimulus we intended to resolve whether a spatial rearrangement of transmembrane molecules was required for the transformation of a T cell contact from an immature to a mature stage. Hybridoma cells coexpressing the ZAP-70-YFP fusion protein alone or in combination with a CFP fusion protein of the CD3ζ-chain were generated as read-outs for signalling events affecting the CD3-complex. Cell lines applied in this study were generated by Anne-Marie Lellouch.

3.3.1 Functional integrity of fusion proteins. Fusion proteins of ZAP-70-YFP and CD3ζ-CFP were overexpressed in the 3A9 hybridoma cell line using a retroviral infection system affording efficient and highly stable expression. Western blotting of total cell lysates using an anti-GFP antibody revealed that both proteins were expressed at the expected molecular weights of 95 kDa and 41 kDa. No degradation products could be detected. Incubation of the coexpressing cells with 0.5 mM sodium pervanadate followed by anti-phosphotyrosine immunoprecipitation and western blotting against GFP revealed that both ZAP-70 and CD3ε fusion proteins were phosphorylated in an activation-dependent manner (Fig. 3.1). Furthermore, using anti-CD3ε-coated coverslips as a stimulus, the recruitment of the ZAP-70 fusion protein to the CD3 complex was demonstrated by immunoprecipitation (see below).

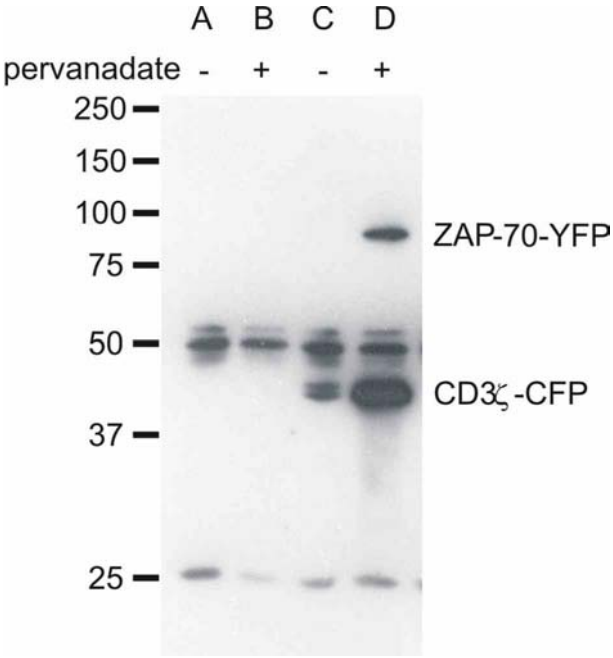

Figure 3.1 Activation-dependent tyrosine phosphorylation of CD3ζ-CFP and ZAP-70-YFP. Cell lysates from 3A9 cells alone (A,B) or coexpressing CD3ζ-CFP and ZAP-70-YFP (C,D) were immunoprecipitated with an anti-phosphotyrosine mAb before (-) or after (+) a 5-minute treatment with 0.5 mM sodium pervanadate. Immunoprecipitates were subsequently blotted with anti-GFP mAb. The bands at 25 kDa and 50 kDa probably result from cross-reactivity of the secondary anti-mouse antibody with the antibody used for immunoprecipitation. Figure provided by Anne-Marie Lellouch.

3.3.2 Transient recruitment of ZAP-70-YFP to CD3 clusters. First, the dynamics of cell spreading and ZAP-70 recruitment were investigated by exposing 3A9 ZAP-70-YFP transfectants to coverslips coated with anti-CD3ε antibodies. In contrast to work reported previously, in our case the adsorption of the antibodies was enhanced by

rendering the surface of the cover slip hydrophobic by silanization with octadecyl-trimethoxysilane. In order to prevent surface functionalization with extracellular matrix proteins contained within the cell suspension that could mediate the attachment of cells via integrins, after incubation with antibody, coverslips were blocked by incubation with 1 % BSA/PBS. In addition, cells were washed and added in serum-free medium. Upon contacting the anti-CD3ε-functionalized cover slip, the cells spread rapidly and small (approx. 0.5 μm) discrete clusters of ZAP-70-YFP began to form (Fig. 3.2). Analysis of the surface distribution of the anti-CD3ε antibodies by immunofluorescence excluded inhomogeneities as the the origin of ZAP-70-YFP clustering (data not shown). No cell spreading or ZAP-70-YFP clusters were observed for control coverslips coated with poly-lysine, anti-CD4 antibodies or BSA.

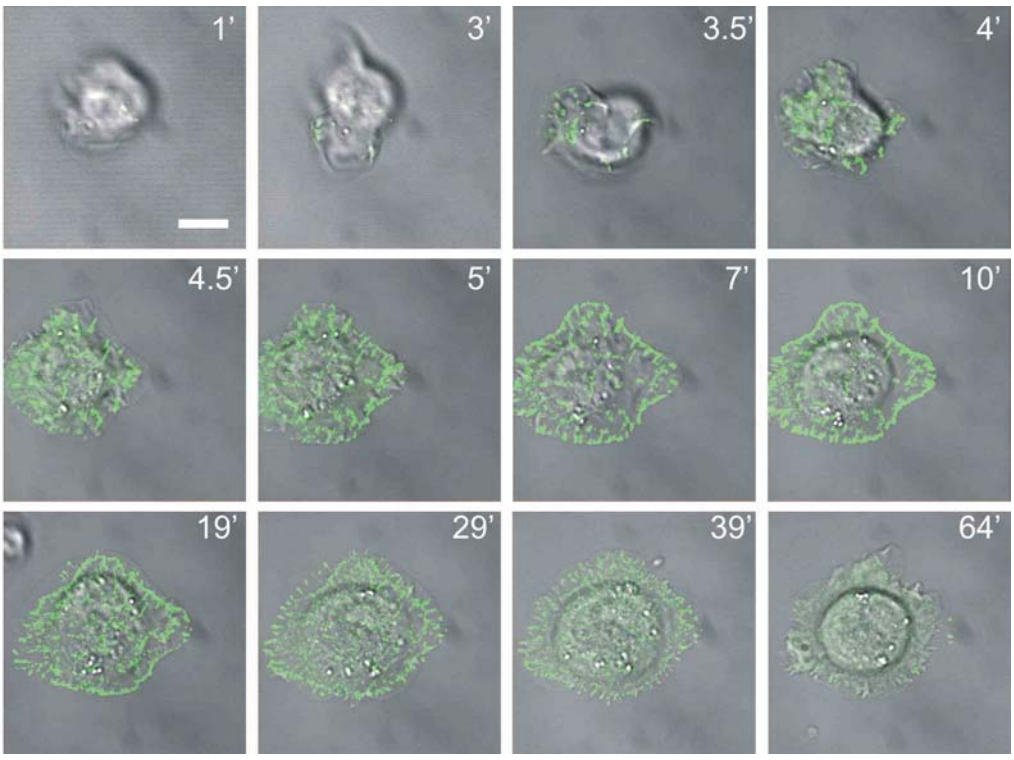

Figure 3.2 Cell spreading and clustering of ZAP-70-YFP fusion proteins in a ZAP-70-YFP transfected 3A9 cell contacting an anti-CD3ε-coated coverslips. The cell was imaged by time-lapse confocal microscopy. In order to ensure recording of cover slip-proximal fluorescence, a confocal stack consisting of five slices was recorded for each time point and slices containing surface-proximal fluorescence were selected for the figure. Times are given in minutes in the figures. The bar denotes 10 μm.

Maximal cell spreading was detected within 5 min. Concomitant with cell spreading, clusters appeared at the leading edge of the cells culminating into a near complete peripheral ring of ZAP-70-YFP clusters at about 10 min. The time-lapse imaging demonstrated that the formation of clusters at the periphery resulted from engagement of CD3 complexes at newly formed contact sites, rather than lateral diffusion or transport of aggregated proteins along the proceeding cell edge. The ring of clusters started to disappear after about 15 min to become completely undetectable about 25 min after formation, i. e. about 30 to 40 min after the initial cell-substrate contact. At the same time, the cells slowly started to retract their extensions from the cover slip. Furthermore a dissipation of central ZAP-70-YFP clusters was observed, which remained barely visible after 60 min. The time frame of ZAP-70-YFP recruitment observed in our system resembles the dynamics of ZAP-70 association with a T cell-APC immunological synapse [6]. The dissipation of ZAP-70 clusters is indicative of the initiation of down-regulatory events limiting the duration of the ZAP-70-dependent signal. Functional TCR engagement by surface-coated anti-CD3ε antibodies was further confirmed for this system by the detection of the nuclear translocation of the transcription factor NFAT (data not shown). For experiments using fixed cells, the 40 min time point was chosen. At this stage, the cells still fully adhered but ZAP-70 clusters had partially dissipated. When using inhibitors of signalling, this time point should therefore reliably reflect changes in signalling activities that influence ZAP-70 recruitment and cell attachment.

3.3.3 ZAP-70-YFP colocalizes with CD3 receptor complexes. In order to identify the molecular basis for the formation and dissipation of ZAP-70 clusters, we first determined whether the dynamics of ZAP-70-YFP clustering was correlated with the formation of CD3ζ-CFP clusters. For this purpose, 3A9 hybridoma cells coexpressing the ZAP-70-YFP fusion protein and a CD3ζ-CFP fusion protein were examined by confocal microscopy using the same stimulus (Fig. 3.3). CD3ζ-CFP formed discrete clusters, which fully colocalized with ZAP-70-YFP in the early stages of stimulation. This colocalization suggests that ZAP-70-YFP clustering resulted from recruitment to phosphorylated CD3 ITAMs, notably the CD3ζ chain. In contrast to ZAP-70, the CD3ζ clusters persisted over the whole 60 min time course of the experiment. The persistence of CD3ζ clusters indicates that the dissipation of ZAP-70-YFP clusters was not due to CD3ζ internalization but to other down-regulatory mechanisms that modulate ZAP-70

recruitment to the plasma membrane. These experiments, using fixed cells confirmed that the loss of YFP-fluorescence was not due to photobleaching. The confocal optics restricted the detection of fluorescence to an optical section next to the coverslip. It was therefore difficult to determine, whether the loss of YFP fluorescence was due to a redistribution of the fusion protein throughout the cell or due to a degradation of the fusion protein. For this purpose, cells were seeded onto anti-CD3ε-coated coverslips and the level of the fusion protein and endogeneous protein probed by Western blot. The ZAP-70 levels remained unchanged throughout the experiment (Figure 3.3 B).

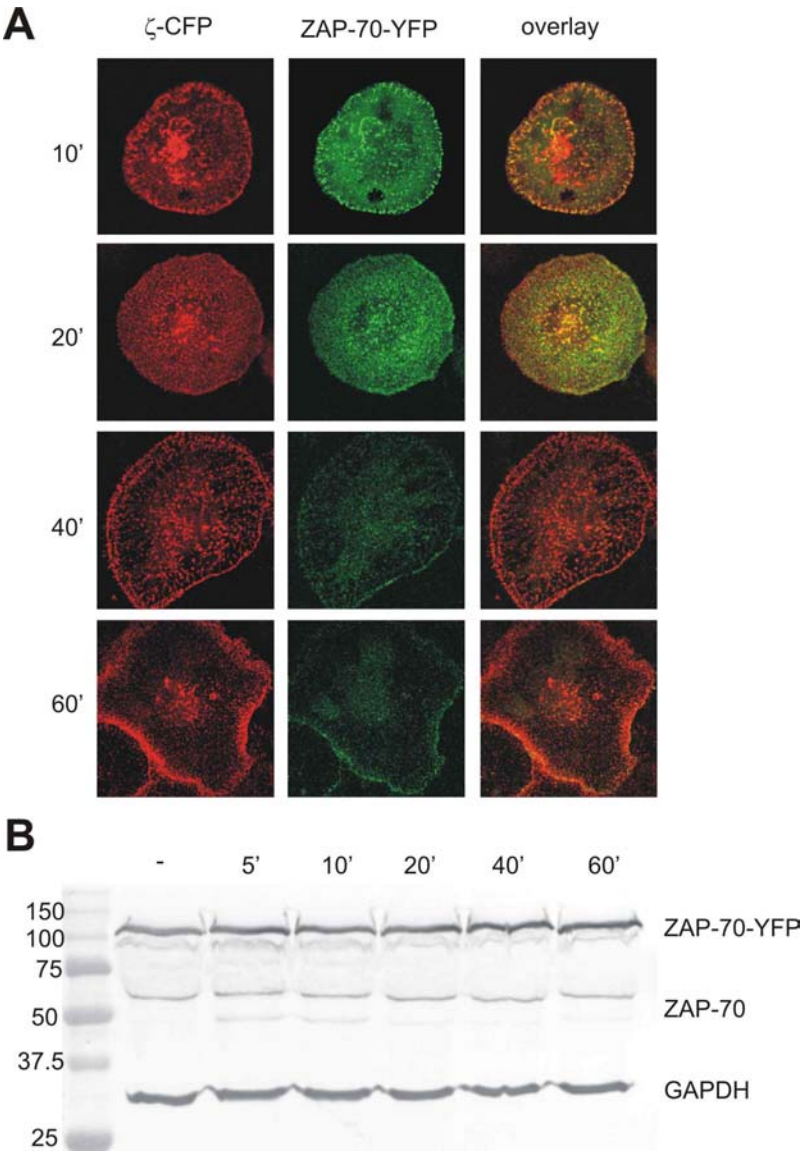

Figure 3.3 Corecruitment of TCR CD3ζ-chains and ZAP-70. (A) 3A9 cells cotransfected with CD3ζ-CFP and ZAP-70-YFP were exposed to anti-CD3ε-coated coverslips, fixed after 10, 20, 40, and 60 min of stimulation and imaged by confocal laser scanning microscopy. Left panels: CFP fluorescence (red); center panels: YFP fluorescence (green); right panels: superposition of both channels. A confocal section corresponding to the surface of the cover slip is shown in each case. The bar denotes 10 µm. (B) An anti-ZAP-70 Western blot was performed in order to determine whether the decrease in fluorescence was due to a degradation of the fusion protein. 3A9 cells expressing ZAP-70 YFP and CD3ζ-CFP were left unstimulated (-), or stimulated on CD3ε-functionalized coverslips for 5, 10, 20, 40 and 60 min. Lysates were subsequently blotted with an anti-ZAP-70 antibody. An anti-GAPDH antibody served as a control for the amount of cellular protein. The band at 50 kDa likely resulted from the cross-reactivity of the secondary antibody with residual stimulatory antibody washed off the coverslip during lysis of cells. Image 3.3 A was generated by Antje Hoff.

3.3.4 Continuous Src-family kinase activity is required for maintenance of cell contacts only in the early phase of cell attachment. To this end we had established that anti-CD3ε-coated coverslips induced a focal engagement of CD3 complexes leading to a transient recruitment of ZAP-70 with a time course similar to the one in the T cell APC contact [6]. In order to reveal the role of LCK in the formation and maintenance of the clusters an inhibitor-based strategy was chosen. Small molecule inhibitors represent powerful tools for rapidly interfering with cellular signalling processes. The specificity of the effects observed for inhibition of LCK activity was established through a combination of results obtained with the Src-family kinase inhibitors PP2 and SU6656. Of the kinases involved in early signalling in T lymphocytes PP2 inhibits the Src-family kinases LCK and Fyn with an IC_{50} value of 4-5 nM[110]. In contrast, the Src-family kinase inhibitor SU6656 (Sigma) was applied at 1 μM, a concentration inhibiting the kinases Src (IC_{50}=0.28 μM) and Fyn (IC_{50}=0.17 μM), but insufficient to inhibit LCK (IC_{50}=6.88 μM) [111]. In addition, SU6656 and PP2 vary greatly in their activity profiles for inhibition of non-Src-family kinases [112].

Pretreatment of the cells with 20 nM PP2 completely inhibited the capacity of the cells to adhere and spread on the anti-CD3ε-coated coverslips. Signalling-active LCK is associated with the immature immunological synapse for the first 10 min after contact formation. When PP2 was added 5 min after contact formation, ZAP-70 clusters, especially those in the periphery of the cells, dissipated. The cells retracted their contacts and the contour of the cell changed from a convex to a concave shape within 5 min (Fig. 3.4). This rapid and strong retraction was a phenomenon observed exclusively for more than 60 % of the PP2-treated cells at this stage. The detachment of cells prompted us to also add the inhibitor at a time point, when the ZAP-70 clusters started to dissipate. We hypothesized that at a time point, when early signalling events had been passed, contacts might be functionally different. In fact, in contrast to addition after 5 min, addition of PP2 20 min after contact formation had no significant effect on cell attachment. The size and distribution of the ZAP-70-YFP clusters corresponded to those of untreated cells (Fig. 3.4). Furthermore, the kinetics of the dissipation of clusters was comparable to that of the control. Apparently, in the early phase of CD3 engagement a requirement for continuous Src-family kinase activity exists in order to maintain cell attachment and ZAP-70 clustering. Later, this requirement vanishes. In order to validate biochemically the

inhibitor effects at the different time points, the interaction of the CD3-complex with ZAP-70 was probed by anti-CD3ε immunoprecipitation followed by an anti-ZAP-70 Western blot. Considering the fact that the addition of 20 nM PP2 caused a dissipation of clusters over a time course of several minutes, first, the concentration dependence of the effect of PP2 was assessed (Figure 3.4 C). To this end in different cellular model systems this inhibitor has been used at very different concentrations, ranging from the lower nanomolar range, into the micromolar range [7;110;111;113]. Cells were stimulated on the same anti-CD3ε-coated coverslips used for cell biological experiments and lysed after 10 min total time of stimulation. As expected, the recruitment of ZAP-70 to the CD3 complex was stimulus-dependent. To our surprise, no effect on ZAP-70 recruitment was detected at 20 nM PP2, neither when the inhibitor was added before initiation of stimulation nor afterwards. When the inhibitor was added at 200 nM or higher concentrations before the initiation of stimulation or 20 min afterwards, the ZAP-70 signal was strongly reduced. Interestingly, the inhibitory effect was even more pronounced when PP2 was applied at 200 nM 5 min after initiation of stimulation (Figure 3.4 D). While the prominent sensitivity of cells, 5 min after initiation of stimulation, observed by microscopy was reproduced by the immunoprecipitation, these data suggest that the cellular response reacts more sensitively to a shift in the extent in the kinase activity than may be detected biochemically.

Exposure of cells to SU6656 at a concentration of 1 μM had no effect neither on the attachment and spreading of cells, nor on ZAP-70 clusters, indicating that PP2-dependent effects are specifically related to the inhibition of LCK (not shown). In order to confirm that SU6656 had the potential to exert a specific inhibitory activity, human Jurkat lymphoma cells were exposed to coverslips coated with an antibody directed against the integrin LFA-1. This integrin acts as a coreceptor in T cell signalling [114]. Propagation of integrin-dependent signals is Src-kinase dependent. As expected, preincubation with both PP2 (20 nM) and SU6656 (1 μM) strongly reduced the attachment of Jurkat cells. On anti-CD3-coated coverslips, PP2 exerted a significant effect, while SU6656 showed a weak effect at best (not shown).

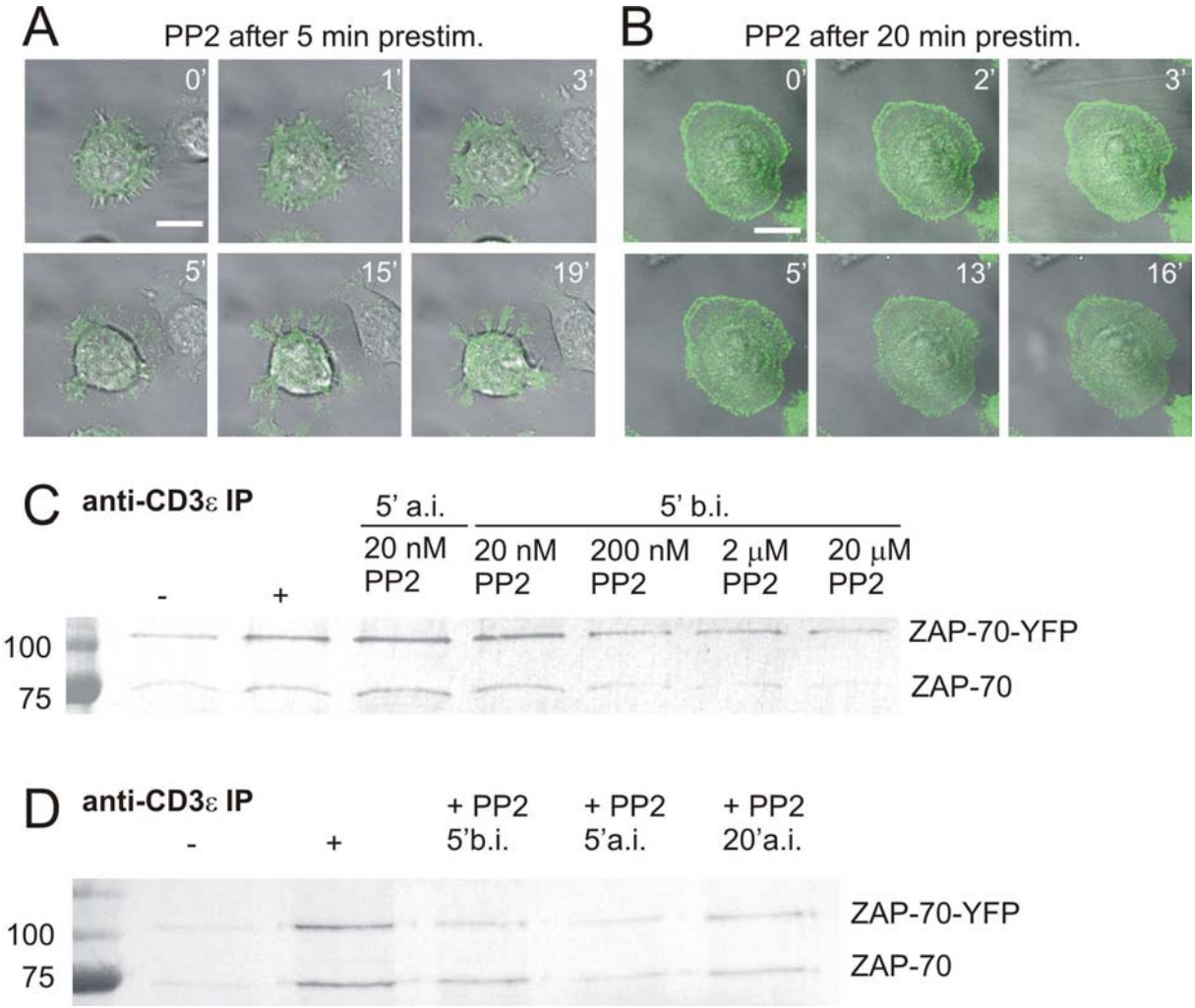

Figure 3.4 Effect of Src-family kinase inhibition on cell attachment and ZAP-70 clustering. (A, B) Time-lapse confocal microscopy of ZAP-70-YFP expressing cells before and after addition of 20 nM of the SFK PP2. Cells were allowed to establish contacts with the coverslips for (A) 5 min and (B) 20 min before addition of the inhibitor. A confocal section corresponding to the surface of the cover slip is shown in each case. The time points after the addition of the inhibitor are shown. The bar denotes 10 μm. (C) Biochemical validation of the effect of PP2 on ZAP-70 recruitment. 3A9 cells expressing ZAP-70-YFP were left unstimulated (-), or stimulated on CD3ε-functionalized coverslips without inhibitor (+) or with 20 nM PP2 added 5 min after initiation of stimulation (a. i.) or 20 nM, 200 nM, 2 μM, and 20 μM PP2 added 5 min before initiation of stimulation (b. i.). Cells were stimulated for a total time of 10 min. Lysates were immunoprecipitated with antibodies against CD3ε and subsequently blotted with an anti-ZAP-70 antibody. (D) Dependence of the inhibition of ZAP-70 recruitment on the timing of the inhibitor application. Anti-CD3ε immunoprecipitates of lysates of cells left unstimulated (-), or stimulated on anti-CD3ε-coated coverslips for a total time of 30 min, without (+) or with 200 nM PP2 added at the indicated time points were probed for ZAP-70 by Western blot.

3.3.5 Cell detachment is actin independent. In order to address the molecular basis for the PP2-dependent cell detachment, we decided to investigate the role of actin reorganization on cell attachment, ZAP-70 clustering and cell spreading. Reorganization of F-actin at the immunological synapse has been related to the stabilization of the cell-APC contact [115]. Both LCK and Fyn have been implicated in the T cell stimulation-dependent actin reorganization [116;117]. T cell spreading on a functionalized surface is accompanied by the rearrangement of F-actin into circumferential rings [7;109].

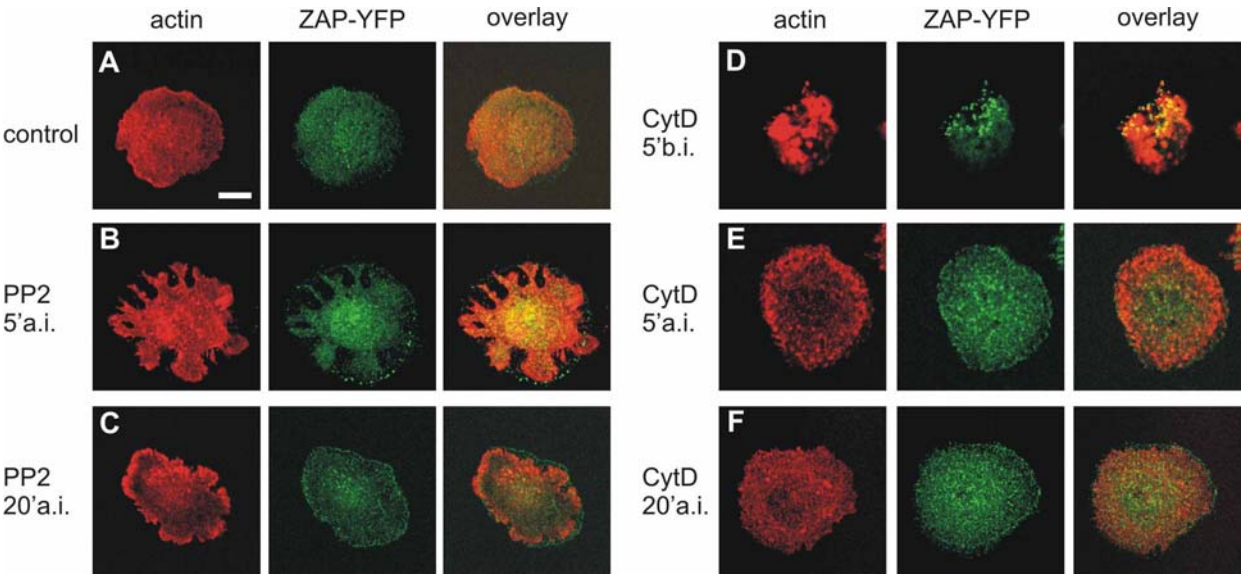

Figure 3.5 Effect of inhibitors on F-actin, cell attachment and ZAP-70 clusters. (A) Untreated controls, (B, C) cells exposed to 20 nM PP2 after (B) 5 min (5' a. i.) and (C) 20 min (20' a. i.) incubation time, (D) cells pre-treated with 10 µM CytD 5 min before exposure to the coverslips (5' b. i.), (E) incubated after 5 min and (F) 20 min of preincubation. In the figure, the time point when the inhibitor was added is given in each panel. In each case, including the control, the cells were incubated for a total of 40 min before fixation, i. e. a further 35 min when inhibitor was added after 5 min and a further 20 min when inhibitor was added after 20 min. Actin was visualized using 100 µg/ml biotin-conjugated phalloidin in combination with Cy5-conjugated streptavidin. The left panels (red) represent actin, the center panels (green) ZAP-70-YFP. In the right panels a superposition of both channels is shown.

When cell detachment was induced by addition of PP2 after 5 min of stimulation, a fragmentation of F-actin was observed (Fig. 3.5 A, B). In contrast, little effect on F-actin was observed when PP2 was added to cells after 20 min stimulation (Fig. 3.5 C). Again, the characteristic detachment was visible for the majority of the PP2 treated cells, while

only rarely seen in untreated cells. In order to ascertain whether the fragmentation of F-actin was the reason for cell detachment, cells were incubated with CytD, an inhibitor of actin polymerization. In contrast to PP2, preincubation of cells with 10 μM CytD did not inhibit the formation of ZAP-70-YFP clusters at the cell-substrate contact and adhesion of cells (Fig. 3.5 D). However, consistent with results reported previously for Jurkat cells, the actin-mediated spreading of the cells on the surface was inhibited [118]. Unlike PP2, CytD treatment of cells contacting the coverslips for 5 min did not cause detachment or retraction of the cells from the surface. Instead, the cells were spread out on a smaller area, demonstrating that only cell extension was inhibited (Fig. 3.5 E). No peripheral actin ring formed and actin did not colocalize with ZAP-70-YFP clusters. For cells treated with CytD after 20 min, the only visible effect was a mild disruption of F-actin compared to the controls (Fig. 3.5 F). In addition, CytD inhibited not only the spreading of the cells, but also abolished the dissipation of ZAP-70-YFP clusters, since the ZAP-70-YFP clusters appeared brighter in CytD-treated cells than in the control cells stimulated for the same total time. In contrast to PP2, ZAP-70 clusters in CytD treated cells persisted over the whole 60 min time course of the experiment. In order to address whether this persistence of clusters was due to an inhibition of actin-dependent internalization, confocal stacks of CytD treated cells and controls were acquired. No evidence for actin-dependent internalization of ZAP-70-rich vesicles was obtained. The observations made for the inhibitors and the loss of colocalization in controls at the 40 min time point support the notion that ZAP-70 clustering is only indirectly coupled to F-actin polymerization. However, cell spreading driven by stimulation-dependent actin reorganization is a prerequisite for the formation of peripheral contacts and clusters.

3.3.6 Cell retraction upon Src-family kinase inhibition occurs by detachment of contacts. The results obtained so far indicate that the PP2-induced detachment of cells is not due to an inhibition of actin polymerization. Instead, LCK may exert a direct activity on the CD3 complex or CD3-associated proteins that act upstream and/or independent of actin polymerization and that destabilize the cell-substrate contact. In order to probe the intimacy of the cell-substrate contact, cells were fixed but not permeabilized and coverslips incubated with a Cy5-conjugated anti-Armenian hamster antibody. In the absence of permeabilization the surface of the cover slip underneath the cell is accessible for the Cy5-labelled antibody only from the side (Fig. 3.6). In control

cells, the area of contact of the cells with the cover slip was completely inaccessible to the antibody, indicative of a tight cell-substrate contact (Fig. 3.6). In contrast, in the periphery of PP2 treated cells, the anti-CD3ε fluorescence colocalized with ZAP-70-YFP fluorescence. This distribution of fluorescence strongly suggests that cell retraction induced by PP2 occurs by disengagement of cell contacts from the antibody-coated surface. The peripheral CD3 contacts were destabilized to the point that even for the contacts themselves the surface became accessible to the antibody. Finally, detachment occurred in a highly disordered fashion. Instead of a uniform retraction of the cell edge, some contacts were maintained and large bay-like shapes formed. Formation of these shapes can be explained by a generalized destabilization of contacts across the contact surface and a random detachment of contacts.

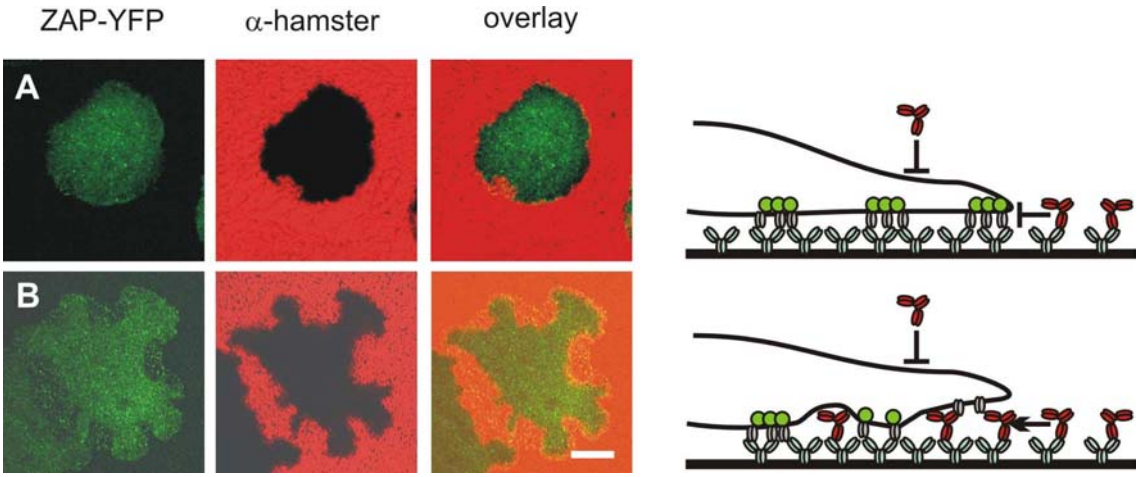

Figure 3.6 Analysis of the mechanism of PP2-induced cell detachment. (A, B) Tightness of cell-substrate contacts determined by the accessibility of surface-bound Armenian hamster anti-CD3ε antibody to Cy5-labelled anti-Armenian hamster antibody. Cells were stimulated for 5 min, followed by incubation for 20 min in the absence (A) or presence (B) of 20 nM PP2. ZAP-70-YFP fluorescence is shown in green (left panels), Cy5 fluorescence of anti-Armenian hamster antibody in red (center panels) and superpositions of both channels in the right panels. To the right, schematics of the surface staining by Cy5-labelled anti-Armenian hamster antibodies are shown. The cells were fixed but not permeabilized. Surface bound Armenian hamster anti-CD3 antibodies in the cell-substrate contact were therefore only accessible to the anti-Armenian hamster antibody by lateral diffusion of the molecules into the contact area. The bars denote 10 μm. The scheme on the right was generated by Roland Brock.

3.4 Discussion

The results presented in this paper introduce chemical genetics in combination with high resolution confocal microscopy for the analysis of the timing of signalling activities in cellular signal transduction pathways. The application of inhibitors of Src-family kinases as well as microfilament dynamics at various stages before and after contact formation provided new insights in the initial steps of CD3-dependent signal transduction in T cells.

3.4.1 Maturation of signalling clusters on anti-CD3ε-coated surfaces. In our experiments, glass coverslips homogeneously coated with anti-CD3ε antibodies were used as a minimal stimulus engaging CD3 complexes in a manner that precludes the ordered rearrangement of transmembrane molecules by lateral diffusion. Three different stages of susceptibility to inhibition of Src-family kinases by PP2 could be distinguished. First, cells pretreated with PP2 failed to establish contacts, which is consistent with the finding that PP2 pretreatment inhibits induction of tyrosine phosphorylation upon subsequent TCR/CD3 cross-linking[119]. Second, cells that had established contacts for 5 to 10 min continued to be sensitive to PP2. Third, at 20 min after initial engagment, the ZAP-70 cluster dynamics were no longer sensitive to the inhibitor and the dissipation and detachment followed its normal time course. By combination of inhibitors with different specificities, especially by taking advantage of the recently described inhibitor SU6656, we were able to show that the effect of PP2 could most likely be attributed to inhibition of LCK (Fig. 3.7). While PP2 acts as an inhibitor of the Src-family kinases LCK, Fyn, Hck, and Src, SU6656 is expected to act on the Src-family kinases Src, Fyn, Yes and Lyn, but not on LCK at the concentration used in our experiments [120]. In addition, at a concentration of 20 nM LCK and Fyn are the primary activities relevant for T cell attachment inhibited by PP2. Moreover, the LCK-deficient Jurkat cell line JCaM1.6 failed to spread on anti-CD3ε functionalized coverslips, while LCK retransfected cells were able to spread, as seen in the second paper in this section. The significance of LCK in the maintenance of ZAP-70 clusters is consistent with the observation that the effect of LCK mutations on cell adhesion cannot be complemented by Fyn [116]. Since LCK is the primary kinase involved in CD3-dependent signalling, validation of the inhibitory activity of SU6656 had to rely on an independent assay.

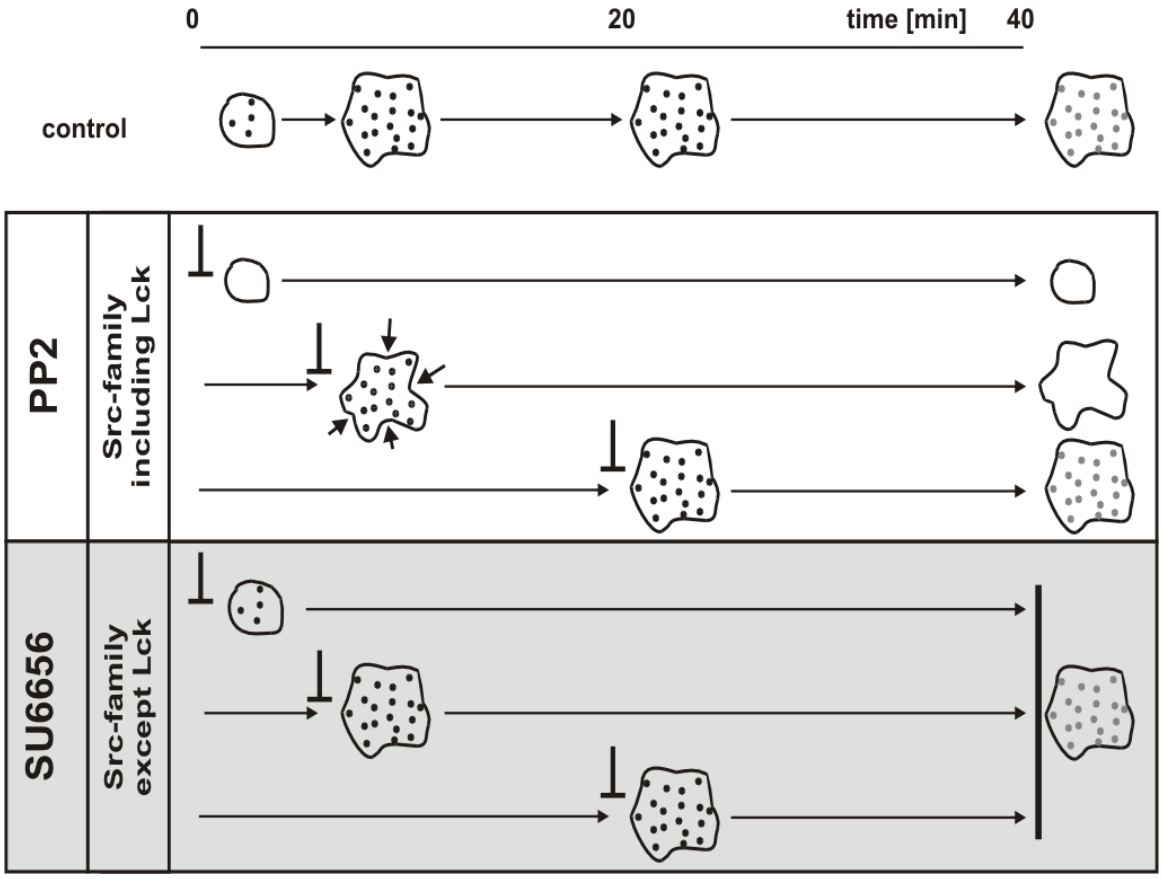

Figure 3.7 Schematic, summarizing the effects of inhibitors on cell morphology and ZAP-70 aggregates observed for addition of compounds before or 5 min and 20 min after contact of cells with the anti-CD3-coated coverslips. Scheme by Roland Brock.

Using a very similar experimental design, we could demonstrate that this compound inhibited the attached of Jurkat T cell lymphoma cells on anti-LFA-1 coated coverslips. As expected, given the activity profiles, both PP2 and SU6656 had the same effect. Given the importance that has been attributed to the lateral mobility of receptor molecules, the formation and maturation of the immunological synapse has most often been investigated in the T cell APC contact or for T cells exposed to ligands incorporated into supported lipid bilayers [106].Our results show, that stimulation by a well defined and highly simplified non-diffusive stimulus, as well, induces a transformation of contacts from a stage sensitive to Src-family kinase inhibition to an inhibition-insensitive stage. Apparently, CD3 clusters alone undergo a time-dependent maturation.

3.4.2 Molecular mechanism of contact maturation and detachment. Actin remodelling has been described as a hallmark both of immunological synapse formation and contact formation of T cells with anti-CD3-coated surfaces. Both LCK and Fyn have been implicated in these processes [117;118;121]. Consistent with these prior results, addition of PP2 affected the distribution of F-actin, both at the early and late time point. However, inhibition of microfilament dynamics by CytD only affected cell spreading. Neither cell attachment nor ZAP-70 clustering were affected by this compound. Apparently, the LCK-dependent regulation of CD3 engagement is controlled by mechanisms acting upstream of actin polymerization at the contact site. At present, we can only speculate how such disengagement occurs on the molecular level. The failure of cells preincubated with PP2 to adhere to anti-CD3-coated coverslips indicates that the presence of receptor and ligand is insufficient for establishing of strong receptor-ligand contacts and suggests some sort of a feedback of early intracellular events necessary to allow adhesion, even to such a simplified and strong stimulatory surface. The observations made for the CD3-dependent attachment bear ressemblance with the modulation of integrin-mediated cell adhesion [122-124]. The results suggest that Src-family kinases act on the CD3 complex in a way that modulates the avidity of these receptors for a polyvalent ligand.

3.4.3 Analyis of T cell contacts by chemical genetics. To this end, contact maturation between a T cell and an APC has been based largely on morphological criteria. The demonstration that T cell contacts acquire an unsensitivity to the inhibition of LCK introduces a pharmacological concept of contact maturation. Moreover, the different phenotypes obtained for the inhibition of LCK before and at various stages after formation of contacts stress a major advantage of chemical genetics over alternative methods for interfering with the function of a protein. Knock-down strategies as well as the down-regulation of protein expression by small interfering RNAs (siRNA) precludes the analysis of protein signalling activities that are vital for the initiation of a signal.

In the analysis T cell signal transduction evidence is accumulated that the kinetics of signalling critically determines the functional response of a T cell [125]. Chemical genetics represents a powerful means to investigate in detail the functional implications of such signalling kinetics. As an alternative to the application of an inhibitor after a certain duration, for low affinity compounds one may also imagine to remove the signalling block by wash-out of a compound. In addition to investigating the function of a gene

product with compounds of known activity, chemical genetics screens are performed by testing of compound collections with unknown targets for the induction of phenotypes, e. g. in the development of organisms [98]. In these applications, kinetics also plays a role. Such screens, as well, therefore greatly benefit from the addition of compounds at different time points.

Interestingly, the cellular phenotype provided a more sensitive sensor to the presence of the inhibitor than the biochemical analysis of the recruitment of ZAP-70. When cells were preincubated with 20 nM PP2 no spreading of 3A9 cells on anti-CD3-coated coverslips was detected. Still, ZAP-70 was recruited into the CD3 complex. At present, the molecular details of this phenomenon remain elusive. We may only speculate that subtle changes in the balance of kinase and phosphatase activities are translated into different degrees of cell spreading. Given that T cells react sensitively to differences in MHC-peptide complexes and that the kinetics and balance of the recruitment of signalling proteins is discussed as the basis for this discriminatory ability, these results are not fully surprising [126]. In our analyses we aimed at using the same anti-CD3 coated coverslips used for cellular experiments for the stimulation of cells used for biochemical experiments. Larger number of cells and a more detailed analysis of the pattern of phosphorylation may resolve the molecular details of this observation.

One possible limitation of chemical genetics is the lack of specificity of some inhibitors. However, for the LCK-dependent signalling addressed in this study, only two members of the group of SFK target proteins have been implicated in the investigated signalling pathway. Of these two proteins, LCK and Fyn, LCK was singled out as the relevant target by incubation of cells with an inhibitor with a different activity profile. Given the availability of diverse compound collections with different activity profiles, a strategy, in which the specificity of an observed effect is confirmed by application of different inhibitors at various time points, may be realized for a large number of molecular targets. In order to perform such analyses efficiently, a robust stimulation protocol providing a maximum in information on the respective signalling pathway is required. For the analysis of T cell signalling, this prerequisite was fulfilled by exposure of cells to anti-CD3-coated coverslips, a stimulus that reproduces major characteristics of TCR-dependent signalling events initiated by more complex stimuli. We are well aware that cellular experiments using such simplified stimuli cannot replace the analysis of T cell signalling in physiological T cell APC contacts. However, our approach may

complement the latter in several ways. First, by providing highly defined stimuli revealing new and interesting characteristics of components of the signalling machinery. Second, by acting as a filter to screen for experimental conditions that are interesting enough for a further detailed analysis. The considerable extra effort required for the analysis of T cell APC contacts precludes the systematic testing of a large number of experimental conditions.

The stimulation and image acquisition protocols presented in this study can readily be implemented into automated experimental procedures. Initial experiments have shown, that cell attachment, size and kinetics of signalling clusters respond sensitively to inhibition of a large number of down-stream events. Moreover, the approach may be extended to stimuli other than CD3-directed antibodies. The anti-LFA-1-coated coverslips used to confirm the activity of SU6656 were a first step in this direction. By taking advantage of a large repertoire of available inhibitors targeting distinct steps in T cell signalling it will be interesting to address systematically the involvement and timing of downstream signalling components controlling T cell adhesion, cytoskeletal reorganization and the dynamics of signalling clusters.

4. Functional Profiling of Chemical Inhibitors and Therapeutic Antibodies using Cellular Microarrays

4.1 Summary

Pharmaceutical inhibitors play an important role in immunology. In basic research, the role of specific enzymatic activities in signal transduction are routinely addressed. In addition, there is an ongoing search for immunomodulatory compounds serving as therapeutics. Specificity of small molecules is a general concern. For this reason, especially in the testing of new compounds, methods are required that sensitively reveal differences in biological activities. As a solution to this problem we have developed microarrays in which cells are exposed to a multitude of mixtures of stimulatory antibodies directed against combinations of cell surface receptors. Microarrays are spotted in a microtiter plate format and the response of cells to each combination of stimuli is detected by automated fluorescence microscopy. In Jurkat cells, inhibitors of T cell signalling with identical primary targets showed remarkable differences in their biological effects in the presence of various combinations of CD3- and CD28-directed stimuli, validating the potential for a profiling of pharmaceutical inhibitors. Furthermore, the application of the microarrays to the functional characterization of a therapeutic antibody is demonstrated. The cellular microarrays increase by more than an order of magnitude the data obtained for cellular assays and enable a detailed analysis of the interplay of signalling pathways requiring a minimum of cells.

All cellular microarray experiments in this section were performed by the author. All stimulatory antibodies applied here were produced by Prof. Dr. Gundram Jung and Dr. Ludger Grosse-Hovest. Dr. Thomas André was involved in microarray establishment.

4.2 Introduction

The combination of sometimes conflicting signals into a physiologically meaningful response is a remarkable characteristic of the molecular signalling machinery. In the past years a wealth of information has been accumulated on the molecular events of individual signalling pathways and on factors that contribute to linking these pathways into

networks. It is now required to validate the functional relevance of these factors and to define the interplay of signalling pathways [127]. In basic research, such information is required in order to identify a functionally relevant network topology, a requirement for model building in systems biology [128;129]. In drug development, the parallel activation of several signalling pathways may induce compensatory activities within a signalling network that override the activity of a compound [130]. A drug candidate should therefore be tested in the presence of a large number of different stimuli in order to obtain information with higher physiological relevance. However, using standard protocols for cellular assays, i. e. one readout per sample, the testing of large numbers of different combinations of stimuli is costly and cumbersome.

Signal transduction in T lymphocytes is paradigmatic for a sensitive dependence on the molecular environment. Depending on the nature of the stimulus, the differentiation and activation state of a T cell, and the molecular environment, a T cell can respond with activation and proliferation, anergy, or apoptosis [3]. For the activation of naive T cells, two signals are necessary to induce persistent activation (reviewed in [75]): The crosslinking of T cell receptor (TCR)/CD3 complexes by specific MHC/peptide complexes of antigen presenting cells (APCs) and a costimulatory signal that is primarily provided through engagement of the CD28 coreceptor. TCR engagement leads to the recruitment of the Src-family kinase LCK, which phosphorylates tyrosine residues within the TCR/CD3 complex [107]. The Syk-family kinase ZAP-70 binds to the phosphorylated CD3ε chains and propagates the activation by phosphorylating downstream components [131], leading to a phospholipase Cγ (PLCγ-mediated increase in intracellular Ca^{2+} and the phosphorylation of membrane lipids by phosphatidylinositol-3'-kinase (PI3K). PLCγ-dependent calcium signalling leads to the activation of the phosphatase calcineurin, which dephosphorylates the nuclear factor of activation in T cells (NFAT), leading to its nuclear translocation [82]. The activity of calcineurin is antagonized by a glycogen synthase kinase-3 (GSK-3)-dependent phosphorylation of NFAT which leads to the nuclear export of NFAT. GSK-3, in turn, is inhibited by a PI3K-dependent signalling pathway. For costimulation by CD28, most signalling molecules involved in this pathway also play a role in CD3-dependent signalling. Therefore, it is still under dispute whether CD28 engagement only quantitatively enhances CD3-dependent signalling or activates qualitatively different signalling activities [75].

We sought to develop a strategy by which the interplay of signalling pathways in generating a cellular response could be analyzed systematically and to apply this strategy to the testing of the activity of low molecular weight inhibitors. Given its significance for the activation of cellular immunity, the CD3-/CD28-dependent signalling network provides a highly interesting target for this approach. In order to sample systematically combinations of CD3 and CD28 stimuli, Jurkat T cell leukaemia cells were exposed to an antibody microarray in the presence or absence of pharmacological inhibitors. Jurkat cells are a human T helper cell leukemia line [132;133] that has been extensively used for the research on T cell signalling in the past 25 years [134]. The arrays were produced in a microtiter plate format, enabling an efficient processing of multiple samples. Each spot of the array contained a distinct mixture of stimulatory anti-CD3 and anti-CD28 antibodies. As a substitute for the APC, antibody-functionalized surfaces have been shown to reproduce major T cell signalling events [118;135]. Cell spreading and NFAT translocation were recorded by immunofluorescence microscopy followed by automated image analysis. For the entire microarray, the cellular responses were a function of the composition of the stimuli. The selected pharmacological inhibitors, including several well-established compounds used for the analysis of T cell signalling, showed remarkable difference with respect to their response profiles. Moreover, different response profiles were obtained for pairs of inhibitors for which the same primary targets had been described, providing new information on the specificity of these compounds. In addition, the application of the method to the functional profiling of the supraagonistic anti-CD28 antibody rM28[136] is demonstrated. The rM28 represents a bispecific single-chain antibody directed to a melanoma-associated proteoglycan (MAPG) and the CD28 receptor, which has shown to induce T cell stimulation independent from TCR/CD3 stimulation.

4.3 Results

4.3.1 Implementation of cellular microarrays. For the immobilization of stimulatory antibodies on different surfaces, we first evaluated the effect of different surfaces on the stimulatory properties of immobilized antibodies using an enzyme-linked immune assay (ELISA). Also, we analyzed the effect of stimulating antibodies on IL-2 expression in this experiment. We compared the effect of different surfaces on the

functional immobilization of different antibodies: Untreated glass coverslips, the hydrophobic but noncovalent-binding octadecylsilane surface, GOPTS (100 %, and 2.5 % (v/v) in ethanol), and an aminopropylsilane-based, noncovalently absorbing hydrogel (Nunc). Taking into account the surface to volume ratio, for the macrostructured format a concentration of 2 μg/ml of the stimulatory anti-CD3 and/or anti-CD28 antibodies was considered sufficient for surface saturation. In addition, a BSA-coated coverslip was included as a negative control. $1.25*10^5$ cells/surface were stimulated for 16 h, then the supernatants were removed and IL-2 expression quantified by ELISA (performed by Ludger-Grosse Hovest and Elke Hoffmann). On all surfaces, the IL-2 expression induced by anti-CD3 engagement was higher than that for anti-CD28 engagement alone (Fig. 4.1). The most intensive IL-2 signal was observed for anti-CD3 stimulation plus anti-CD28 costimulation and was much higher than the sum for both single stimuli. The supraagonistic anti-CD28 antibody induced a much stronger signal than the clone 9.3. On the untreated slides and the hydrogel, the IL-2 signal was more intense than anti-CD3 engagement alone. The most intensive IL-2 signal was observed for anti-CD3 plus anti-CD28 stimulation for the untreated slides, the hydrophobized slides, and the hydrogel surface, while the epoxy-functionalized slides only generated weak signal.

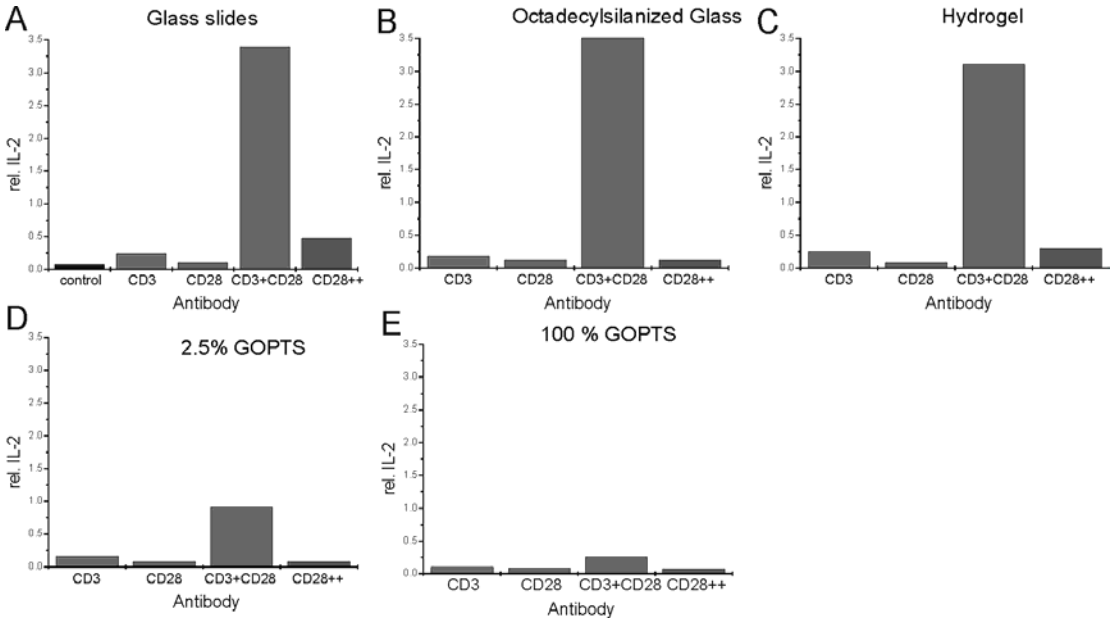

Figure 4.1 Evaluation of different functionalization methods for the immobilization of stimulatory antibodies. Surfaces were functionalized with 2 μg/ml of each of the stimulatory antibodies, and blocked with BSA. PBMC cells were stimulated for 16 h on the surfaces and IL-2 expression quantified by ELISA.

The different surfaces were also tested for the suitability for antibody spotting. Solutions of anti-CD3 antibodies (OKT3) were spotted as described for the stimulatory antibody microarrays in the experimental procedure section, blocked with 1 % BSA, washed with PBS and stained with fluorescently-labelled secondary anti-mouse antibodies. Microscopy showed that the unfunctionalized glass slides only provide relatively low binding including wash-out effects. Coating of protein surfaces with 2.5 % epoxy-silane provided high protein binding, but due to difficulties in the removal of residual silane from these surfaces, detectable by impurities, self-produced epoxysilane surfaces were not suitable for the reproducible spotting of antibodies (data not shown), and also were only able to induce weak stimulation of the cells as determined by ELISA. Providing the best spot quality, hydrogel substrates were selected as substrates for the cellular microarrays. The substrates from Nunc and Schott-Nexterion both showed a highly homogeneous distribution of antibodies within a spot over a wide concentration range. The Schott-Nexterion Slide H hydrogel, a succinimidyl ester-activated polyethylenglycol-based hydrogel was selected as an antibody microarray substrate because of its insensitivity for the adhesion of cells on non-functionalized areas, enabling a direct correlation of attachment and spreading to activation. The saturation binding capacity of this hydrogel was determined at an antibody concentration of about 200 µg/ml, which represents a concentration of about $6.4*10^{-6}$ ng per μm^2 hydrogel, which is about 700 molecules per μm^2.

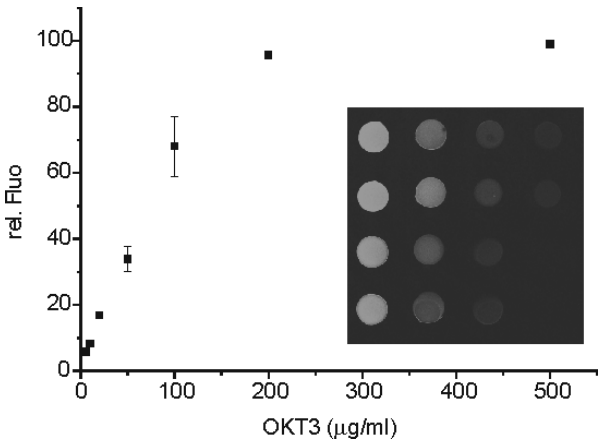

Figure 4.2 Quantification of antibody binding to a succinimidyl-ester functionalized hydrogel (Schott-Nexterion). Anti-CD3 antibodies (OKT3) were spotted in different concentrations and bound antibodies detected by anti-mouse Alexa 488 staining, fluorescence microscopy and quantified using Image Pro Plus.

The composition of the spotting and blocking buffer was adapted from the manual for Hydrogel Slides H. In order to enhance spot homogeneity and to prevent evaporation, 0.5% (w/v) trehalose was added to the spotting buffer. In addition to the blocking of the reactive groups by ethanolamin, an additional blocking step against unspecific adhesion of proteins and cells with the albumine supplement 1% (w/v) Top Block (Sigma) was incorporated [137].

4.3.2 Attachment of cells to the microarrays. To systematically probe the interplay of CD3 and CD28 in T cell activation a matrix of mixtures of anti-CD3 and anti-CD28 antibodies was spotted. A polylysine spot served as a negative control to determine NFAT translocation in the absence of a stimulus. In addition rM28, a single-chain bispecific antibody against anti-CD28 and the melanoma-associated proteoglycan (MAPG) [136], was spotted. This protein has been shown to induce a CD3-independent, supraagonistic stimulation of the CD28 molecule on human T cells, resulting in tumour cell killing. After pipetting of the arrays, a frame was attached to the microarray substrate, yielding 16 wells in a standard microarray-plate format per microarray substrate (Fig. 4.3). In this way, in each well a multitude of different conditions, corresponding to the number of spots of the microarray, could be tested. Cell spreading, serving as a measure for activation-dependent reorganisation of the actin-cytoskeleton [118] and translocation of the transcription factor NFAT were quantitated by laser scanning microscopy and image processing. One multi-channel fluorescence image was recorded for each spot. An overview of a typical cellular antibody microarray, scanned in a mosaic-like fashion is shown in Fig. 4.3.

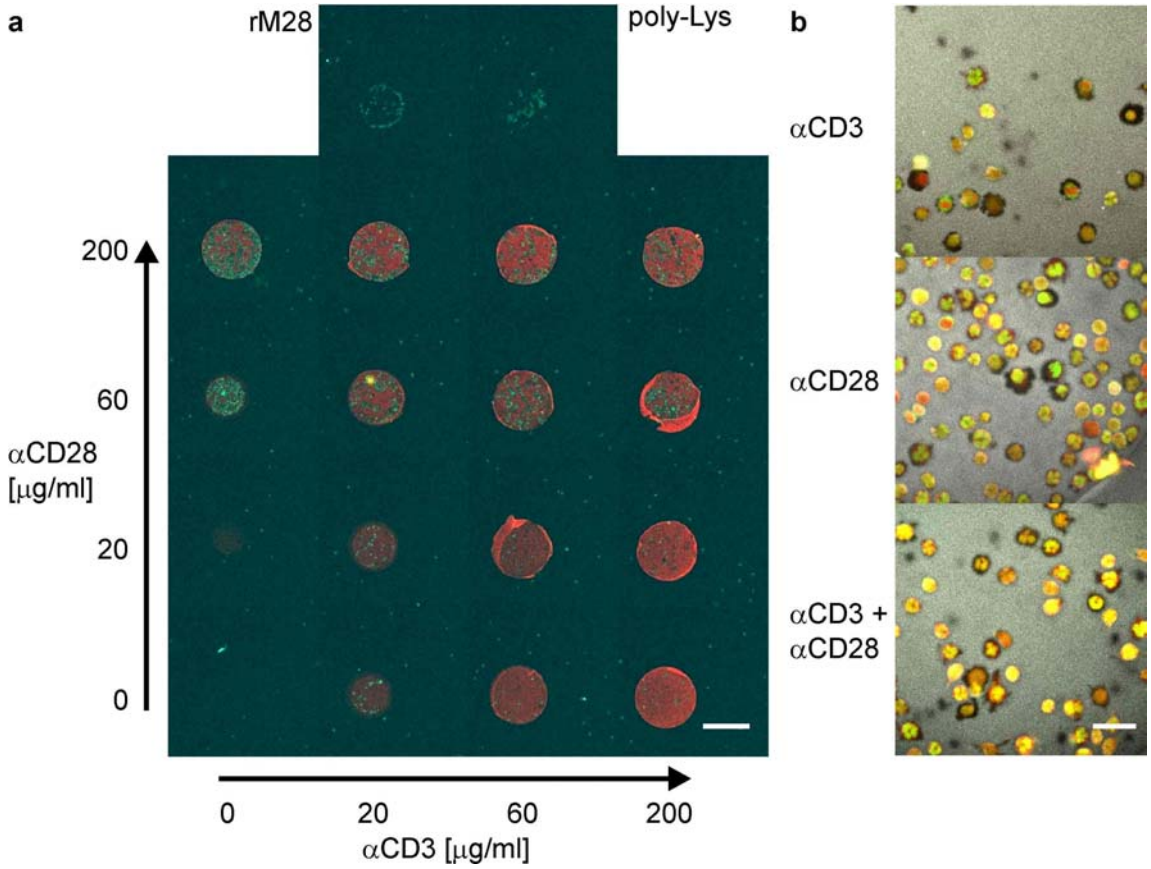

Figure 4.3 Anti-CD3/anti-CD28 antibody microarray. (A) Overview: Mixtures of anti-CD3 and anti-CD28 antibodies were spotted at the indicated concentrations and visualized by staining with an Alexa546-labeled anti-mouse antibody (red). Jurkat cells are visualized by nuclear TOPRO staining (blue). As a control to mediate cell-attachment without activation, polylysine was spotted. The supra-agonistic anti-CD28 antibody rM28 had little reactivity for the secondary antibody. The scale bar represents 400 μm. (B) Spreading and NFAT translocation of Jurkat cells on spots functionalized with 200 μg/ml of anti-CD3, anti-CD28 or a mixture of both antibodies. The immobilized antibody is visualized in grey. Nuclei are colored red, NFAT green, resulting in yellow color in the case of colocalization. The scale bar represents 20 μm.

Cells were incubated on the microarrays for 60 min before fixation, a time required to observe pronounced NFAT translocation. In some cases, 20 μg/ml of either antibody was not sufficient to induce the attachment of a sufficient number of cells to determine NFAT translocation. Overall, the number of cells per spot showed a positive correlation with antibody concentration in the range of about 5 to 200 cells with measurable properties present on each spot. Initial experiments had shown that spreading of Jurkat cells on anti-CD3 reached its maximum after about 10 min of cell stimulation and was strongly reduced after 60 min, in accordance to [118], while on anti-CD28 spreading was

stronger after 60 min than after 10 min (Fig. 4.9). This suggests a higher persistence of the anti-CD28-induced spreading compared to that induced by anti-CD3. The observations for the 60 min time point were extended by the concentration matrix (Fig. 4.4). Interestingly, cell spreading was reproducibly weaker on the 200 μg/ml anti-CD3 spot than on the 60 μg/ml anti-CD3 spot at that time point. For mixtures of both antibodies cell spreading was observed for total antibody concentrations at which each of the antibodies alone failed to induce a response. With regard to NFAT, anti-CD28 alone induced a stronger translocation than anti-CD3 alone. Again, cells exposed to a mixture of both antibodies showed an enhanced response, which was reproducibly strongest for the spots with maximum anti-CD28 concentration and intermediate anti-CD3 concentrations. For both, cell spreading and NFAT translocation a gradient of activation was obtained for the whole array, confirming that the antibody concentrations were appropriately selected for probing the interplay of both stimuli. The data on cell spreading and nuclear translocation were obtained on a single cell level. However, for individual cells, no strong correlation between both responses was observed (Fig. 4.8 A). In contrast for the average of all cells on one spot, for those spots for which a significant average cell spreading was observed, (>60 μg/ml total antibody) spreading showed a weak positive correlation with the translocation of the transcription factor (Fig. 4.8 B).

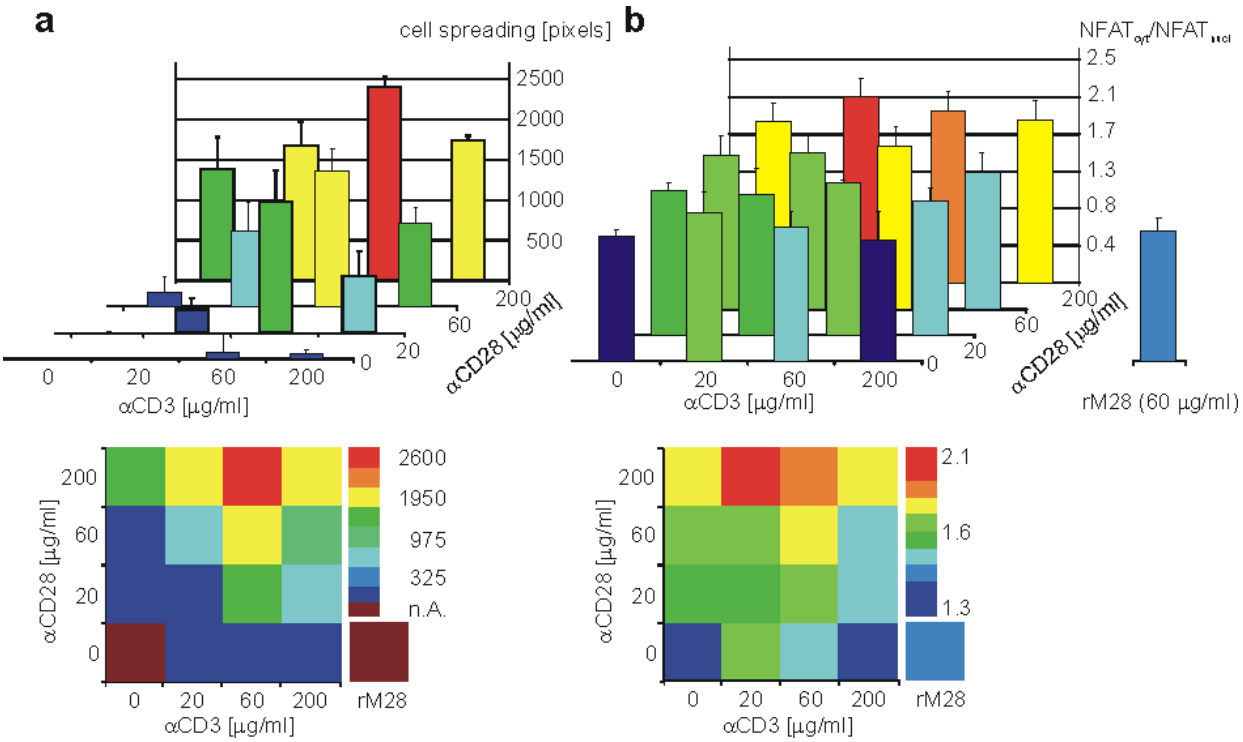

Figure 4.4 Cellular responses on an anti-CD3/anti-CD28 concentration matrix and on the supraagonistic single chain fragment rM28. (A) Cell spreading expressed by the average number of pixels covered per cell, with 1 pixel corresponding to 0.05 µm^2. (B) Nuclear NFAT translocation expressed by the average of the ratios of fluorescence in the nucleus and fluorescence in the cytoplasm for each cell. An increased translocation is reflected by a higher ratio. Top panels: bar graphs, error bars correspond to the mean deviation of 3 (translocation) and 2 (spreading) experiments. Bottom panels: The respective array depicted in a colour matrix, each coloured field corresponds to one spot in the microarray. The brown hue indicates that on this spot cell spreading could not be quantified. The data for the polylysine spot was included as a negative control.

4.3.3 Effects of small molecule inhibitors. Having established that the anti-CD3/anti-CD28 antibody microarray yielded a gradient of the cellular response over the whole concentration range, we next aimed at determining the effects of signalling inhibitors on this response profile. Pharmacological inhibitors are a frequently used tool for addressing the involvement of a specific enzyme in T cell signalling. However, specificity of these compounds is a general concern and most compounds inhibit several targets [138]. We intended to explore to which degree the matrix of stimuli would reveal functionally relevant differences between inhibitors, especially for those having the same primary target. The latter case reflects a typical situation in drug development, where a

screening of molecules in vitro produces several 'hits' inhibiting an enzyme, however, these hits may have different in vivo activities due to the inhibition of further secondary targets. The collection of inhibitors included established inhibitors of T cell signalling as well as compounds for which little information on specificity was available (See Fig.4.5 for an overview of inhibitor interferences in the T cell signalling network). Cytochalasin D inhibits actin polymerization [139] and thus the formation of stable T cell-APC contacts on anti-CD3-coated surfaces [118]. The Src family kinase inhibitor PP2 is a prototypical inhibitor of early CD3-dependent signalling with LCK as the primary target [110], while piceatannol inhibits ZAP-70 [140], but has also been reported to inhibit PKC [141]. Ro-31-8220 [142] and alsterpaullone [143] were both described as inhibitors of GSK-3, albeit with different activity profiles for the inhibition of further kinases [112; 144]. PD98059 acts an inhibitor of MAPK1 (= MEK1), by disrupting its activation via Raf or MEK kinase [145]. FK506 is an inhibitor of the NFAT activator calcineurin [146]. (For the PI3K inhibitor LY-294002 an inhibitory effect on T cell activation had been reported [147]. ML-3403 [148] and SB-203580 [149] have been described as highly potent inhibitors of the MAP kinase p38 with similar IC_{50} values for inhibition of LPS-dependent TNF release in human PBMCs (SB-203580, IC_{50} 0.6 μM; ML-3403, IC_{50} 0.2 μM) [148]. With respect to NFAT, p38 has been shown to play a dual role. First, the kinase phosphorylates the transcription factor thereby promoting nuclear export. Second, a p38-dependent induction of of NFATc expression leads to an overall activation of NFATc-dependent transcription [150]. The concentrations applied for the individual inhibitors were selected based on concentrations commonly used in the literature or on known IC_{50} values.

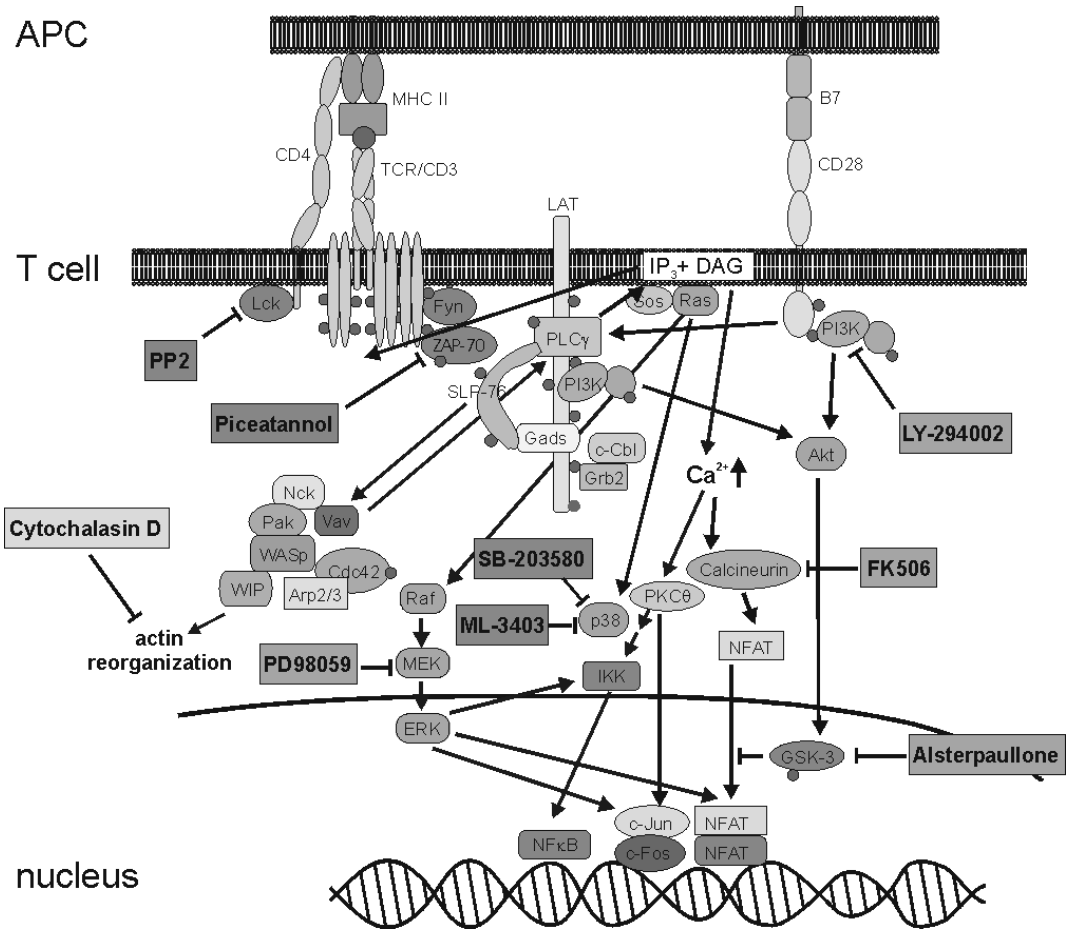

Figure 4.5 Schematic of T cell signalling and the principal targets of the inhibitors applied in this study. The scheme gives a simplified overview about the components involved.

In addition to the NFAT translocation and cell spreading, which represent a signal at a certain time point, an IL-2 ELISA was additionally performed in order to yield a quantitative signal integrated over time. For all inhibitors, except Ro-31822 we observed a clear inhibitory effect on anti-CD3/anti-CD28 dependent IL-2 secretion in the concentrations applied to the cellular microarrays (Fig. 4.6). As expected for a compound directly targeting actin, 10 µM cytochalasin D exerted a uniform inhibitory effect on cell spreading. In contrast, NFAT translocation was not affected (Fig. 4.7). This result correlates with findings, that cell spreading, but not the formation of signalling-active clusters is inhibited by cytochalasin D (Fig. 3.5). The LCK-inhibitor PP2, on the other hand, uniformly inhibited NFAT translocation, and weakly inhibited cell spreading at the 60 min time point. Previously, a pronounced effect of PP2 on cell spreading had been reported [118]. In fact, spreading was much more strongly inhibited by PP2 when cells were fixed after 10 min (Fig. 4.12), consistent with these earlier results. For piceatannol (10 µM), cell spreading was reduced for all combinations of stimulatory antibodies, while

NFAT translocation was more strongly reduced for spots containing anti-CD28. For the calcineurin-inhibitor FK506, we observed a strong inhibition of NFAT translocation. For alsterpaullone, as expected for a GSK-3 inhibitor, a potentiation of NFAT translocation was observed. Cell spreading was not affected. For Ro-31-8220 a strong fluorescence of the compound compromised an automated analysis of NFAT translocation. By eye, no effect could be detected. Ro-31-8220, with an IC_{50} of 6.8 nM for GSK-3 [142] was the only inhibitor analyzed in this study for which we could not detect a significant inhibition of CD3/CD28 dependent IL-2 expression (Fig. 4.6). For the PI3K inhibitor LY-294002, which acts upstream of GSK-3 and should act as an inhibitor of NFAT translocation, no strong effect on NFAT was observed. Surprisingly, the p38 kinase inhibitor ML-3403 exerted a pronounced concentration-dependent effect on NFAT translocation. At 1 μM a slight inhibitory effect on NFAT translocation was observed for spots containing only anti-CD28. With increasing concentration the inhibitory effect successively also affected spots containing a higher fraction of anti-CD3. The NFAT inhibition profile for 3 μM ML-3403 was similar to the one of 10 μM of the Syk/ZAP-70 inhibitor piceatannol. While for the second p38 inhibitor, SB-203580 only a slight inhibitory effect on NFAT translocation was present even at 30 μM, both p38 inhibitors inhibited IL-2 expression. The MEK inhibitor PD98059 induced a weak, but reproducible inhibitory effect on NFAT translocation.

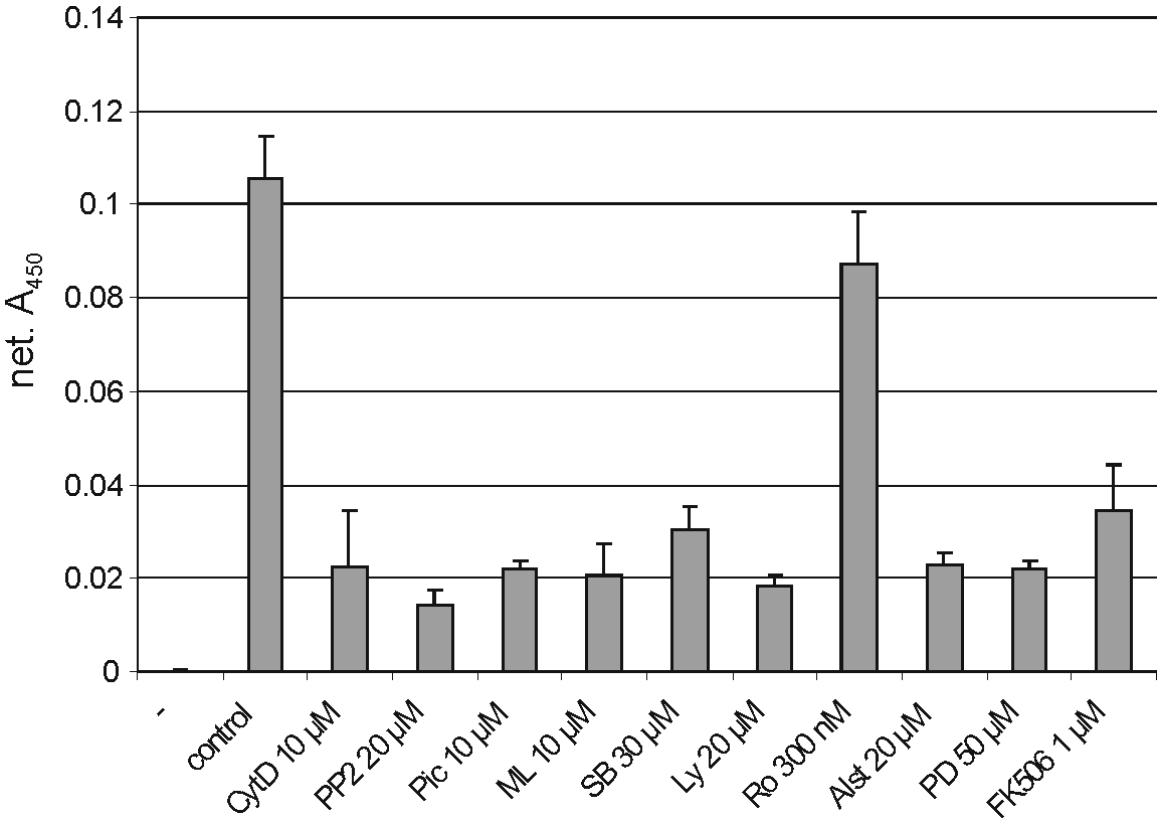

Figure 4.6 ELISA quantitation of the IL-2 expression of Jurkat cells that were stimulated with plate-bound anti-CD3 + anti-CD28 for 16 h. The A_{450} value corrected by that of the unstimulated control is given. Cell vitality after inhibitor incubation was controlled by an MTT assay.

4.3.4 Functional characterization of the supraagonistic antibody. The recombinant supraagonistic anti-CD28 antibody rM28 elicits a strong T cell activation in the absence of the primary CD3-dependent signal. We employed the antibody microarray to determine to which degree cellular signals elicited by the supraagonistic antibody rM28 combined features of CD3- and CD28-dependent signalling. rM28 consists only of the variable regions of heavy and light chains for each binding specificity, i. e. anti-CD28 and anti-MAPG and lacks all constant immunoglobulin domains. For this reason, this protein was poorly detectable by the secondary antibody used for surface staining. In our case, the MAPG-directed specificity was irrelevant. Quantification of cell spreading by the automated protocol was therefore impossible. Optical evaluation indicated that the cells were clearly spread after 60 min. Only little NFAT translocation was observed compared to the anti-CD28 clone 9.3. Nevertheless, the effects of the inhibitors on NFAT translocation corresponded to the effects of these compounds exerted on spots with high anti-CD28 content (Fig. 4.7). In no case was the effect similar to a spot with an excess in anti-CD3.

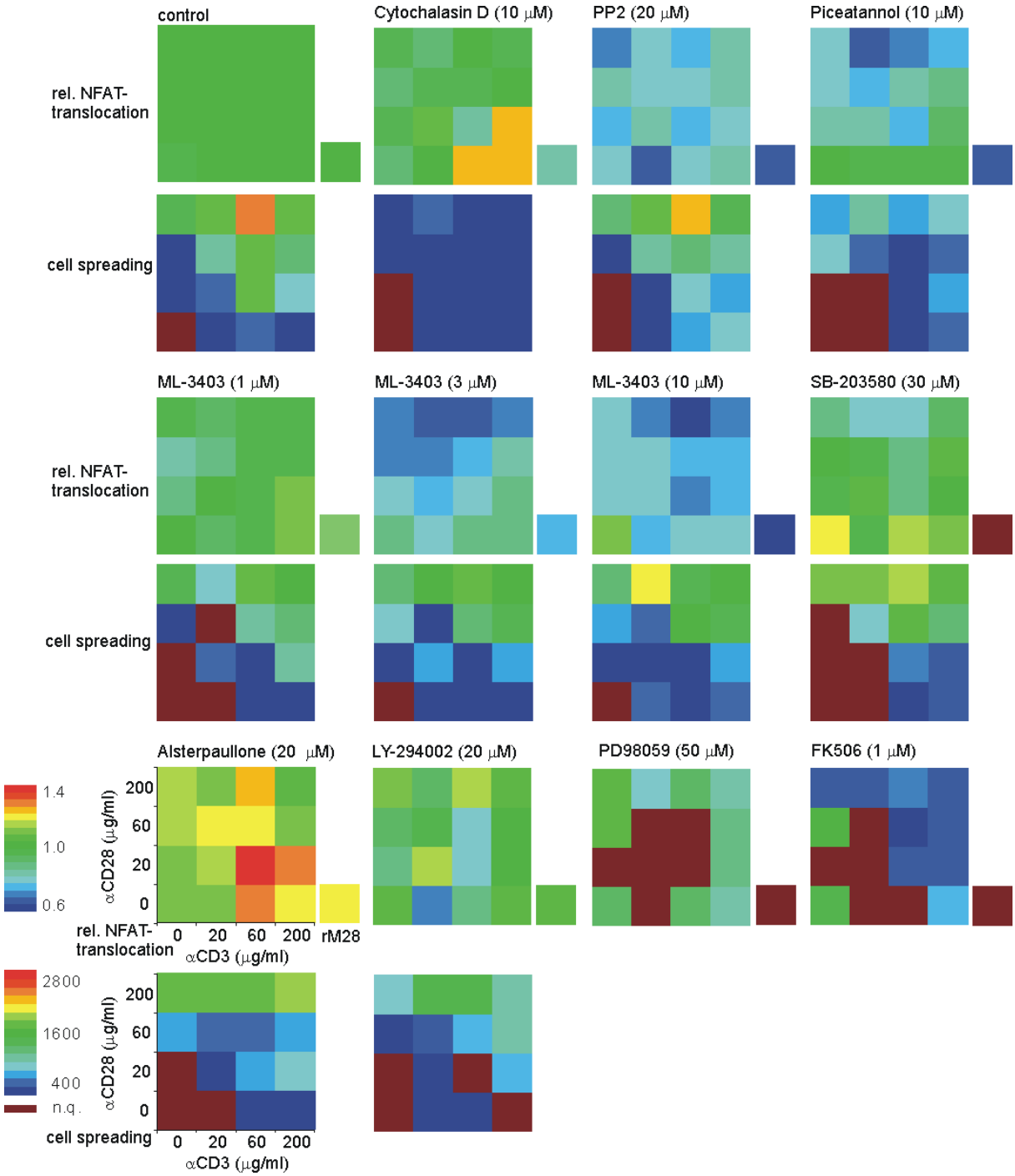

Figure 4.7 Response profiles in the presence of inhibitors. NFAT translocation, the ratio of nuclear versus cytoplasmic fluorescence in the presence of inhibitor was divided by the ratio in the absence of inhibitor. Blue hues represent an inhibitory effect, yellow and red hues an activating effect on NFAT translocation. For spreading, absolute values instead of ratios inhibited/non-inhibited are shown. The figure legends are the same as for Fig. 4.4.

Whereas different intensities of stimuli influence cell spreading and NFAT translocation of untreated Jurkat cells in the same way, for the cell population on one spot NFAT translocation and cell spreading are not correlated (Fig. 4.8).

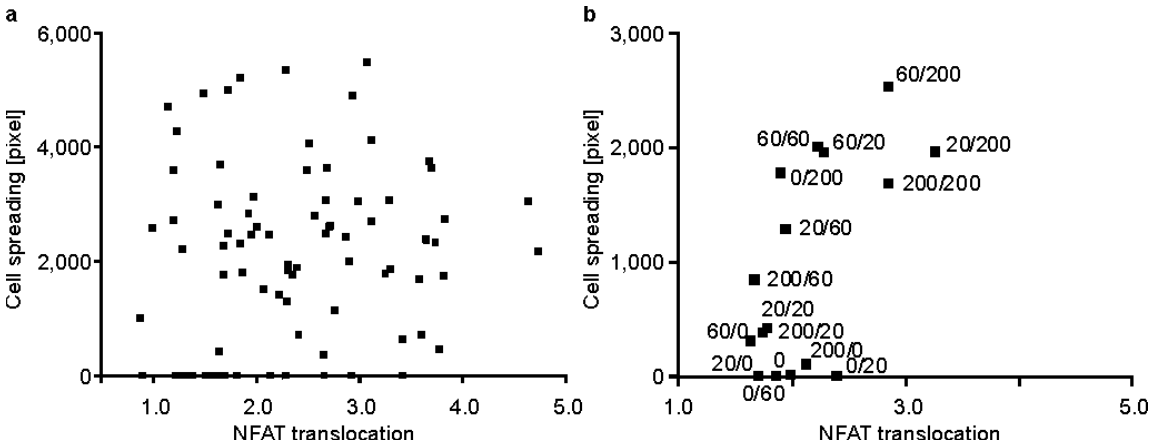

Figure 4.8 Correlation between cell spreading and NFAT translocation. (A) Cell spreading plotted against NFAT translocation for a population on the spot containing 200 mg/ml of anti-CD3 and anti-CD28 each. (B) Cell spreading plotted against NFAT translocation for the mean of cell populations on different peptide spots of a representative array, with the first number representing the anti-CD3 concentration immobilized on the spot, and the second number the anti-CD28 concentration. The x-axis represents the NFAT fluorescence in the nucleus compared to one in the cytoplasm

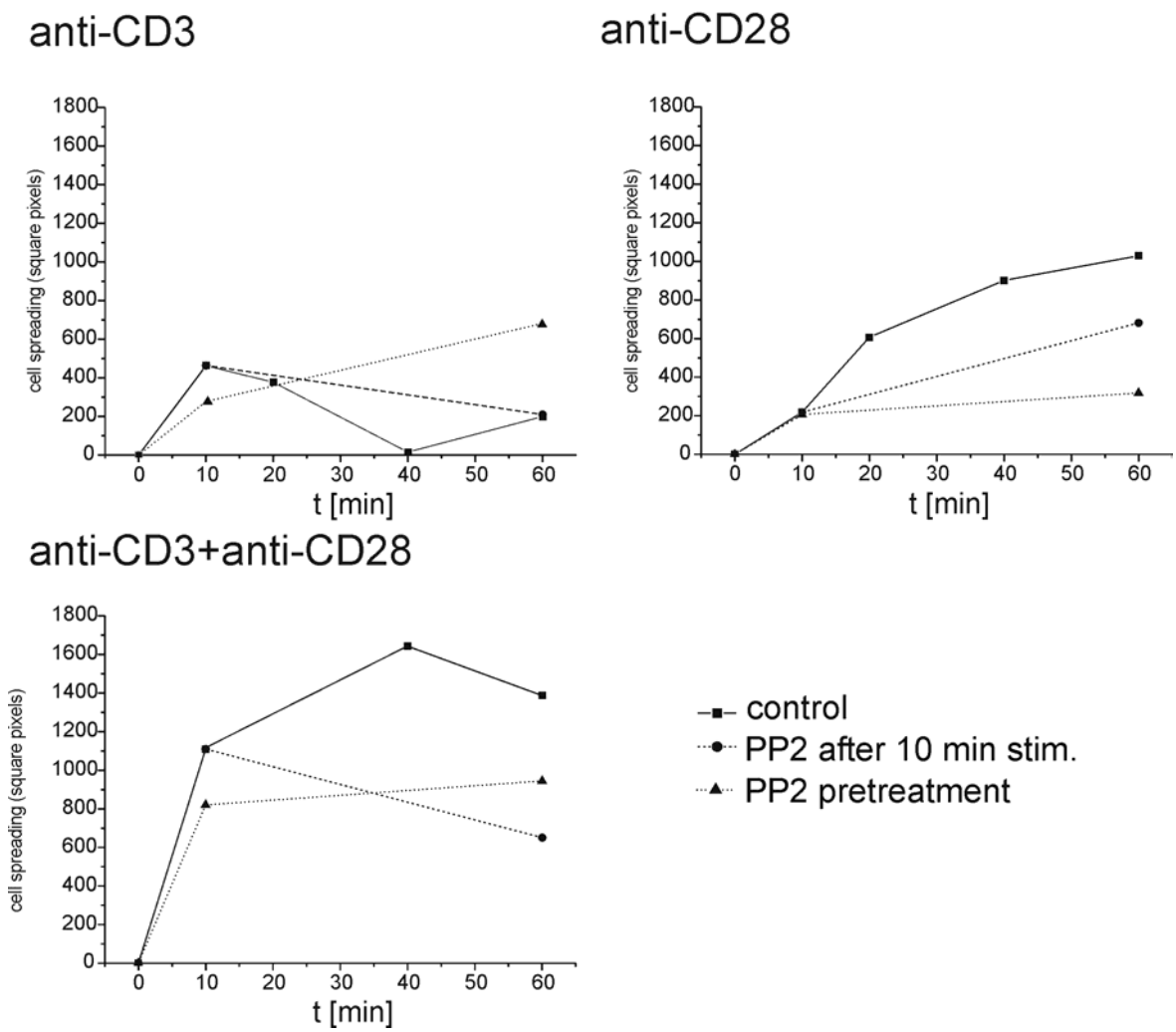

Figure 4.9 Time dependent changes in the spreading of Jurkat T cells under the influence of 20 μM of the SFK inhibitor PP2. Single anti-CD3 and anti-CD28 antibodies were spotted at a concentration of 200 μg/ml each, the antibody mixture contained 60 μg/ml anti-CD3 and 200 μg/ml anti-CD28. Cells were left untreated (black line) or either pretreated with PP2 (dotted line), or treated after 10 min after the initiation of contact formation (dashed line). 1 pixel corresponds to 0.05 μm^2. The data are from one representative experiment.

4.3.5 Analysis of protein clustering by confocal microscopy. With the NFAT translocation being a relatively late readout for T cell activation, it was our goal to extend the application of microarrays to further and earlier readouts for signalling. For this purpose, we analyzed the CD3-dependent recruitment of different proteins involved in T cell activation to the site of contact formation using confocal microscopy. In Jurkat cells stimulated by immobilized anti-CD3 antibodies for 10 minutes, we observed intense clusters of the phosphoproteins LAT (phosphorylated on tyrosine 226) and PLCγ (phosphorylated on tyrosine 783) as well as for the GADS protein. Clusters of these proteins localized mainly to the outer rims of the cell at the 10 min time point. The observed clustering of the proteins is in accordance with findings by the peptide microarray experiments on the molecular level, which shows a strong and parallel tendency in the association of LAT, PLCγ and GADS to signalling complexes upon CD3 stimulation or pervanadate stimulation (see Figs 7.3 and 7.5). A weak protein clustering was observed for the proteins GRB2, ZAP-70, LCK and SHP2 and PI3K under these conditions. In contrast to the other proteins, PI3K clusters localized strongly to the centre of the cell. Upon CD3 engagement, GRB2 also strongly localizes to a perinuclear compartment, which may be involved in cytoskeletal reorganization, and Gab2 also shows nuclear localization for a part of the cells. The partially fibrous distribution of Nck and Vav may indicate an association with the cytoskeletal components. As an enzyme which is partially constitutively associated with the plasma membrane, SHP-1 shows a membrane-associated staining.

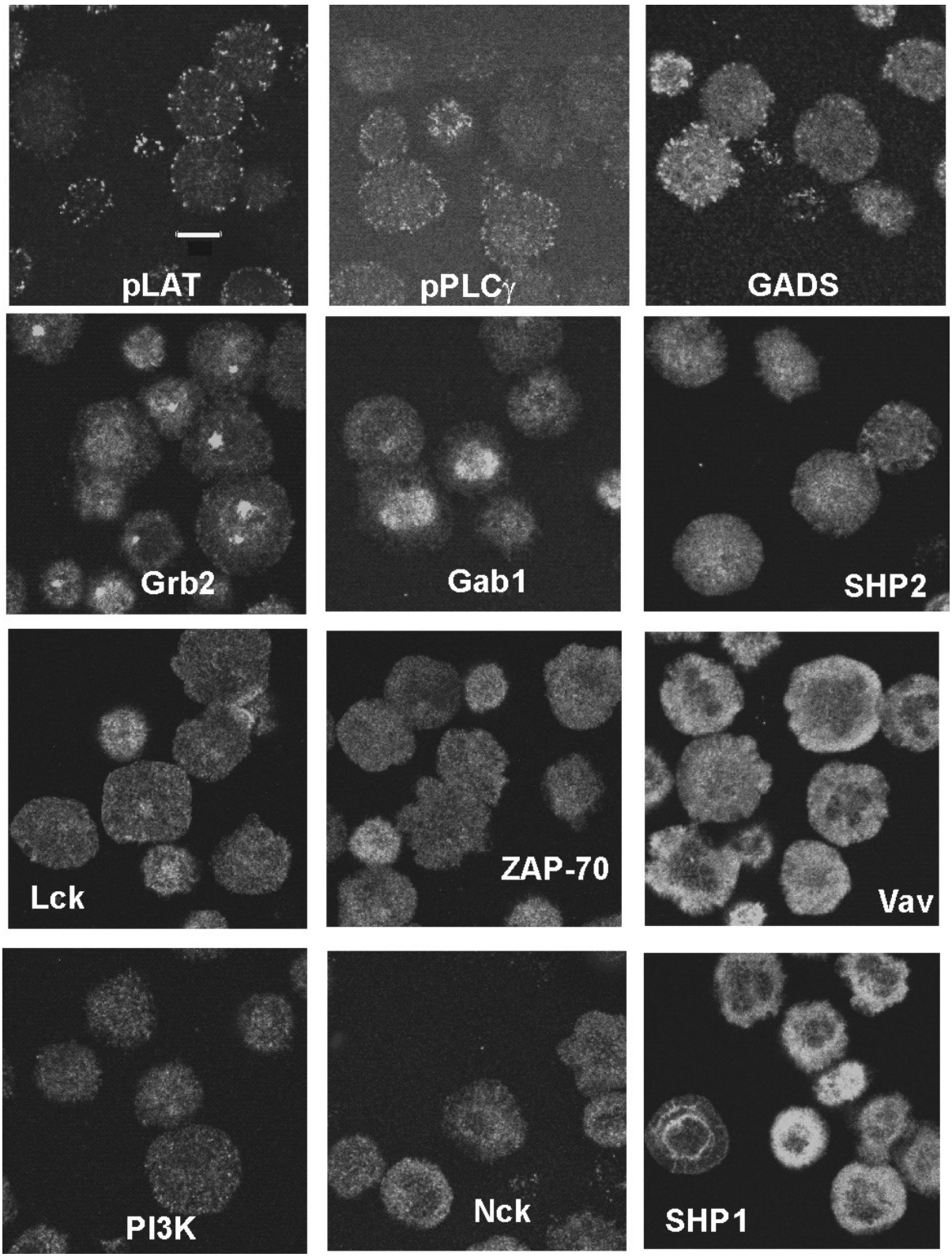

Figure 4.10 For the analysis of TCR/CD3-dependent protein clustering Jurkat cells were exposed to anti-CD3 coated surface for 10 min. White represents the immunostaining against the represented antigen with 2 µg/ml of the respective antibody (see table 8.1). The white bar corresponds to 10 µm for all images.

4.3.6 Quantification of protein clustering. The activation of PLCγ is mediated bythe TCR-induced recruitment into the LAT signalosome on the one hand, and by PIP3-dependent phosphorylation of tyrosine 783 by Itk on the other hand, and thus might be involved in the integration of stimulatory signals from the TCR and the CD28 coreceptor. Due to the central relevance for the spreading of the activation signal via calcium, the activation of PLCγ is a central event in T cell activation. Due to this relevant function as an integrator of CD3 and CD28-dependent signalling, we selected the recruitment of PLCγ phosphorylated on tyrosine 783 to the site of surface antibody engagement as an activation marker. Protein clustering was analyzed by confocal microscopy using the 10 min time point for different stimuli. Compared to anti-CD3 stimulation, both cell spreading and clustering of phospho-PLCγ was weaker in anti-CD28 stimulated cells at that time point (Fig. 4.11). Also, clustering and phosphorylation of PLCγ and cell spreading were strongly reduced in cells pretreated with 20 μM of the SFK inhibitor PP2. In contrast, the actin inhibitor cytochalasin D completely abrogated cell spreading, but in some cases very intensive phospho-PLCγ staining at the areas of antibody engagement was visible, indicating no inhibitory effect of the actin inhibitor on PLCγ activation.

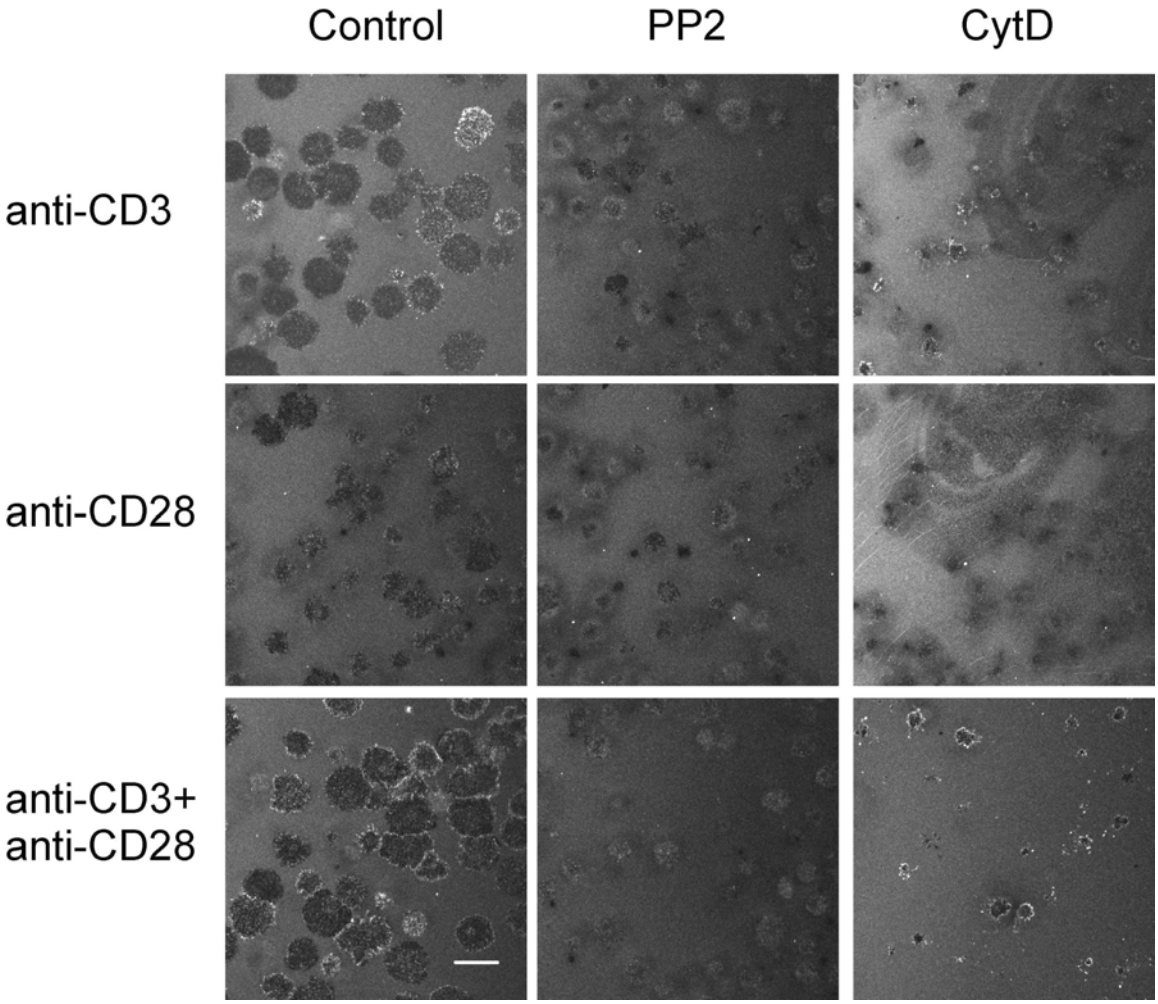

Figure 4.11 Overview of the effects of signalling inhibitors on the spreading and phospho-PLCγ clustering (light grey) of Jurkat cells stimulated on different surfaces for 10 min. The surface antibody was detected by staining with a secondary antibody (dark grey), resulting in a dark patch at sites of cell attachment. The white scale bar represents 20 μm.

Image quantitation shows that CD28 coengagement augments the anti-CD3 induced phospho-PLCγ staining per area (Fig. 4.12). The effects of anti-CD3 engagement are completely counteracted by the inhibitor of TCR-dependent signalling, PP2. In contrast, the supporting tendency of the effect of CD28 coengagement on PLCγ activation seems to be reproduced even under the conditions of impaired cytoskeletal functions. The effects of both inhibitors on PLCγ recruitment correspond to those observed for the NFAT translocation.

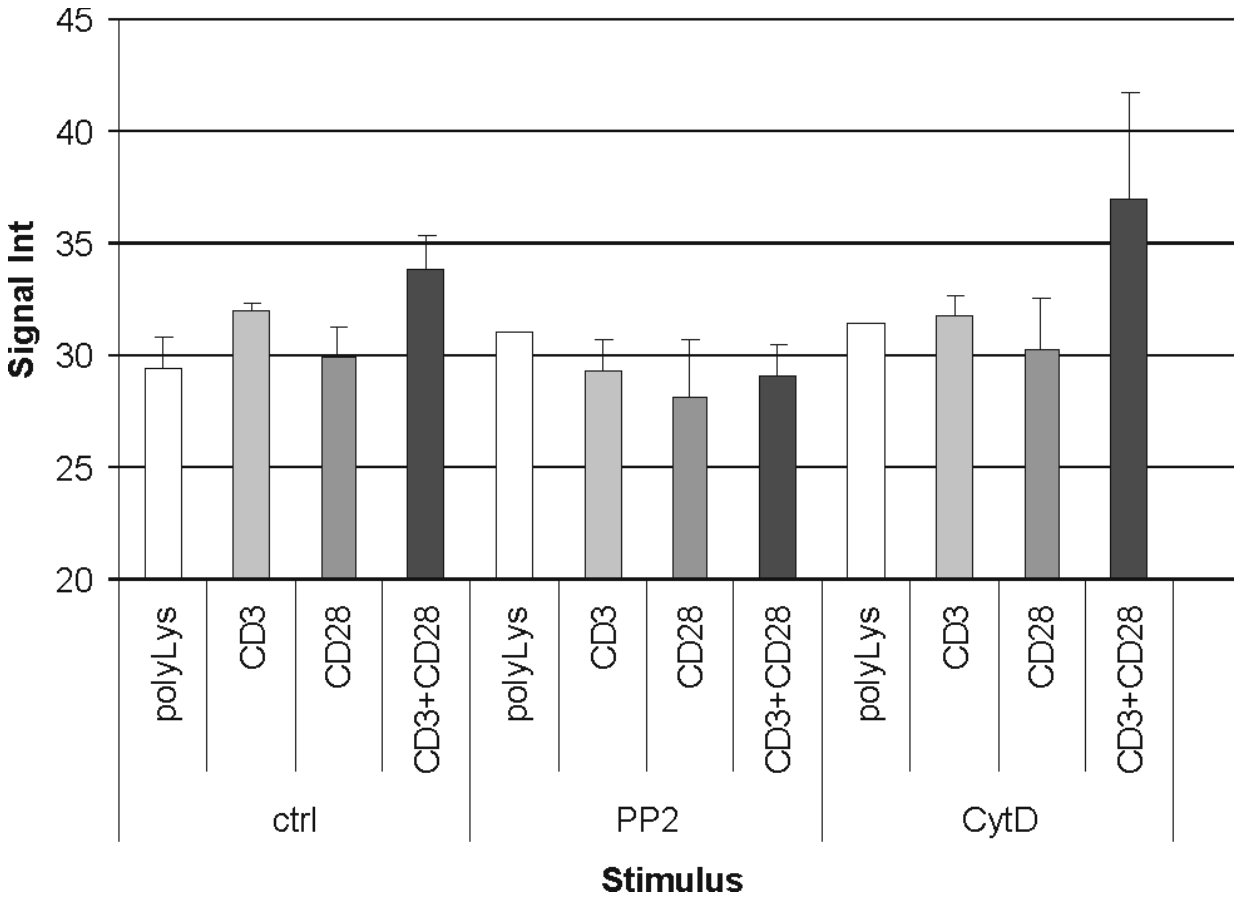

Figure 4.12 Quantification of the density per area of the immunostaining against PLCγ phosphorylated on pY783. The contact site of Jurkat cells with different stimulatory surfaces after 10 min of contact was imaged by confocal microscopy. Before stimulation, cells were treated with PP2 (20 μM), Cytochalasin D (10 μM), or the respective DMSO control. The threshold for protein clusters was adjusted manually for each set of experiments. The figure represents the combined and normalized data from two experiments.

4.4 Discussion

In order to understand the activation of cells, it is required to understand how different signals are integrated into a cellular response. The cellular antibody microarrays provide the means to systematically probe different combinations of stimuli in a multiwell format. With one array per well an order of magnitude more data is generated for a limited number of cells – in our case typically 100,000 per well. For combinations of different concentrations of CD3- and CD28-directed stimuli a gradual response matrix for the activation of T cells was obtained (Fig. 4.4). This demonstrates that for T cell activation, unlike e. g. for epidermal growth factor-dependent signalling [151], the cellular response strongly depends on the strength of the signalling activities. Crosslinking of CD28 in addition to anti-CD3 stimulation induced not only a higher protein tyrosine phosphorylation, for example for PLCγ1 at the contact surface, but also enhanced the persistence of cell spreading.

4.4.1 Inhibitor effects on cell spreading and NFAT translocation. NFAT translocation was affected negatively by PP2, ML-3403 and FK-506 and positively by alsterpaullone, while for all three compounds cell spreading remained nearly unchanged at the 60 min time point. PP2 strongly delayed the kinetics of cell spreading, leading to a strong inhibitory effect at early time points (Fig. 4.7, Fig. 4.11), and only a weak effect at later time points (Fig. 4.9, 4.11), which corresponds to published observations [118]. For the Jurkat-derived LCK-inactive JCaM 1.6 cells, cell spreading and NFAT translocation on all stimuli were also strongly inhibited but not fully abolished (not shown), again indicating partial compensation for the loss of LCK activity by other enzymes. Piceatannol clearly reduced cell spreading also at later time points. In accordance with its key role in the initiation of T cell receptor-dependent signalling, the inhibition of LCK by PP2 strongly affected NFAT translocation for all stimuli. At the concentrations of 10 μM piceatannol and 20 μM PP2, similar levels of inhibition for the anti-CD3/anti-CD28 containing spots were obtained. Though both inhibitors of the upstream kinase activities strongly inhibit CD3+CD28-dependent NFAT translocation and IL-2 expression, their response profiles (Fig. 4.7) show clear differences for CD3 stimulation alone, which were also present at higher concentrations of piceatannol (50 μM, not shown). On the spot

containing only polylysine, PP2 also reduced NFAT translocation, indicative of some basal level of NFAT translocation, while piceatannol was without effect.

While the PI3K inhibitor LY-294002 inhibits IL-2 expression, its lack of effect on NFAT translocation might be due to the fact that Jurkat cells do not express the phosphatase PTEN that antagonises the action of PI3K [152]. Alsterpaullone also inhibits LCK [112], in addition to inhibiting GSK-3. Concerning TCR-dependent NFAT translocation, the inhibitory effect of alsterpaullone on LCK was obviously compensated by the stimulatory activity on GSK-3 inhibition. In contrast, the IL-2 expression is inbibited by alsterpaullone, suggesting that its stimulatory effect on NFAT translocation is irrelevant for induction of IL-2 expression.As the GSK-3 inhibitor Ro 31-8220 does not inhibit IL-2 expression, we assume that GSK-3 inhibition alone exerts no effect on IL-2 expression.

The comparison of the activities of ML-3403 and SB-203580 illustrates the potential of the stimulatory cellular microarray in the functional profiling of inhibitors. The pair of inhibitors was selected as p38 kinase inhibitors and both inhibited IL-2 expression, but exerted very different effects on NFAT translocation. At concentrations higher than 1 μM ML-3403 had a pronounced inhibitory effect on NFAT translocation while not affecting cell spreading. In contrast, for SB-203580 (30 μM) only a weak inhibitory effect was observed. Of the 15 kinases against which ML-3403 had been screened, only for JNKs was a considerable inhibitory activity of ML-3403 (10 μM) observed, while the in vitro GSK-3 activity was enhanced by 30 ± 9% (S. Laufer, personal communication). SB-203580 was screened against a panel of 119 kinases [138]. For this reason, one has to assume that for ML-3403 the observed activity should be due either to GSK-3 stimulation or to inhibition of a kinase not included in this large scale screen.

Fig.4.8 a shows that, on the single cell level, NFAT translocation and cell spreading are not correlated. This observation is in accordance with the effects of the actin inhibitor cytochalasin D, which completely inhibited cell spreading but had no significant effects on NFAT translocation (Fig. 4.7) and PLCγ activation (Fig 4.12) considering the single-cell level. On the other hand, cytochalasin D inhibited IL-2 expression. This observation is consistent with reports that the disruption of the contact between the CD3 and the actin cytoskeleton does not affect phosphorylation cascades, which eventually lead to NFAT

translocation, but [153]. Thus, the integrity of the actin cytoskeleton a prerequisite for the integration of TCR stimulation and CD28 costimulation into signalling leading to IL-2 expression [154]

In summary, very similar inhibitory profiles were obtained for cells exposed to anti-CD28 alone or a combination of anti-CD3 and anti-CD28. These data illustrate that pharmacologically, CD28-dependent signalling is very similar to CD3/CD28-dependent signalling, but different to CD3-dependent signalling. Consistently, CD28 initiated different cellular response kinetics than CD3. In early signalling (first minutes), engagement of CD3 is therefore a prerequisite for CD28 to exert its auxiliary role, for prolonged and strong engagement CD28 also acts as an independent signalling unit, at least with respect to cell spreading and NFAT translocation. For ML-3403 the relative cellular response was affected more strongly on spots with a high density of stimuli. The higher the inhibitor concentration, the lower was the concentration of stimuli at which an effect could be observed. However, one should also note that for the spots with higher antibody densities, inhibition did not increase any further. As a consequence, even at high inhibitor concentrations, activation at these spots was still higher than at spots with little stimuli (Fig. 4.13), an observation with major relevance for the action of immunosuppressants [130]. These data illustrate the capability of the cellular antibody microarrays to reveal the environment dependence of drug action, a phenomenon that is mostly neglected in classical cellular screens.

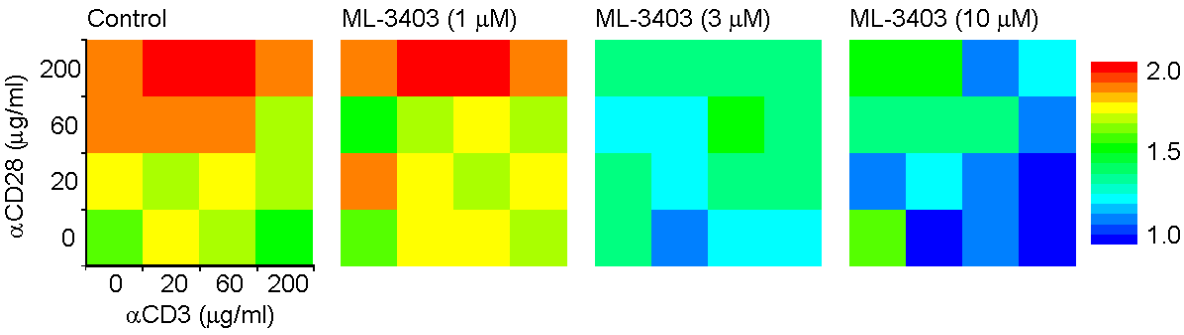

Figure 4.13 Dependence of NFAT translocation on ML-3403 concentration. Shown are absolute values for nuclear versus cytoplasmic fluorescence. The data represent the mean of three independent experiments. The data shown for the control corresponds to the data given in Fig. 4.4, albeit with a different scaling for the look-up table.

4.4.2 Functional profiling of a supraagonistic antibody. The supraagonistic anti-CD28 antibody rM28 induced only a low NFAT translocation. It is not fully clear, whether this observation is a functional characteristic of this molecule or due to a lower density of rM28 binding sites on the array than for anti-CD28. With a molecular weight of 55 kDa and one CD28 binding site per molecule, the concentration of 50 µg/ml used for spotting corresponds to a concentration of 70 µg/ml of an IgG, a concentration at which for anti-CD28 a stronger NFAT translocation was observed. Moreover, in spite of weak NFAT translocation, the inhibitory effects exerted by the different compounds corresponded to the ones observed for spots with high anti-CD28 and anti-CD28/anti-CD3 densities. The pronounced inhibitory effects in the presence of little translocation indicate that even though rM28 stimulates qualitatively similar signalling pathways, functional differences exist. When tested in a conventional ELISA, rM28 induced a significantly higher IL-2 expression than anti-CD28 (Fig. 4.1). Further analyses will be required to determine the basis for the strong IL-2 expression in the presence of weak NFAT translocation. It has been demonstrated that CD28 upregulates IL-2 expression via two pathways: A PI3K-dependent pathway leading to an increase in gene expression and a second one inducing the stabilization of the IL-2 mRNA [83].

The cellular antibody microarray adds a further dimension to functional cellular analyses in T cell immunology. The simultaneous testing of many different stimuli in combination with two readouts, i. e. cell spreading and NFAT translocation, provides abundant information on the interplay of stimuli in generating a cellular response. In addition, the technology is readily compatible with further multidimensional readouts such as the testing for the translocation of other transcription factors or for the phosphorylation of a large number of signalling proteins [155;156]. Compared to ELISA experiments integrating signal intensities over time, cellular microarrays with microscopical readouts allow signal quantification at different, defined time points in a parallel manner. In drug development the response profiles for drug candidates reveal differences in the target spectrum of these compounds. By exposing cells to many different environments the technique yields important information on the range of potential activities of a compound that may be elicited in the physiological context. Therefore the stimulatory microarrays should assist in the selection of promising compounds in preclinical drug development.

Our analyses confirm that the specificity of small molecule inhibitors is indeed a concern when using these compounds for the analysis of signalling pathways. Given highly selective compounds, including siRNA for the down-modulation of protein expression, the cellular antibody microarrays may provide information on the role of a specific protein in the interplay of different signalling pathways.

5. T Cell stimulation using microstructured surfaces

5.1 Introduction

Previous experiments performed in this thesis concerning CD3 and CD28 costimulation analyzed the immobilizations of mixed antibodies. Both the TCR/CD3 complex [84] and the CD28 coreceptor [157] have been described to reside in special membrane areas described as "lipid rafts", or GEMs, with anti-CD28 facilitating the clustering of lipid rafts at the sites of TCR engagement [84]. This observation raises the question, if a spatial proximity of the stimuli and costimuli is necessary for optimal TCR-dependent stimulation. In order to analyze the interplay of CD3 stimulation and CD28 costimulation in the respect of spatial engagement, we tested the effect of spatially distinct stimuli on cell activation. For the microstructured manufacturing of stimulatory surfaces, we introduced the method of microcontact printing using polydimethylsiloxane (PDMS)-stamps onto glass slides. The stimulation of cells with microstructured has the potential for the analysis of cells in contact with spatially defined arrays of stimuli systems, such as the immunological synapse. Also, it allows the exposition of cells to stimuli of different sizes, geometries and intensities.

All cellular experiments described in this section were performed by the author. The PDMS stamps were produced by Günter Roth and Alexander Ganser, and the stimulatory antibodies were kind gifts from Dr. Ludger Grosse-Hovest, Prof. Dr. Gundram Jung and Alexander Ganser.

5.2 Results and Discussion

PDMS stamping allows a spatially confined transfer of proteins to glass surfaces. The glass areas printed with protein (Fig. 5.1, top left) are blocked against attachment of further protein (Fig. 5.1, top right). Image inspection also shows also that no blurring of border occurs during also during longer incubation times and protein remains associated to the stamped area also during following washing, incubation and staining steps.

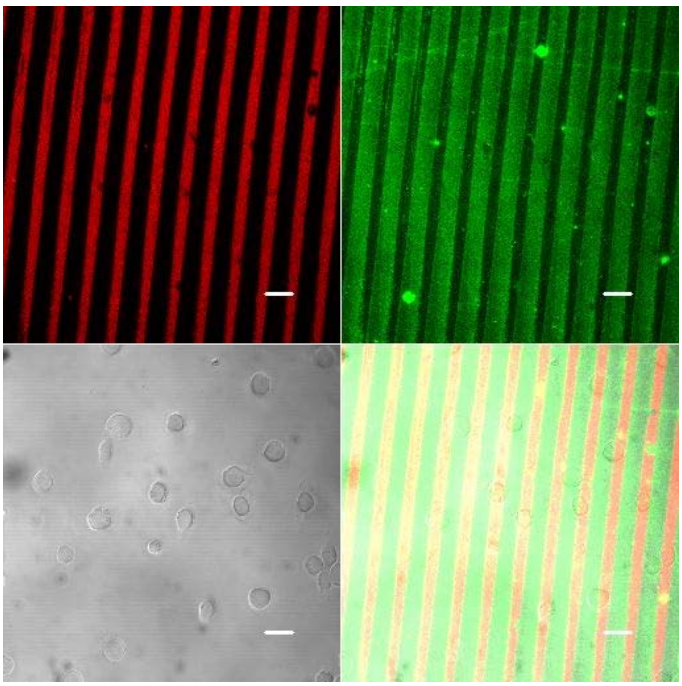

Figure 5.1 Determination of the spatial separation of printed and overlayed stimulatory antibodies. A mixture of 100 µg/ml anti-CD3 antibody and 15 µg/ml Alexa 633-labelled goat anti-rabbit antibody (top left) was printed by PDMS stamps to a glass surface. Subsequently, the glass was overlayed with 15 µg/ml Alexa 488-labelled goat anti-rabbit antibody (top right), and incubated with Jurkat cells (transmission chanel, bottom left). The spectral properties of the antibody pair for visualization was selected to minimize quenching, and thus to maximize sensitivity for the detection of overlayed antibody. The white bar corresponds to 20 µm.

5.2.1 Actin cytoskeletal rearrangements. Fluorescence microscopy indicates that printed stimuli are able to induce the specific attachment of cells (Figs 5.1 and 5.2). Phalloidin staining of filamentous actin shows that CD3 engagement initiates local actin polymerization to a higher degree than CD28 (see Fig. 8.2). The effects of local anti-CD3 stimulation on global actin reorganization are limited. This observation corresponds to findings that stimulation on an anti-CD3 surface leads to cell spreading mediated by widespread actin polymerization [109], while anti-CD28 coated surfaces induces the formation of local "mikrospikes" [135].

5.2.2 Analysis of influences of local stimulation on local and global protein phosphorylation. With tyrosine phosphorylation representing an essential step in the generation of a T cell response, it was our goal to find out about the local and global effects of spatially distinct CD3 and CD28 engagement on the formation of phosphotyrosine-rich signalling clusters. When the surface outside the stamped area was

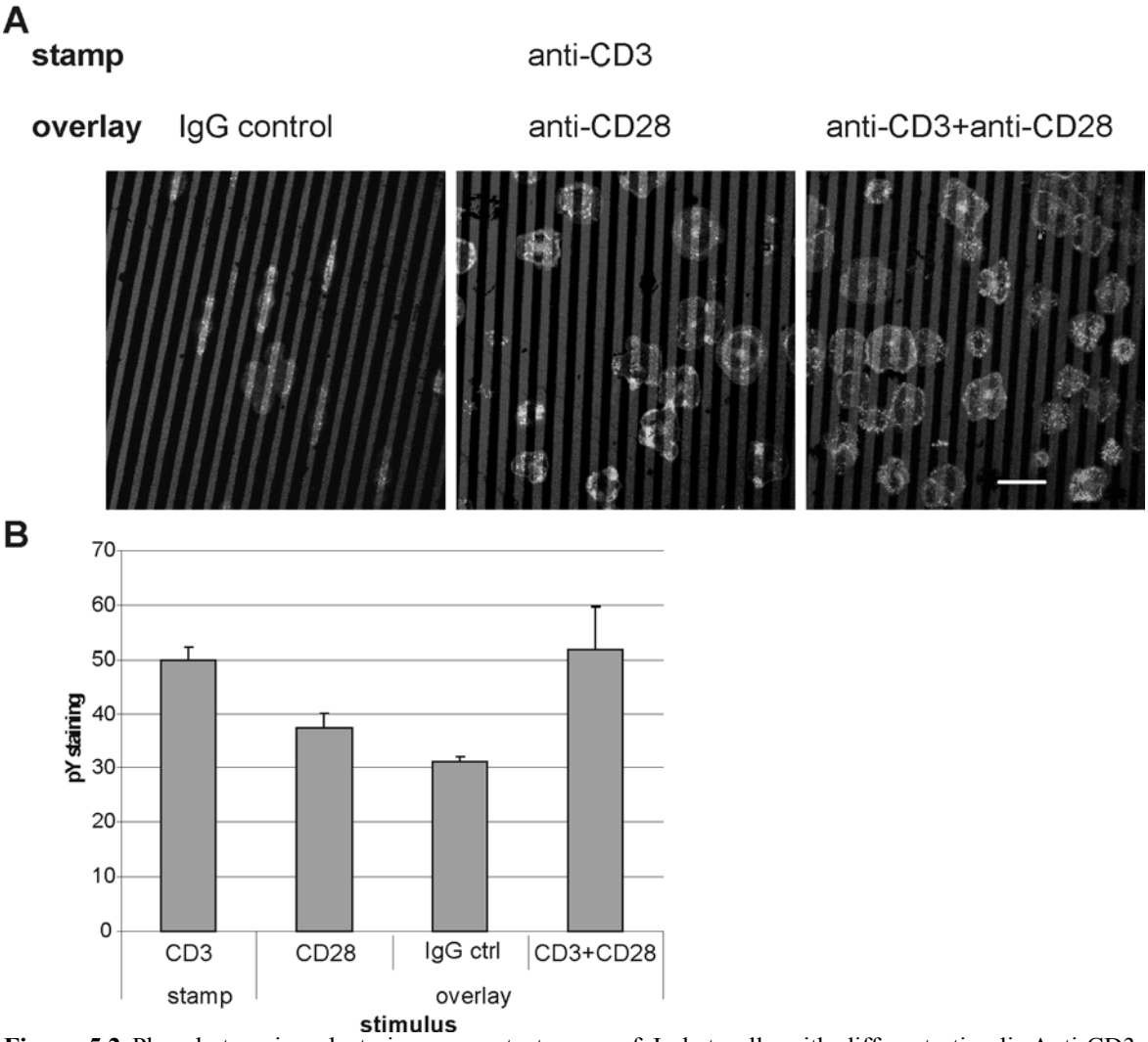

Figure 5.2 Phosphotyrosine clustering on contact areas of Jurkat cells with different stimuli. Anti-CD3 antibodies (100 μg/ml) were stamped to glass slides, which then were overlayed with IgG2a control antibodies, anti-CD28 or anti-CD28 (with a total concentration of 15 μg/ml). Jurkat cells were stimulated on the microstructured surfaces for 10 min. The localization of tyrosine-phosphorylated proteins on the plane of surface contact was analyzed by staining with a Zenon-Alexa 633 labelled anti-pY antibody and confocal microscopy. A) Fluorescent images, with the grey lines representing the stamped antibodies B) Quantification of pY staining on different areas (combined from three experiments). The white bar corresponds to 20 μm.

blocked with non-binding control antibodies, cells established only firm contacts at sites of stimulatory antibody engagement, leading to a "catamaran shape". Intracellular tyrosine phosphorylation depends on the type of the stimulus. Anti-CD3 engagement induced higher phosphorylation than anti-CD28 engagement (Fig.5.2), This was also the case for the direct comparison of stamped antibodies. Contact of Jurkat cells with surfaces and areas functionalized with a mixture of anti-CD3 and anti-CD28 antibodies resulted in a stronger pY clustering than anti-CD3 areas (Fig. 5.2).

This result demonstrates that, while anti-CD28 stimulation induces only a very weak tyrosine phosphorylation, accounting for an additive effect on simultaneous anti-CD3 engagement. A possible mechanism for this is the CD28-mediated activation of PI3K, which is involved in the phosphorylation and activation of PLCγ1 (see introduction, compare Fig. 4.12). The first question was, whether a proximal, but spatially distinct engagement of CD3 and CD28, possibly within one lipid raft, initiated an enhanced tyrosine phosphorylation. Spatially separated engagement of stimuli occurs on the CD3 borderlines between surfaces functionalized with different antibodies. In many cases, an enhanced localization of pY-rich clusters was observed on the border-proximal anti-CD3 functionalized area (see Fig. 5.3). However, image quantification did not yield a significant result, possibly because the direct contact area is relatively small compared to the whole area of cell contact.

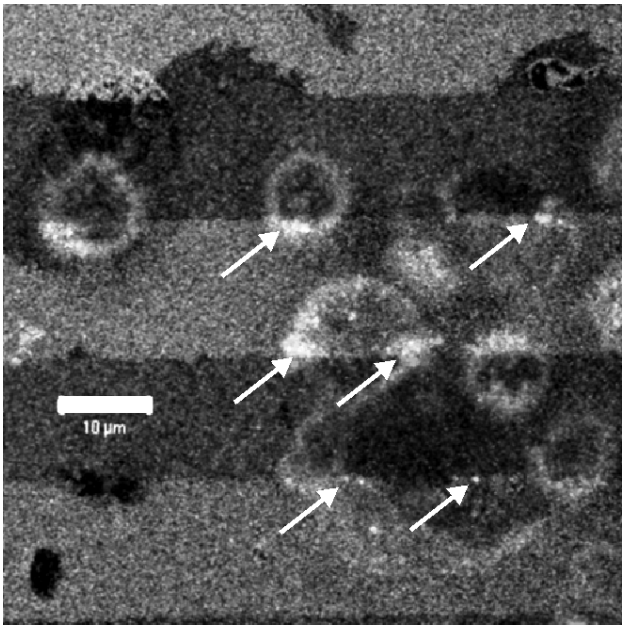

Figure 5.3 Confocal image indicating enhanced phosphotyrosine clustering (white, indicated by arrows) at the borders between stamped surfaces of anti-CD3 (middle grey) and anti-CD28 generated by overlay (dark grey). The white bar represents 10 µm.

This result demonstrates that, while anti-CD28 stimulation induces only a very weak tyrosine phosphorylation, accounting for an additive effect on simultaneous anti-CD3 engagement. A possible mechanism for this is the CD28-mediated activation of PI3K, which is involved in the phosphorylation and activation of PLCγ1 (see introduction, compare Fig. 4.12). The first question was, whether a proximal, but spatially distinct engagement of CD3 and CD28, possibly within one lipid raft, initiated an enhanced tyrosine phosphorylation. Spatially separated engagement of stimuli occurs on the CD3 borderlines between surfaces functionalized with different antibodies. In many cases, an

enhanced localization of pY-rich clusters was observed on the border-proximal anti-CD3 functionalized area (see Fig. 5.3). However, image quantification did not yield a significant result, possibly because the direct contact area is relatively small compared to the whole area of cell contact.

The second question was, whether the local engagement of CD3 quantitatively affected the tyrosine phosphorylation induced by contact with anti-CD28 surfaces in *trans*, such as by the means of diffusible factors. In order to test this question, we stamped mixtures of anti-CD3 antibodies and IgG2a isotype control antibodies with a total antibody concentration of 100 µg/ml. The stamped antibodies were overlayed with 15 µg/ml anti-CD28, and analyzed for the effect on tyrosine phosphorylation at the cell/antibody contact surface for the total area of each stimulus. Data were analyzed in a similar manner as depicted in Fig. 8.3.

We observed a strong dependence of tyrosine phosphorylation on the intensity of anti-CD3 engagement with signal saturation occurring at concentrations higher than 30 µg/ml. In contrast, on areas with CD28 engagement, the induced phosphorylation was only marginally higher than on unfunctionalized areas (Fig. 5.4). This suggests that anti-CD3 engagement does not have intense effects on areas of only anti-CD28 engagement. This corresponds with results, that, in contrast to engagement of CD3 and CD28 in the immunological synapse, anti-CD28 engagement outside the immunological synapse only causes indirect effects leading to IL-2 expression by enhancing IL-2 mRNA stability [158].

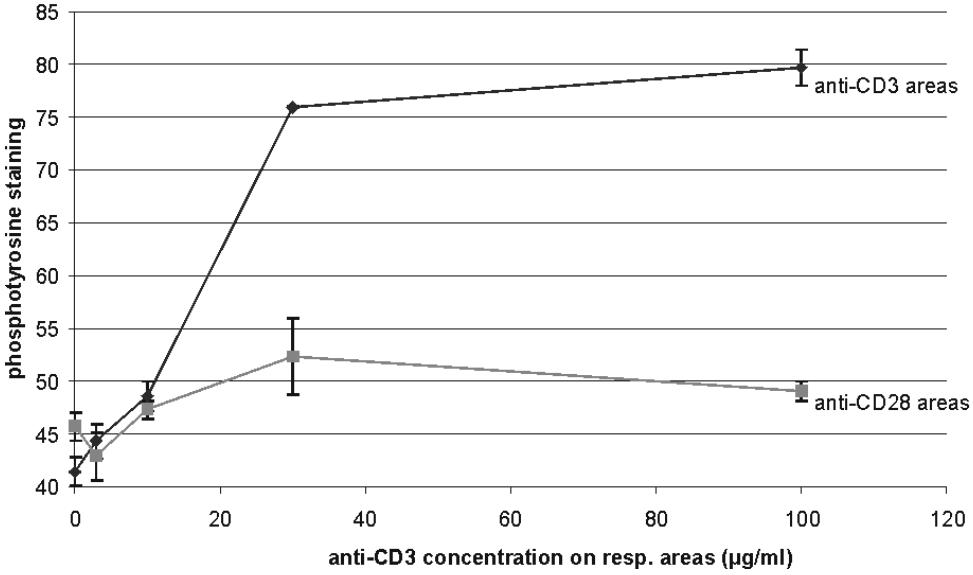

Figure 5.4 Effect of local CD3 engegement on CD28 phosphorylation in *trans*. Dependence of global phosphotyrosine clustering on local anti-CD3 engagement. Anti-CD3 antibodies in different concentrations were mixed with with isotype control antibodies adding up to a total concentration of 100 µg/ml and stamped to glass slides. Slides were subsequently overlayed with anti-CD28 (15 µg/ml). Jurkat cells were stimulated on the microstructured surfaces for 10 min. The localization of phosphotyrosine on plane of surface contact was analyzed by staining with a Zenon-Cy5 labelled anti-phosphotyrosine antibody and confocal microscopy.

5.3 Effects of stimulus size on phosphotyrosine clustering. As the stimulation intensity of Jurkat cells depends on the density of the anti-CD3 antibody, we were interested if stimulation also depends on the size of the stimulus. In this context, it was our goal to distinguish the effect of the size of the site of CD3 engagement on the tyrosine phosphorylation in general and per area. For this, we employed PDMS stamps with round studs of diameters between 2 and 20 µm. Due to instability of stud units smaller than 2 µm during stamping, these protein spots of that size could not be employed successfully. Evaluation of immunofluorescence microscopy indicates that, concerning the area of the stimulatory surface, the mean phosphotyrosine intensity appears more intense and evenly located on anti-CD3 spots of smaller size than on bigger spots (Fig. 5.5). While on spots allowing full spreading of cell (>15 µm in diameter), phosphotyrosine localized preferentially at the outer rim of the cell, the staining on smaller spots was more intense and covered the whole area of cell contact with the anti-CD3 antibody (see Fig. 5.5 A). Quantification of phosphotyrosine intensity followed the same protocol as for the lines, with only taking surface of the stamped antibody

representing the area of TCR stimulation into account. Quantitative analysis shows that the total fluorescence intensity is higher on bigger spots, but the relative phosphotyrosine staining intensity per area is higher on smaller spots (see Fig. 5.5 B). A possible explanation for this is that the number of proteins actively and passively involved in tyrosine phosphorylation might be the limiting factor. Because only limited cell spreading is allowed to occur on the stimulus, the contact area on which signalling proteins are distributed is reduced. This observation may correspond to the effect of Cytochalasin D (Fig 4.12), for which we observe often a higher phospho-PLCγ staining intensity per area than in the control, but with an overall weaker effect on T cell stimulation.

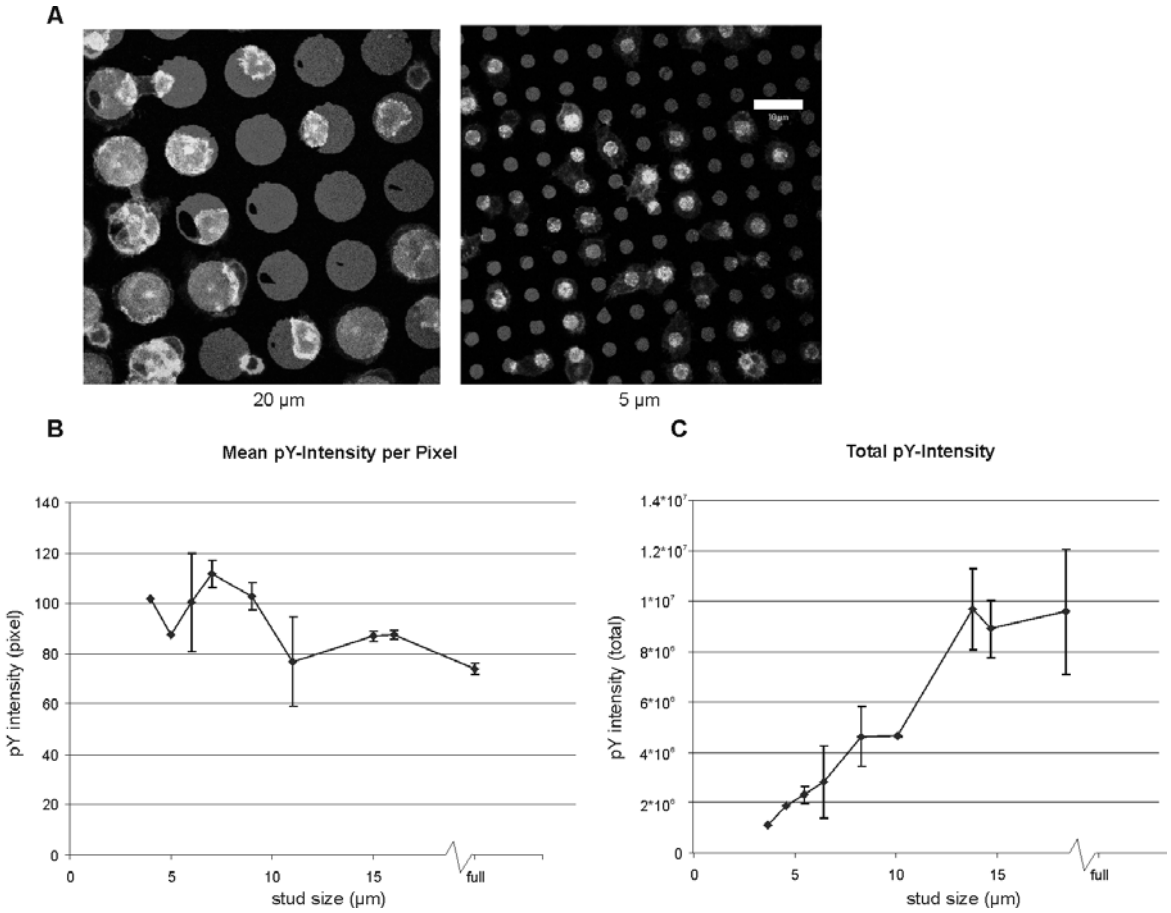

Figure 5.5 Dependence of intracellular phosphotyrosine fluorescence on stimuli size. Jurkat T cells were stimulated for 10 min on stamped anti-CD3 surfaces (100 µg/ml), which had been overlayed with anti-CD28 antibodies (15 µg/ml). Phosphotyrosine fluorescence in the contact surface was imaged using confocal microscopy in fixed cells. A) pY staining (light grey) on studs of 20 and 5 µm diameter. B) Quantification of the mean pY intensity per pixel, and C) total pY intensity per spot. On the graphs, the x-axis defines the stud size, with "full" representing representing conditions that allow full spreading on a homogeneously anti-CD3 functionalized surface. The data represent the means of two experiments.

6. Label-free Characterisation of Cell Adhesion using Reflectometric Interference Spectroscopy (RIfS)

6.1 Summary

Reflectometric Interference Spectroscopy (RIfS) is a label-free, time-resolved technique for detecting interactions of molecules immobilized on a surface with ligands in solutions. Here we show that RIfS also enables the detection of the adhesion of tissue culture cells to a functionalized surface in a flow system. Jurkat T cell leukemia cells rapidly attached to a transducer functionalized with a monoclonal antibody directed against the T cell receptor (TCR)/CD3 complex followed by activation-dependent cell spreading. For the Jurkat derivative JCaM 1.6 that lacks the key signalling protein LCK, cells preincubated with the inhibitor of actin polymerization cytochalasin D, and for surfaces functionalized with an antibody directed against the co-receptor CD28, RIfS curves were obtained that differed with respect to the maximum signal and the initial slope of the increase in optical thickness. Interactions of T cells with other leukocytes or epithelial cells of blood vessels are crucial steps for the regulation of the immune response and inflammatory reactions. The testing of chemical inhibitors, cell surface molecules and gene products relevant for a key event in T cell immunity illustrates the potential of label-free techniques for the analysis of activation-dependent cell-surface contacts.

This chapter has been adapted from:

Möhrle, B., Köhler, K., Jaehrling, J., Brock, R., Gauglitz, G. (2006): Label-free characterisation of T cell adhesion using reflectometric interference spectroscopy. Anal. Bioanal. Chem. 384 (2):407-13

Cellular and microscopy experiments in this section were performed by the author. All RIfS measurements themselves, and the generation of RIfS transducers were performed by Bernd Möhrle.

6.2 Introduction

Cell-cell contacts are mediated through specific receptors that, in addition to establishing a physical link between cells, also act as signal transducing molecules. Due to the significance of cell-cell interactions in health and disease there is a keen interest in the development of analytical techniques that enable the analysis of contacts with respect to kinetics, strengths and the underlying signalling processes. Reflectometric Interference Spectroscopy (RIfS) is a label-free, time-resolved technique, which is able to detect biomolecular interactions of molecules immobilized on the surface of a transducer with analytes in solution [159]. The binding of the analyte leads to an increase in the so-called optical thickness of the transducer-bound layer of molecules. The increase in thickness results in a change of the interference spectrum of light reflected at its boundaries. In contrast to surface plasmon resonance spectroscopy (SPR) the RIfS method is temperature independent [160] and has a higher depth of penetration into the solution (about 300 nm for SPR and up to 40 μm for RIfS, depending on the wavelength) [161]. RIfS has been employed to measure the interaction kinetics of a variety of biomolecular interactions such as antibodies [162], biotin [163] and peptides [164] . The RIfS setup is described in detail in the work of Schmitt et al. [8]. In spite of their potential for detecting interactions of molecules, cellular applications have been limited. SPR has been used for the analysis of the adhesion of bacteria [165;166] and erythrocytes [167] to surfaces. So far label-free techniques have not been used for the analysis of activation-dependent cellular interactions. Moreover, there is little information in which way the signal depends on the molecular and morphological characteristics of a cell in contact with the transducer.

Cell-cell contacts play a key role in the immune system and especially in the immune surveillance exerted by T lymphocytes: T cells continuously circulate in the blood and lymphatic system, and engage in transient contacts with other cells mediated by interactions of their T cell receptors (TCR) with major histocompatibility complex (MHC)-peptide complexes on the target cell, and by interactions of other surface receptors [2]. The molecular mechanisms of contact formation between T cells and antigen-presenting cells have been investigated in great detail under static conditions, i. e. in the absence of flow. Activation of a T cell is a function of the affinity of the interaction, the density of specific MHC-peptide complexes on the cell surface, and the differentiation

and activation state of the T cell [3]. Activation of cytotoxic T cells leads to the killing of a target cell and cytokine expression; T helper cells interact with professional antigen presenting cells and contribute to the orchestration of an immune response. The cytokine-mediated guidance of T cells to their targets proceeds via adhesion-molecule contacts to the surface of the blood vessel epithelia, followed by active migration of the cells into the surrounding tissue [168;169].

In order to better understand the events that precede T cell activation, such as extravasation, approaches that enable an analysis of T cell contacts under flow conditions are required. Ideally, such approaches should simultaneously provide information on the kinetics of an intercellular interaction and the cellular response. In drug development such analyses will provide the basis for the screening of compounds that interfere with contact formation of T cells and therefore be useful for the identification of immunomodulatory compounds.

Here, we demonstrate the application of RIfS to the analysis of T cell contacts and activation in a flow system. With ligand-functionalized surfaces, T cells form contacts that vary in intimacy and contact area depending on the nature of the ligand and the cell activation. T cells are therefore also especially suited for evaluating to which degree cellular responses to different stimuli can be discriminated based on a RIfS signal. Transducers were functionalized with different antibodies that served as well established and well defined stimuli. Antibodies directed against the CD3ε chain of the TCR/CD3 complex represent a strong T cell stimulus. Contact of T cells with anti-CD3-functionalized surfaces leads to a rapid spreading of cells on the surface within 2-5 minutes (Fig. 3.2). This process depends on the reorganization of the actin cytoskeleton and thus can be completely inhibited by the addition of 10 μM cytochalasin D, an inhibitor of actin polymerization [109]. Surfaces functionalized with antibodies directed against the CD28 coreceptor were described to mediate specific T cell attachment but, instead of cell spreading, the formation of small “mikrospikes” was observed [135]. Characteristic RIfS curves were obtained for Jurkat T cell leukemia cells perfused over anti-CD3- and anti-CD28-functionalized transducers and for cells inhibited with cytochalasin D and cells lacking the CD3-dependent upstream kinase LCK. Correlation of

the results obtained by the label-free technology with those obtained by fluorescence microscopy yielded the morphological basis for these findings.

6.3 Results and Discussion

6.3.1 Spreading of T cells on antibody-functionalized surfaces. Antibody-functionalized coverslips represent a well-defined T cell stimulus that enables the analysis of T cell signal transduction and the effect of chemical inhibitors under highly controlled conditions [170]. First, the spreading of Jurkat T cells on antibody-functionalized surfaces was determined using immunofluorescence microscopy in a stopped flow protocol. Antibodies were immobilized on epoxy-activated glass surfaces in order to mimick most closely the conditions used for the immobilization of antibodies on the RIfS transducers. The high reflectivity compromised the analysis of cell contacts on RIfS transducers using fluorescence microscopy. Cells were allowed to settle on antibody-functionalized coverslips and were fixed after 20 min. On anti-CD3-functionalized coverslips, for most cells the formation of tight contacts with the surface was observed, and about 15% of the cells showed a spreading of more than twice the cell diameter (Fig. 6.2 A). The detection of surface contacts was based on by staining fixed but not permeabilized cells as described in the first paper of this section. In the presence of tight contacts, a fluorescently labelled secondary antibody, directed against the antibody used for stimulation of cells, can only stain the part of the surface of the coverslip that is not shielded by the cells.

In contrast, on an anti-CD28 functionalized surface, the cells attached to the surface, but spreading and contact formation were strongly reduced (Fig. 6.2 B). The difference in cell spreading was also evident in a phalloidin staining of the actin cytoskeleton. On the anti-CD3-coated surface a strong polymerization of actin was present in the leading edge of the spread cells. Little actin was present in the contact zone (Fig. 6.2 A). On anti-CD28-coated surfaces, cells adhered tightly, however no spreading was observed, and the contact zone was poor in polymerized actin. JCaM 1.6 cells, a Jurkat derivative cell line deficient in the CD3-dependent upstream kinase LCK, showed a strong reduction of cell-

spreading, and polymerized actin was distributed around the periphery of the cells, especially in the contact zone (Fig. 6.2 C). Pretreatment of cells with the inhibitor of actin polymerization cytochalasin D completely abolished firm cell attachment and spreading and inhibited the actin localization to contact sites (Fig. 6.2 D). The cells showed little contact with the surface. Finally, on BSA the cells attached, but no spreading was observed (Fig. 6.2 E), and actin was localized evenly in the membrane-proximal region of the cell. In conclusion, each surface led to a distinct pattern in spreading and reorganization of the actin cytoskeleton.

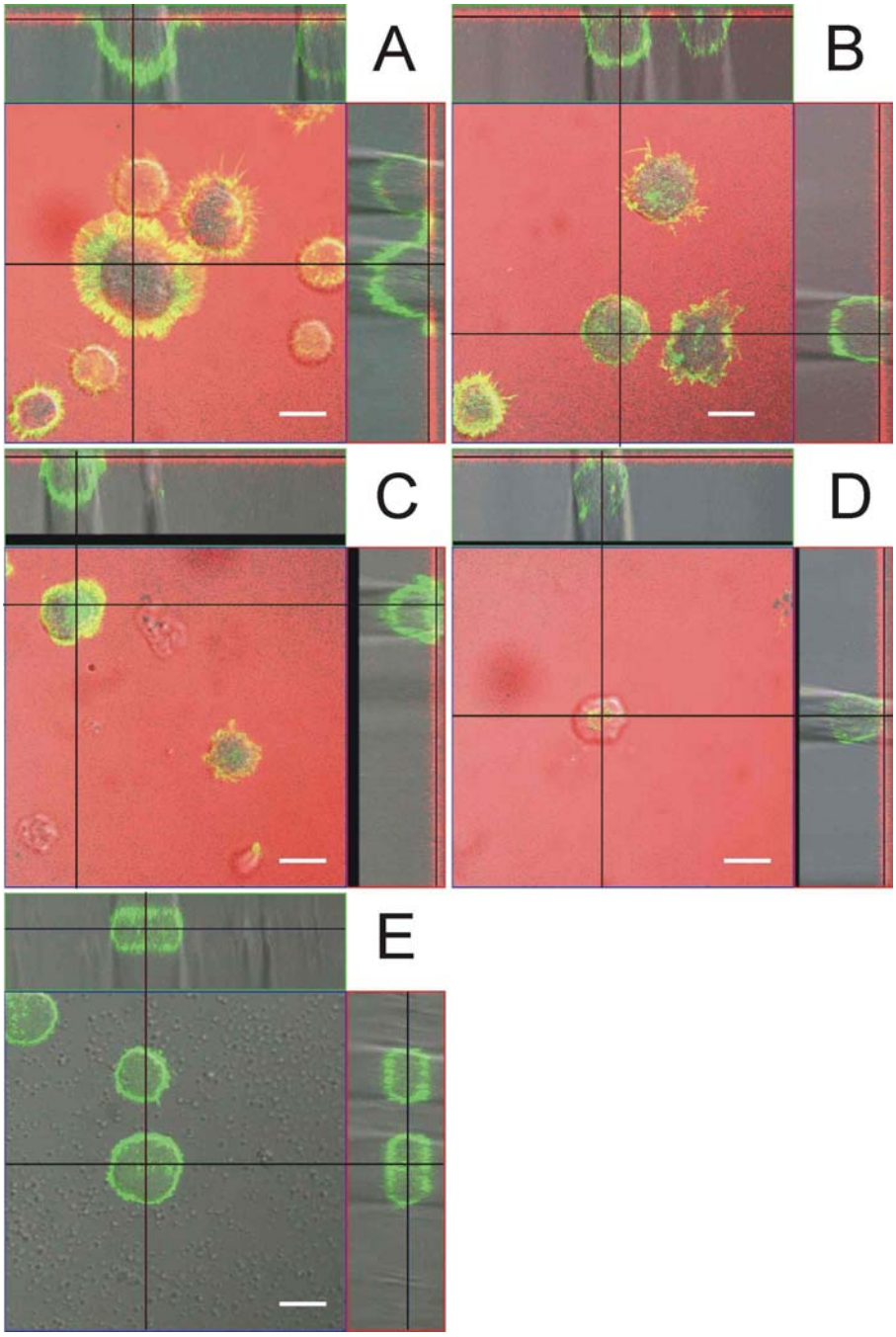

Figure 6.2 Contact formation of cells on antibody- and BSA-functionalized surfaces. Jurkat cells (A, B, D, E) or the LCK-deficient Jurkat derivative JCaM 1.6 (C) were exposed to coverslips functionalized with anti-CD3 antibodies (A, C, D), with anti-CD28 antibodies (C) or BSA (E) in the absence (A-C, E) or presence (D) of the inhibitor of actin polymerization cytochalasin D (10 μM). Cells were allowed to establish contacts for 20 min before fixation. The immuno-fluorescence staining of the antibody used for surface functionalization is shown in grey; the Cy5-phalloidin staining of filamentous actin is represented in light grey. Cells were fixed but not permeabilized. For this reason, parts of the surface in close contact with a cell are not accessible to the secondary antibody. In each panel, an x-y section and orthogonal projections through the confocal image stack along the indicated lines are shown. The bar corresponds to 10 μm.

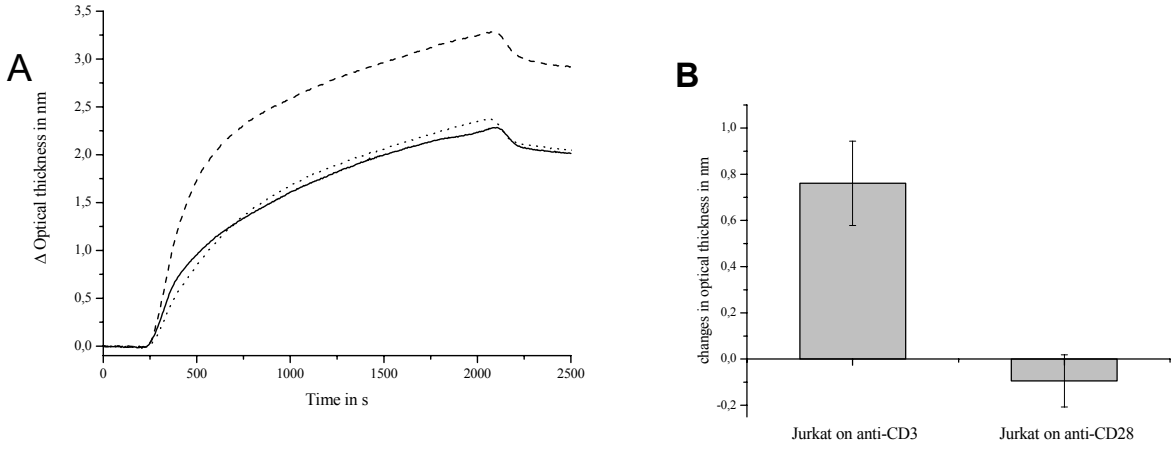

Figure 6.3 A) RIfS measurements of the adhesion of Jurkat T cells on different surfaces. $5*10^5$ Jurkat cells/ml were pumped in a flow chamber over different surface in a flow of 20 µl/min over differently functionalized transducer surfaces. The time-dependent changes in optical thickness for Jurkat attachment on anti-CD3- (dashed line), Jurkat on anti-CD28- (solid line) and Jurkat on BSA-functionalized surfaces (dotted line) are plotted. B) Bar chart of the RIfS-Signal of the attachment of Jurkat cells on anti-CD3- (n=4) and anti-CD28-functionalized (n=3) surfaces referenced against the non-specific binding to BSA at the 2000 s time point. The signal difference between both surfaces is significant (t-test, P=0.05). Picture generated by Bernd Möhrle.

6.3.2 Label-free detection of cell attachment by RIfS. Having established that wild type Jurkat cells showed different phenotypes on anti-CD3-, anti-CD28- and BSA-coated surfaces, next the adhesion of these cells to functionalized RIfS transducers was detected in a flow system with a flow rate of 20 µl per minute. On each type of surface the RIfS signal showed similar general characteristics. In each case, a steep initial increase was followed by second phase of a slower increase. For the anti-CD3-coated surface the maximum increase in optical thickness at 2000 s was about 1.5 times as high as the one detected for the anti-CD28 and BSA-coated surfaces. Once the perfusion of the cell suspension was stopped and instead, the flow cell was perfused with medium alone, very similar absolute decreases in optical thickness were observed in each case (Fig. 6.3 A).

The signals of the adhesion to anti-CD3 and anti-CD28 surfaces were referenced against the non-specific adhesion on BSA surfaces, at the 2000 s time point (Fig. 3 B). The RIfS signal of the adhesion of the T cells on both surfaces was significantly different (t-test,

P=0.05). This high reproducibility was obtained in spite of the use of different transducers, freshly prepared cell suspensions for each experiment and the fact that a complete series of measurements could not always be performed in direct succession. This may also account for the rather high variability of the RIfS signal. Interestingly, on anti-CD28-coated surfaces the maximum optical thickness was slightly but reproducibly smaller than on BSA-coated surfaces.

In addition to the maximum increases in optical thickness a comparison of the initial slopes of the RIfS curves (ΔOT) yielded additional information. Even though the maximum increase of the optical thickness was smaller on the anti-CD28-coated surface than on the BSA control, the initial increase of the RIfS curves for Jurkat cells was much higher on the anti-CD28-coated surface ($\Delta OT=(5.8 \pm 0.4)*10^{-3}$ nm/s) than on the BSA-coated surface ($\Delta OT= (2.6 \pm 1.3)*10^{-3}$ nm/s) (Fig.3). The increase in optical thickness for the anti-CD3-functionalized surface had the highest slope ($\Delta OT= (6.8 \pm 1.6)*10^{-3}$ nm/s).

6.3.3 Characterization of mutant cell lines and chemical inhibitors. The initial measurements demonstrated that RIfS enabled a discrimination of the adhesion behavior of the Jurkat T cells on surfaces functionalized with antibodies that either induce a strong activation of cell spreading or mediate specific adhesion but little spreading, and on surfaces functionalized with BSA that induce only unspecific interactions.
We therefore also explored to which degree the label-free time-resolved detection of cell attachment enabled a characterization (i) of the adhesion behaviour of different cell lines and (ii) of the effects of pharmacological inhibitors of cell attachment and spreading. Each condition was characterized with respect to the maximum increase in optical thickness and the initial slope of the RIfS curve (Fig. 6.4). For JCaM 1.6 cells perfused over the anti-CD3-coated surface the maximum RIfS signal was reduced by 11 % in comparison to the signal of wild type Jurkat cells (Table 1) but still higher than the one of the wild type cells on BSA- and on anti-CD28-coated surfaces. The initial slope of the RIfS curve ($\Delta OT= (4.1 \pm 0.6)*10^{-3}$ nm/s), was lower than the one for Jurkat cells contacting anti-CD28-functionalized coverslips.

The spreading of the Jurkat T cells on the immobilized anti-CD3 antibodies surface is an actin-dependent process. For this reason, the inhibitor of actin polymerization cytochalasin D was selected as a compound to evaluate RIfS for the detection of pharmacological interventions. Cytochalasin D treatment does not inhibit the attachment of cells to anti-CD3-coated surfaces and the formation of signalling clusters, but completely abolishes cell spreading. Preincubation of cells with cytochalasin D led to a reduction of the maximum RIfS-signal by 21.5% ± 12.9% (Table 6.1). Interestingly, the initial slope of the RIfS curve ($\Delta OT=(4.2 \pm 0.6)*10^{-3}$ nm/s), was in the same range as the one observed for JCaM 1.6 cells. Similar to the JCaM 1.6 cells, for cytochalasin D-treated cells, even though the initial kinetics of attachment were slow, the maximum increase in optical thickness was higher than the one for Jurkat cells on anti-CD28-coated surfaces.

Table 6.1 Reduction of the RIfS signal for the 2000 s time point relative to the signal of Jurkat cells on anti-CD3 antibody surface (n=3).

	Reduction of the RIfS-signal in %
Jurkat cells on anti-CD28 antibodies surface	47.3 ± 15.8
Jurkat cells on BSA surface	31.0 ± 4.4
Jurkat cells on anti-CD3 antibodies surface pretreated with 10 µM cytochalasin D	21.5 ± 12.9
JCaM 1.6 cells on anti-CD3 antibodies surface	11.5 ± 3.2

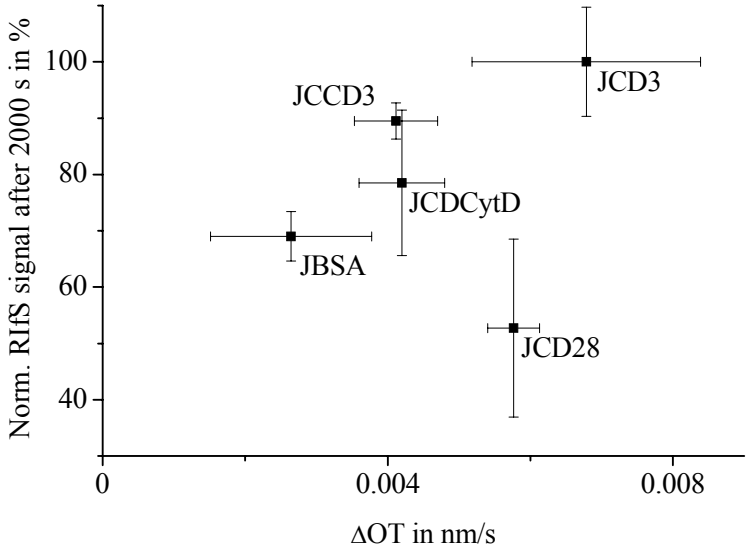

Figure 6.4 Correlation of the maximum optical thickness after 2000 s and the initial slopes of the tangents to the optical thickness curves (ΔOT). JCD3, JCD28 and JBSA indicate Jurkat cells adhering to a surface functionalized with anti-CD3, anti-CD28 antibodies or BSA, JCCD3 the LCK-deficient JCaM 1.6 cells on an anti-CD3 surface and JCD3CytD Jurkat cells pretreated with 10 μM of the actin inhibitor cytochalasin D before perfusion over an anti-CD3-functionalized surface. The average values of the maximal optical thickness were normalized to the spreading of Jurkat cells on anti-CD3-coated transducers.

6.3.4 Correlation of kinetics of cell attachment and cell spreading.

The time-resolved RIfS measurements yielded information on the kinetics of T cell attachment and spreading in the presence of flow. We therefore asked whether correlations existed between the behaviour of the cells in the flow system and in the stopped flow configuration. Interestingly, the initial kinetics of cell attachment rather than the maximum RIfS signal showed a strong positive correlation with the cell spreading determined by immunofluorescence microscopy (Fig. 6.5). The lower maximum RIfS signal in spite of the larger average area for Jurkat cells on anti-CD28-coated surfaces in comparison to JCaM 1.6 cells, cytochalasin D-treated cells and cells on BSA is a non-trivial result that may not be explained by the RIfS analysis alone.

In the analysis of cell attachment and spreading, three factors may contribute to an increase in optical thickness: (i) Cell attachment, (ii) spreading of an already attached cell, and (iii) the refractive index in the contact area. The higher maximum optical thickness

for the latter three cases may readily be explained by the fluorescence microscopy data: For each condition the number of cells was the same even though a loss of cells during fixation and washing cannot be fully excluded. However, in contrast to the anti-CD28-coated surface, for the JCaM 1.6 cells on an anti-CD3-coated surface and the Jurkat cells on BSA, a strong enrichment of filamentous actin in the contact area was observed. The higher RIfS signal is therefore most likely a consequence of the local enrichment of protein.

Especially through the combination of results from immunofluorescence microscopy and RIfS it is now possible to distinguish between modes of binding in which (i) unspecific contacts are formed – as for BSA-coated surface, (ii) contacts establish quickly and induce firm attachment, but no cell spreading, even though contacts are less intimate/or the membrane proximal region is less enriched in protein – as for anti-CD28-coated surfaces, (iii) contacts establish slowly and cells do not spread or spread only in little extent, but the contact area still has a high optical thickness – as for JCaM 1.6 cells and possibly for cytochalasin-treated Jurkat cells, and where (iv) contacts establish quickly and cells spread strongly as for Jurkat cells on anti-CD3-coated surfaces.

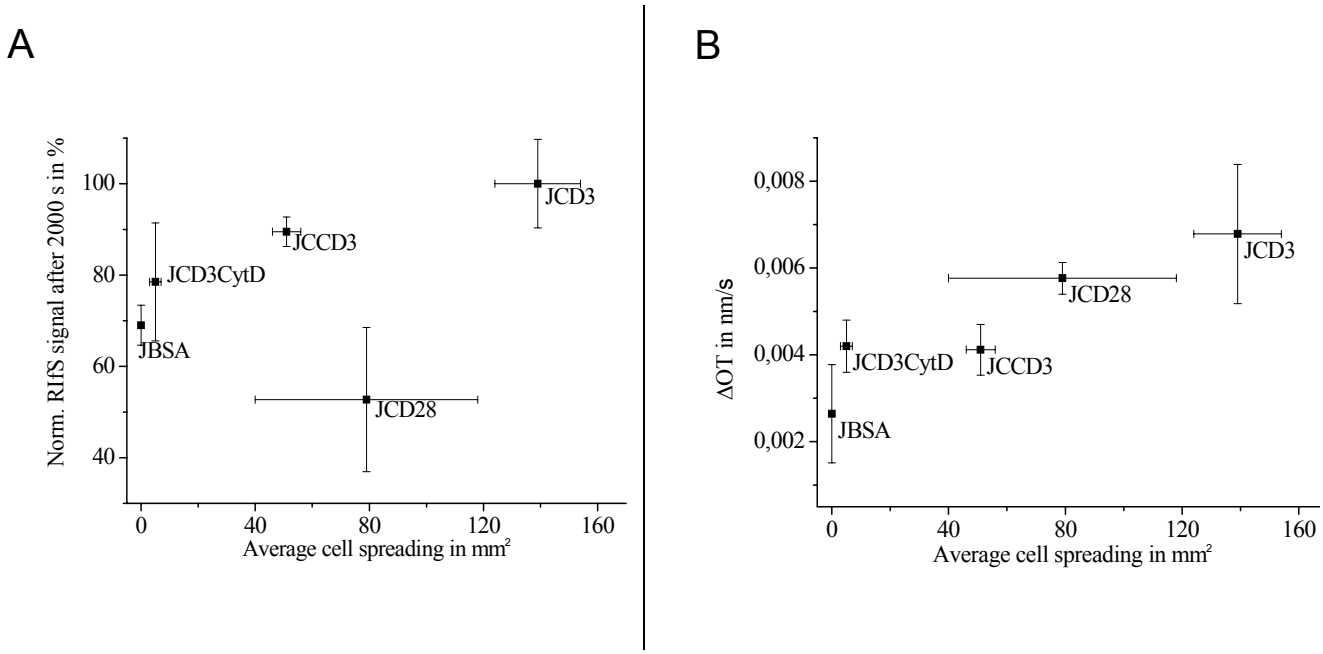

Figure 6.5 Correlation of RIfS and immunofluorescence microscopy. A) Maximum RIfS signal after 2000 s versus the average cell spreading determined by immunofluorescence microscopy and digital image processing. B) Slopes of the tangents to the optical thickness curves (ΔOT) versus average cell spreading determined by immunofluorescence microscopy.

6.4 Conclusion

The results demonstrate that the label-free RIfS technique enables a sensitive distinction between various states of cell adhesion and activation in a flow system. Cells responded differently to surfaces functionalized with different stimulatory antibodies. Moreover, cells lacking a signalling protein and cells treated with an inhibitor of cell spreading yielded characteristics signatures of kinetics and maximum optical thickness. A correlation of the results obtained by RIfS with fluorescence imaging provided an explanation for the increases in optical thickness observed for the individual conditions, a prerequisite for a wider application of label-free techniques in cell biology. Remarkably, the cell spreading observed in a stopped-flow protocol correlated with the initial increase of the RIfS signal rather than with the maximum increase in optical thickness. There is evidence that in T cell receptor-dependent signal transduction the association kinetics of the TCR with the MHC peptide complex is a major determinant for the activation of a T cell [171]. The flow system and especially the correlation of the dynamic data with fluorescence imaging as exemplified in this contribution should enable to address these questions in a highly robust experimental set-up. Finally, the analysis of T cell attachment in the presence of flow enables the screening for compounds that interfere with T cell interactions in a flow system.

7. Analysis of T cell signalling using peptide microarrays

7.1 Abstract

In cellular signal transduction multiprotein complexes play an essential role in the propagation and integration of signals. In spite of enormous progress in the identification of protein complexes and the definition of interaction motifs, systems-based analyses of signalling-dependent changes in the pattern of molecular interactions are still missing (still very limited). In order to overcome this deficit we have implemented peptide microarrays comprising a set of known interaction motifs of signalling proteins. Lysates of resting or stimulated cells are incubated on these arrays and the binding of signalling proteins detected by indirect immunofluorescence. Masking of binding sites or recruitment of proteins into complexes can lead to signal changes. Competition with peptides corresponding to interaction motifs provides detailed information on the architecture of signalling complexes and the functional relevance of individual interaction motifs in the organisation of the interaction network. For molecular interactions in T cell signal transduction this approach reveals detailed information on the presence of preformed complexes and the functional effect of a protein on molecular interactions patterns.

This section has been adapted from:

Stoevesandt, O., Elbs, M., Köhler, K., Lellouch, A.C., Fischer, R., André, T., Brock, R. (2005): Peptide microarrays for the detection of molecular interactions in cellular signal transduction. *Proteomics* 5 (8):2010-2017

The author of this thesis designed and synthesized the bisphosphorylated peptides used in this study and was involved in the microscopical analysis and image quantification.

Stoevesandt, O., Köhler, K., Wolff, S., Hummel, W., André, T., Brock, R.: Dissection of T cell-activation dependent protein complex formation using peptide microarrays. Manuscript submitted

The author of this thesis designed the peptides used in this study, produced the peptide microarrays and was involved in the cellular stimulation experiments and data analysis.

7.2 Introduction

In recent years the molecular characterization of cellular processes has moved to the systemic level. Highly parallel analyses of changes in gene expression using oligonucleotide microarrays and various methods for detecting changes in protein expression have been applied to numerous biological questions. Also, signalling-dependent changes in the pattern of protein phosphorylation have been mapped extensively. T cell signalling has been systematically characterized at the level of transcription [79], translation [172], and protein phosphorylation [173].

In contrast, systems-based approaches for analysing signalling-dependent changes in protein interaction networks are still missing. Complexes of signalling proteins are key determinants for the integration of signals from different cell surface receptors. So far, interaction networks have been inferred by mapping of binary interactions, as exemplified by two-hybrid screens or by mapping of molecular complexes through tag-based pull-down. The physiological relevance of two-hybrid data has been questioned, as partners interact in a foreign molecular and functional context. Pull-down approaches require the introduction of tagged proteins into many separate cell populations and therefore do not provide comprehensive information on the overall pattern of molecular interactions in an unmodified cell population.

Compared to these approaches, the highly parallel detection of signalling-dependent changes in the pattern of molecular interactions in an unmodified cellular system would provide a more physiological data set for systems biological analyses. Here we demonstrate the use of peptide microarrays for this purpose. T cell receptor-dependent signal transduction is representative for signalling pathways in which interactions mediated via linear peptide motifs play a major role. Src homology 2 domains (SH2) interacting with phosphotyrosine (pY) peptide motifs and Src homology 3 domains (SH3) interacting with polyproline (polyP) peptide motifs are prominent examples.

T cell receptor (TCR) crosslinking via a specific MHC/peptide complex initiates T cell activation through different signalling pathways in which kinases mediate phosphorylation-dependent protein-protein interactions. Src homology 2 domains (SH2) interacting with phosphotyrosine (pY) peptide motifs and Src homology 2 domains (SH3) interacting with polyproline (polyP) peptide motifs figure prominently in this network, making its analysis by peptide microarrays attractive. A key step following TCR

crosslinking is the phosphorylation of tyrosine motifs in the TCR/CD3 complex by the Src family kinase LCK, leading to the formation of sites for the binding and activation of ZAP-70 [174]. ZAP-70 in turn phosphorylates various downstream targets, among them the adapter proteins LAT and SLP76. Tyrosine-phosphorylated LAT forms a scaffold for the recruitment of various SH2 proteins (PLCγ1, GRB2, GADS and Vav) [175; 27; 36; 176]. By interaction of pY motifs of LAT with SH2s of PLCγ1 and GADS, and polyP motifs of SLP76 with the SH3s of PLCγ [177] and GADS [35], these four proteins form the core of a protein complex called the LAT signalosome [36;178]. Via further adapter proteins, the LAT signalosome composes a scaffold for the indirect recruitment of other proteins to the TCR, which are involved in dephosphorylation (SHP2 via Gab [37]), cytoskeletal remodelling (e.g. via WASP [179]) and TCR degradation (Ubiquitinylation via Cbl [180]).

7.3 Results

7.3.1 System establishment. Direct detection of protein binding as judged by the intrinsic YFP-fluorescence of the ZAP-70-YFP fusion protein to its immobilized recognition peptide CD3ζpY72/83 shows a linear dependence from the protein concentration up to the highest applicable lysate concentrations (Fig. 7.1 A). However, the detection of endogenous ZAP-70 by immunofluorescent staining showed saturation tendencies for ZAP-70 concentrations below those of ZAP-70-YFP (Fig 7.1 B), most likely due to diffusion-limited binding of antibodies and incubation times below those necessary to reach equilibrium [181]. Binding of ZAP-70-YFP from a pervanadate treated lysate prepared at 10 x 10^6 cells / ml was strongly reduced and showed also a clear reduction of immunostaining. This observation is likely a consequence of the depletion of free ITAM binding SH2 domains for ZAP-70, induced by the recruitment of ZAP-70 to intracellular phosphorylated ITAMs. This effect corresponds to the enforced recruitment of ZAP-YFP towards the plasma membrane in pervanadate-treated cells (data not shown).

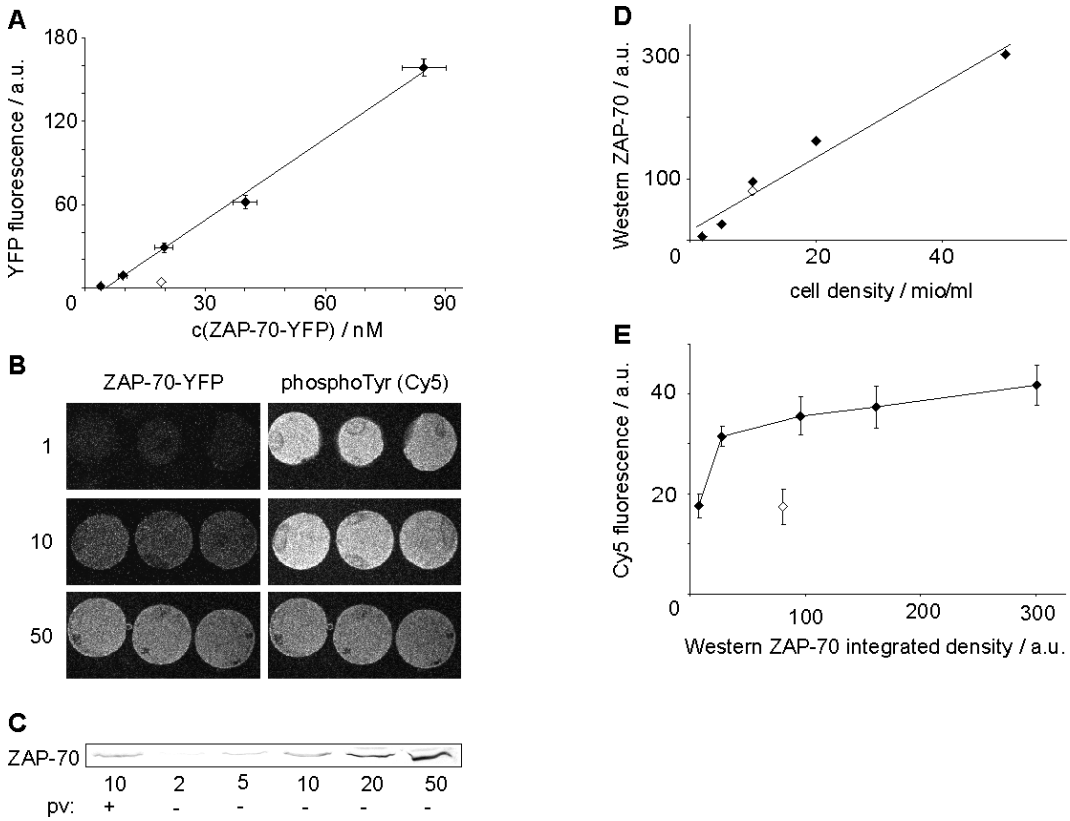

Figure 7.1 Relation between the concentration of ZAP-70 in the lysates of resting cells and array-bound fluorescence on pITAM spots after incubation on microarrays. (A) Lysates of resting cells expressing ZAP-70-YFP were prepared at cell densities of 2, 5, 10, 20 and 50 x 10^6 cells / ml lysate (black diamonds). The concentration of ZAP-70-YFP was determined by fluorescence correlation spectroscopy. Array-bound fluorescence of ZAP-70-YFP increased linearly over the concentration range tested. The open diamond represents the signal of the lysate of 10 x 10^6 cells / ml treated with PV. (B) pITAM spots on arrays incubated with lysates of 1, 10 and 50 x 10^6 cells / ml displayed an increasing fluorescence intensity of ZAP-70-YFP, while indirect immunostaining against phosphotyrosine using a Cy5-labelled secondary antibody revealed that pITAM was not saturated by ZAP-70-YFP. (C) Western blot analysis of endogenous ZAP-70 from lysates of untransfected cells prepared at cell densities from 2 to 50 x 10^6 cells / ml. Equal volumes of lysate were loaded. Pervanadate treatment of the cells prior to lysis is denoted by PV. (D) ZAP-70 Western bands shown in (C) were quantitated by integrating their density and area. The ZAP-70 content inceased linearly with the density of cells in the lysate. (E) Aliquots of the lysates depicted in (D) were incubated on arrays and the arrays indirectly immunostained for ZAP-70. A correlation between ZAP-70-content as determined by Western blotting and intensity of the immunostaining on the array was established for lysates of resting cells (black diamonds) and PV treated cells (open diamond). Error bars represent the mean deviation from the mean. Western blots and FCS measurements were performed by Oda Stoevesandt.

7.3.2 Experimental design. 16 identical peptide arrays were nanospotted per glass slide. The peptides comprised a set of known binding motifs for interaction domains of proteins involved in T cell signal transduction, with a focus on interactions up- and downstream of the scaffolding protein LAT. A 16-well clip-on frame allowed the individual incubation of arrays with cell lysates and indirect immunostaining for various bound proteins. Per array, two proteins were detected simultaneously, using primary antibodies from mouse and rabbit and species-specific distinctly labelled secondary antibodies (Fig 7.2 a, b). To limit redissociation of weakly bound proteins, antibody incubation and washing were kept as brief as possible.

Judged by the intensity of immunostaining on the array, proteins showed a strong preference for peptides representing binding motifs for the respective domain subtype of the protein, notably peptides derived from known binding partners (Fig. 7.2 c). For example, PLCγ1 contains an SHP/PLC type SH2 domain and correspondingly its signal on the peptide LATpY132 (SHP/PLC motif) was about twice as intense as on LATpY191 (GRB2/SFK/PLC motif) and nondetectable on LATpY226 (GRB2/SFK motif). The signal of GADS on the peptide SLP228 (atypical SH3 motif[182]) was about 300fold higher than on SLP179 (type2 SH3 motif).

Table 7.1 Peptides used for peptide microarrays

Peptide	Sequence	Source	Inter-acting Partner	Binding domain
PAG421	CSDLQQGRDITRL-OH [183]	PAG 421-432	EBP-50	PDZ
ZAPpY296	CIDTLNSDG(pY)TPEPARIT-NH2 [21]	ZAP-70 284-300	Cbl	PTB
SHP1pY564	CSKHKEDV(pY)ENLHTKNK-NH2 [184]	SHP1 557-572	LCK	SH2 (GRB2 type)
LATpY226	CEVEEEGAPD(pY)ENLQELN-NH2 [36]	LAT 217-233	GADS, GRB2, Vav	SH2 (GRB2, SFK-type)
ZAPpY319	CVYESP(pY)SDPEELKD-NH2 [185]	ZAP-70 314-327	LCK	SH2 (GRB2, SFK type)
LATpY191	CEASLDGSRE(pY)VNVSQEL-NH2 [27;176]	LAT 181-198	Vav, GADS, GRB2,PLCγ1	SH2 (GRB2, SHP/PLC, SFK type)
CD3zpY72/83	C-Ahx-NQL(pY)NELNLGRREE(pY)DVL-NH2 [186]	CD3ζ ITAM1 69-86	ZAP-70	Tandem-SH2 (ITAM)
PLCγpY783	CEGRNPGF(pY)VEANPMPT-NH2 [187]	PLCγ1 775-791	PLCγ intramol.	SH2 (SFK type)
FYBpY595	CEDDQEV(pY)DDVAEQD-NH2 [188]	FYB 589-604	Fyn, SLP76	SH2 (SFK type)
FYBpY625	CDDDI(pY)DGIEEED-NH2 [188]	FYB 621-634	Fyn	SH2 (SFK type)
FYBpY651	CLDMGDEV(pY)DDVDTSDF-NH2 [188]	FYB 644-663	SLP76	SH2 (SFK type)
LCKpY505	CVLEDFFTATEGQ(pY)QPQP-NH2 [189]	LCK 493-509	LCK	SH2 (SFK type)
LATpY132	CEDEDDYHNPG(pY)LVVLPDSTP-NH2 [27;175]	LAT 121-141	PLC-γ1	SH2 (SHP/PLC type)
SIGpY437	CGEEREIQ(pY)APLSFHKG-NH2 [190]	Siglec-7 430-445	SHP1, SHP2	SH2 (SHP /PLC, SFK-type)
GAB2pY614	CKSTGSVD(pY)LALDFQPS-NH2 [191]	Gab2 607-622	SHP1	SH2 (SHP/PLC type)
CD28pY202	CTRKHYQP(pY)APPRDFAA-NH2 [192]	CD28 196-210	GRB2	SH2 (atyp.)
CblpY699	CEGEEDTE(pY)MTPSSRPL-NH2 [193]	Cbl 693-707	Vav	SH2 (atyp.)
PI3K84	CPTPKPRPPRPLPVAPGSSKT-NH2 [194]	PI3Kp85 84-104	Fyn	SH3 (type I + atyp.)
SLP179	CSGKTPQQPPVPPQRPMAAL-NH2 [195]	SLP76 179-197	PLCγ1	SH3 (type II)
PAK6	CLDIQDKPPAPPMRNT-NH2 [43]	PAK1 6-20	Nck	SH3 (type II + atyp)
GAB2-509	CQPPPVNRNLKPDRKAKPTPLD-NH2 [53]	Gab2 509-529	GRB2	SH3 (atyp.)
SLP228	CAKLPAPSIDRSTKPPLDRS-CONH2 [182]	SLP76 228-246	GADS	SH3 (atyp.)
UBP8-403	CNVPQIDRTKKPAVKLPEE-NH2 [196]	UBPY 8 403-416	Hbp	SH3 (atyp., Hbp type)
WIP446	CEDEWESRFYFHPISDLPPP-NH2 [197]	WIP 446-464	WASP	WH1

7.3.3 Phosphorylation-dependent changes in interaction profiles. To initiate signal transduction by protein phosphorylation, we employed the phosphatase inhibitor pervanadate, a strong supraphysiological stimulus of T cell signalling [198]. Lysates of resting or pervanadate-treated Jurkat cells were incubated on separate arrays (Fig. 7.2 b,c) and signal ratios of corresponding peptides were calculated (Fig. 7.3 a). For interactions of SH2-domain containingproteins on pY peptides representing known binding partners, pervanadate induced a moderate signal decrease, as for GADS, GRB2, and PLCγ1 on the respective LATpY motifs. This decrease was in line with our previously demonstrated concept, that phosphorylation-dependent complex formation masks binding sites of proteins and therefore reduces binding to cognate immobilized phosphopeptides[199]. Remarkably, for GRB2 an increase was observed on SIGpY437, representing an pY-motif of the PLC/SHP subtype. For proteins directly binding to cognate polyP-motifs through SH3 domains, we observed only moderate signal changes, as for example for PLCγ1 binding to SLP179 or Grb2 binding to GAB2-509 [53]. In most cases, these changes were minor signal increases.

In addition, most proteins lacking SH3 domains were also detected on the SH3-binding polyP peptides (Fig. 7.3), suggesting that they were recruited to the array in a complex with a direct binding partner for an immobilized polyP peptide. Remarkably, signal increases for these proteins were much stronger than those of proteins for which direct binding was possible. Signals for which the subtype preference of the respective domain was violated could also originate from the binding of complexes rather than direct interactions. For example, LAT, which has no interaction domains at all, displayed a stimulation-dependent median 74-fold increase of binding of on the polyP peptide SLP228. This binding could be mediated by an SH2/SH3 adapter like GADS or GRB2, which were also detectable, albeit with moderate median signal changes. The LAT-interactor PLCγ1 was detected on SLP228 with a median increase upon stimulation of 4400. Likewise, the increase of the GRB2 signal on SIGpY437 could be explained by a phosphorylation-dependent interaction between GRB2 and SHPTP2, and binding of SHPTP2 to SIGpY437. On LATpY191, the median signal of GADS decreased to 0.7, while the median signals of the GADS-interactor SLP76 and the SLP76-interactor PLCγ1 decreaseḍ to 0.2 of the unstimulated control (Fig. 7.2a). Similar tendencies were found for GRB2 (0.7) and its binder Cbl (0.3), which contains a PTB domain, unlikely to mediate direct interactions with LATpY191 [21].

The absolute signal intensities provided further evidence for the binding of protein complexes to the arrays (Fig. 7.2 c). For lysates of resting cells, immunostaining for PLCγ1 was intense on SLP179 and PAK6 and negligible on SLP228 and GAB2-509. For lysates of pervanadate-treated cells, signals on SLP228 and GAB2-509 were stronger than signals on SLP179 and PAK6. If a mere change in the availability of the SH3 domain of PLCγ1 was the reason for a signal increase, then the signal should increase uniformly on all peptides. The reversal in the order of signal intensities therefore suggests that a portion of PLCγ1 was contained in complexes recruited to the array via the SH3 domain of another protein.

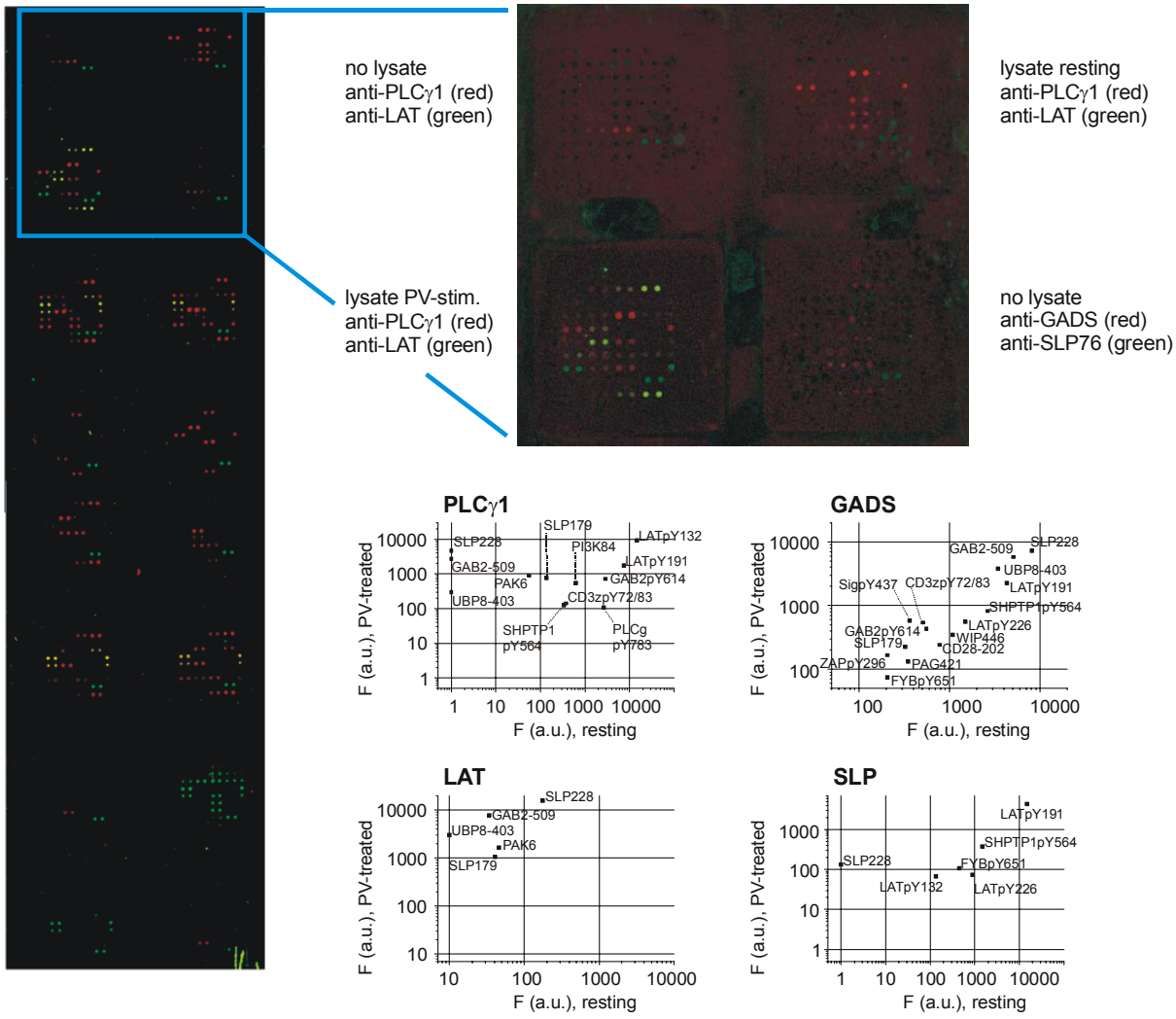

Figure 7.2 a) One coverslip holding 16 identical peptide microarrays, incubated with cell lysates and different antibodies for immunostaining. Each subarray was incubated with lysate of 10^6 Jurkat cells. Green: secondary immunostaining with anti-mouse-Alexa546; red: secondary immunostaining with anti-rabbit-Alexa633. For the total of 31 different immobilized peptides, binding of key proteins in T-cell signal transduction could be detected on 24 peptides, comprising 16 pY-motif peptides, 6 polyP-motif peptides, one PDZ-binding peptide and one WH1-binding peptide. b) Detailed view of the arrays used for determining background binding of anti-PLCγ1 and anti-LAT antibodies, and binding of PLCγ1 and LAT from resting and pervanadate (PV) treated cells. c) Fluorescence intensities F derived for resting and PV treated condition were corrected for background binding of antibodies. Median values of 5 experiments are shown, if in minimum of 4 out of 5 experiments produced a signal above threshold for either one of the stimulated or unstimulated condition. Figure prepared by Oda Stoevesandt.

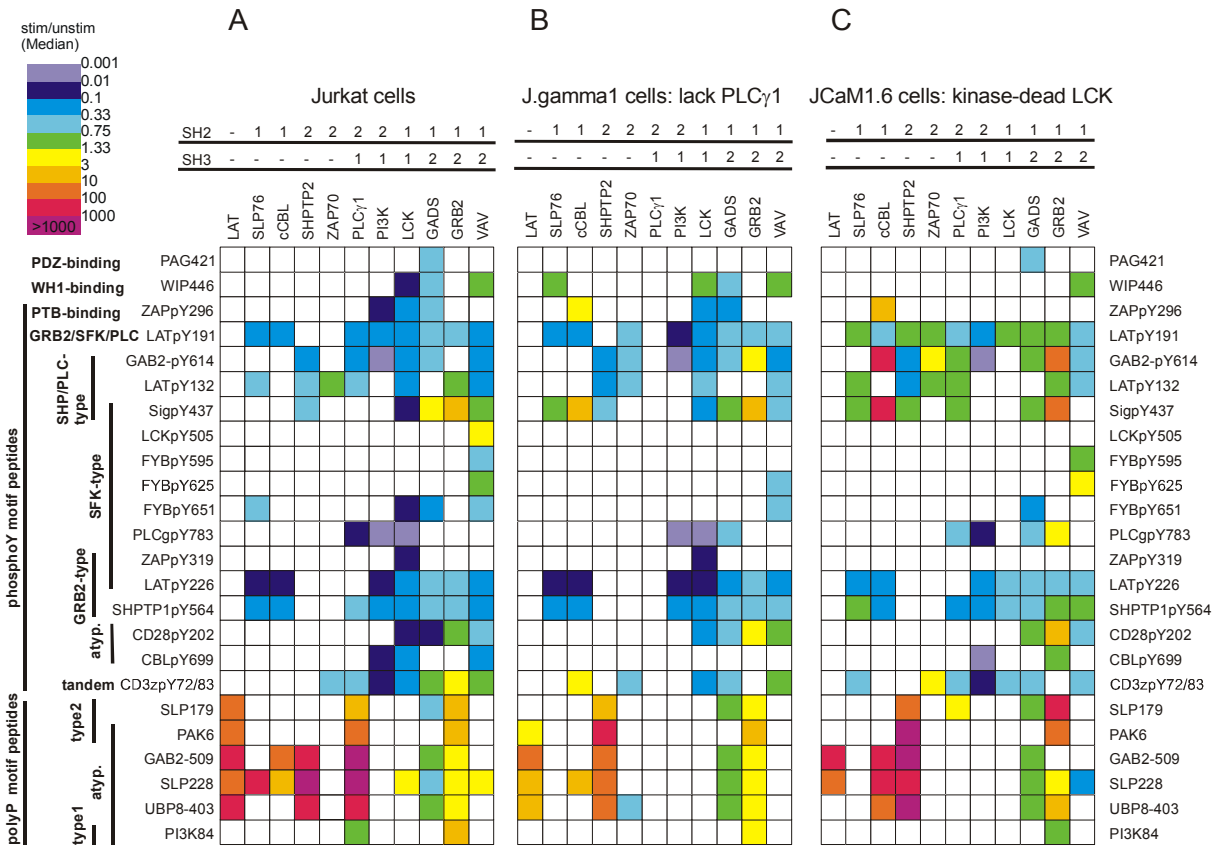

Figure 7.3 Changes in protein signal intensity on the peptide microarrays upon treatment of Jurkat cells and derivative cell lines with sodium pervanadate. Peptides immobilized on the array are plotted vertically, proteins probed by immunostaining horizontally. Above the proteins, their numbers of SH2 and SH3 domains are listed. Ratios of background-corrected fluorescence intensities were calculated for PV-treated to resting cells. a) Jurkat cells. The median ratio of 5 experiments is shown, if a minimum of 4 out of 5 experiments produced a signal above threshold (see Materials and Methods). b) Jgamma1 cells and c) JCaM1.6 cells. The median ratio of 4 experiments is shown, if a minimum of 3 out of 4 experiments produced a signal above threshold.

7.3.4 Dissection of complex architectures by peptide competition and titration. Next we sought to confirm experimentally the binding of complexes on the array and to obtain information on the architecture of these complexes. On the SLP228 peptide spot, we detected GADS, LAT, and PLCγ1 (Fig. 7.4 a). If the proteins were bound as a complete, then incubation with peptides corresponding to individual motif should selectively remove each one, two or all three proteins from the array. We had shown previously, that the PLCγ1-LAT interaction was competed by incubation of lysates with the LATpY132 peptide and less effectively with LATpY191[10]. Peptide concentrations for competition on the arrays were chosen accordingly (Fig 7.4 a). The signals of GADS, LAT and PLCγ1 were all sensitive to SLP228. Upon addition of LATpY191, the signals of LAT and PLCγ decreased, while the signal of GADS was not affected. In contrast to the LAT signal, the PLCγ1 signal was also sensitive to the LATpY132 peptide. Taken together, this suggested the following order of binding: SLP228 directly bound GADS, the SH2 of GADS bound LAT via LATpY191, LAT bound the SH2 of PLCγ1 via LATpY132[27]. Moreover, these results confirm that the binding of PLCγ1 to SLP228 is indirect.

Peptide competition of the signals of GADS, SLP76 and PLCγ1 on the immobilized peptide LATpY191 enabled the dissection of the same set of interactions from yet another perspective (Fig. 7.4 b): All proteins contain SH2 domains. Therefore, instead of binding as a complex, these proteins might bind the peptide independently. Detection of GADS, SLP76 and PLCγ1 was all sensitive to LATpY191. However, only SLP76 and PLCγ1 were sensitive to SLP228. PLCγ1 was also sensitive to SLP179, even though this peptide had some effect on all three proteins. Finally, the sensitivity of PLCγ1 to LATpY132 may suggest that further SH2-interactions stabilize the complex. In contrast to the LAT-containing complex described above, all three proteins were detected on LATpY191 also upon incubation of lysates of resting cells. Inhibitory peptides had similar effect in lysates of resting and pervanadate-treated cells (Fig 7.4 b), indicating the existence of a preformed complex of GADS, SLP76 and PLCγ1. However, the effect of all disrupting peptides on PLCγ1 was weaker in lysates from resting cells, suggesting that direct binding of PLCγ1 to immobilized LATpY191 accounted for a larger part of the signal than after stimulation.

Titration with the peptides LATpY132 and LATpY191 yielded further information on the organisation of signalling complexes through comparison of titration curves obtained (i) for several proteins on the same array spot, or (ii) for one protein on a range of arrayed peptides (Fig 7.4 c). (i) For LAT and PLCγ1 on the SLP228 spot, signal losses upon addition of LATpY191 occurred with the same concentration dependence, while for LATpY132 only PLCγ1 dissociated, supporting the binding order inferred from the simple peptide competition experiment (Fig. 7.4 a). (ii) Upon titration with LATpY132, PLCγ1 fully dissociated from GAB2-509 and SLP228 (atypical SH3-binding motifs), but only partially from PAK6 and SLP179 (type 2 SH3-binding motifs), suggesting different modes of PLCγ1 binding. On SLP228, indirect binding of PLCγ1 as a part of a large complex can be assumed as shown by the competition experiment (Fig. 7.4 a). SLP179 represents a favoured binding motif of PLCγ1 SH3 domains. Still, titration with pY-peptide decreased the signal of PLCγ1, suggesting a role for the SH2-domain of PLCγ1 in the stabilization of binding to the array.

7.3.5 Effect of single protein deficiency on the interaction network. The titration experiments had revealed the significance of individual interaction motifs for the functional organisation of the network. Next, we examined the impact of a loss of a multidomain protein on the organisation of the network, using the PLCγ1-deficient Jurkat-derivative JGamma1 [200].

Loss of PLCγ1 affected the formation of various complexes, notably on the preferential PLCγ1-interacting peptides. SLP76 on LATpY132 and LAT on SLP179 became undetectable, supporting the role of PLCγ1 for their recruitment in Jurkat cells. To analyze the role of PLCγ1 in complex formation, ratios of signal intensities from JGamma1 to Jurkat lysates were calculated for resting and stimulated cells (Fig.7.5). For proteins supposed to bind directly to immobilized peptides (e.g. GADS and GRB2 on LATpY191 and SLP228), only marginal changes were observed. However, PLCγ1-deficiency strongly inhibited phosphorylation-dependent recruitment of LAT to polyP peptides. Furthermore, in JGamma1-lysates, SHPTP2-signals on polyP-peptides were increased compared to WT Jurkat lysates, with no significant differences of SHPTP2 expression detected by Western Blot. As the SH2-domains of SHPTP2 and PLCγ1 share a

common consensus motif, the lack of competing PLCγ1 may enable increased binding of SHPTP2.

The Jurkat derivative cell line JCAM 1.6 displays no LCK activity, due to a mutation affecting the kinase domain of LCK [201]. JCaM1.6 cells were used as a model for generally impaired TCR-downstream signalling capacity. For JCAM1.6 cells (7.3 c), the predominant signal decrease observed on pY peptides for Jurkat cells (Fig. 7.3 a) was largely missing, agreeing with the role of LCK in starting a phosphorylation cascade. A similar reduction of the decrease of PLCγ1 binding to LAT pY-peptides was also observed for cells pretreated with the SFK-Inhibitor PP2 before PV stimulation (not shown). Effects of LCK deficiency were observed for ZAP-70, a binding partner of activation motifs phosphorylated by LCK, and for proteins further downstream the kinase cascade, such as the ZAP-70 substrates SLP76 and LAT. PLCγ1 became undetectable on most polyP peptides, likely due to missing phosphorylated LAT and SLP76 as mediators of binding. By contrast, pervanadate-dependent recruitment of SHPTP2 to polyP peptides was not affected. This suggests an LCK independent, but phosphorylation-dependent formation of a complex between SHPTP2 and an SH3-SH2 adaptor protein.

.

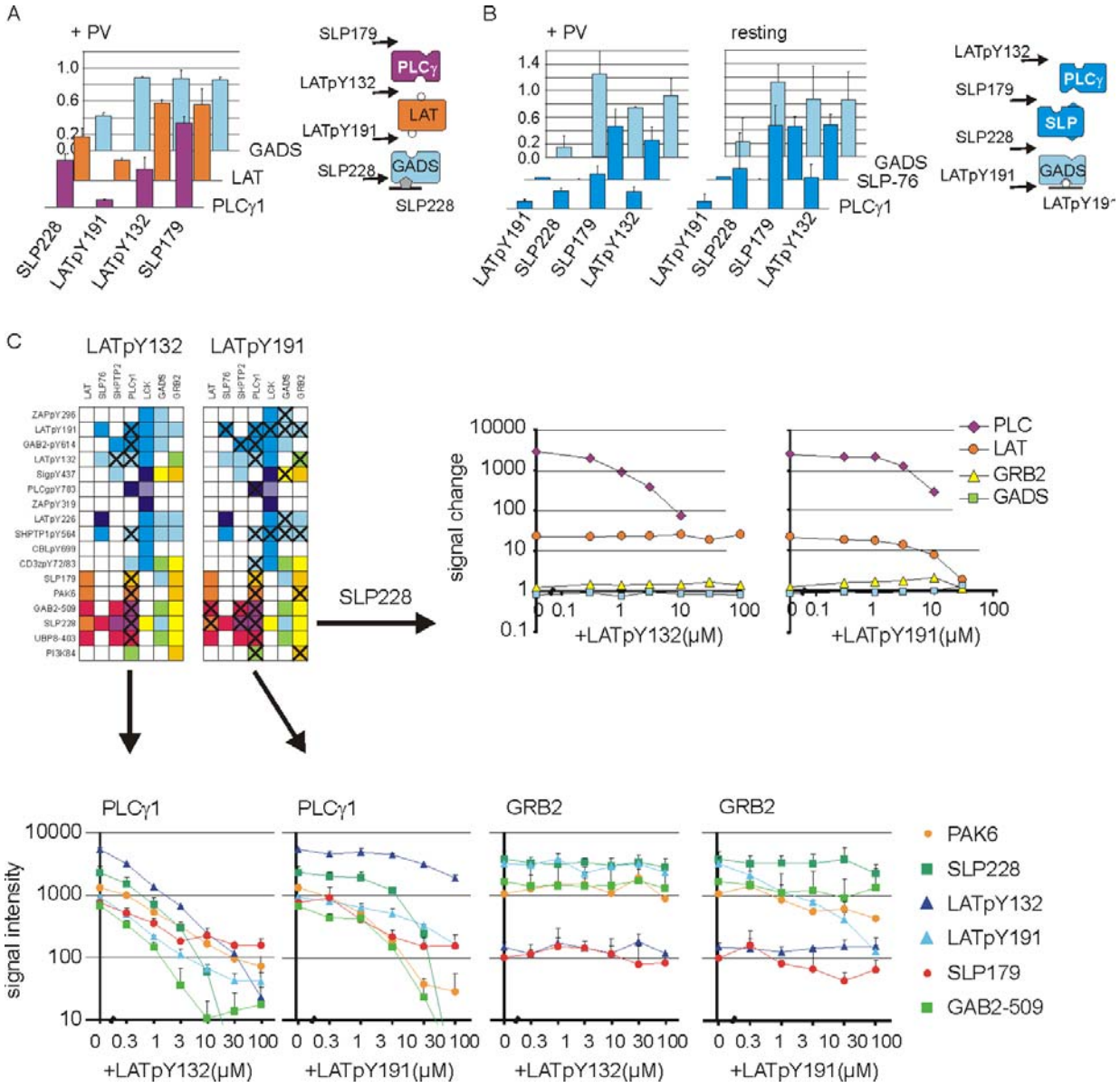

Figure 7.4 Effects of signalling peptides on the detection of proteins in a complex on the array. Jurkat T cells were treated with 0.5 mM pervanadate and lysed in presence of the interactor-peptides in the following concentrations, unless indicated otherwise: (LATpY191 (20 µM), LATpY132 (0.5µM), SLP228 (20 µM) and SLP179 (20 µM)). A) Effects of the different peptides (x axis) to protein detection on the SLP228 peptide B) the LATpY191 peptide under the influence of different interfering peptides. For A and B, relative changes in protein signal compared to the control without peptides are indicated. C) Titration of different proteins associated to the signalling peptides with the LATpY132 and the LATpY191 peptide. A cross represents a signal decrease under the influence of the respective peptide for more than 50 %. The example right to the colour plot represents the recruitment of different proteins to the SLP228 peptide, while that under the colour plot represents that for PLCγ1 on different polyP peptides. On the graphs, the relative signal change to the unstimulated control is given on the y axis.

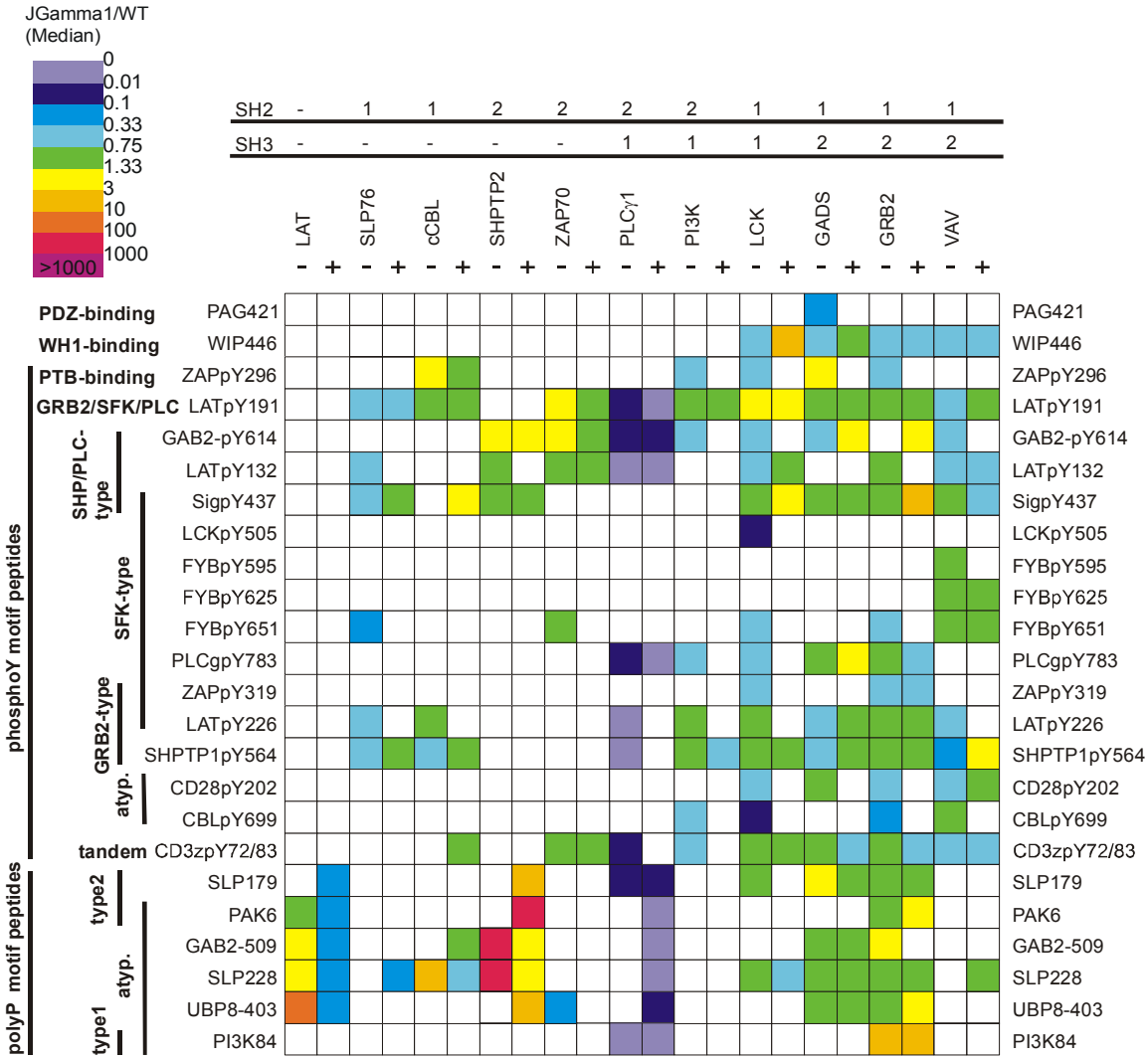

Figure 7.5 Changes in protein signal intensity on the peptide microarrays between PLCγ1 deficient JGamma1 cells and "wildtype" Jurkat cells, expressed as background-corrected ratio JGamma1/WT. Lysates of resting (-) and pervanadate-treated (+) cells were used. The median ratio of 4 experiments is shown, if a minimum of 3 out of 4 experiments produced a signal above threshold.

7.3.6 Stimulus-dependence of protein interactions in T cell activation. We next employed the peptide arrays to profile the time course of protein complex formation in a more physiological model of T cell activation. Jurkat cells were stimulated for variable times with stimulatory anti-CD3 antibodies (clone OKT3), costimulatory anti-CD28 (clone 9.3), or both. On the arrays, distinct and reproducible changes in signal profiles were obtained for PLCγ1, LAT, SLP76 and PI3K (Fig. 7.6). For PLCγ1, signal increases on polyP peptides were strongest after 2 min of CD3-stimulation, and then diminished. Only on SLP228, CD28 stimulation alone induced slight increases in PLCγ1 recruitment. CD3-CD28 costimulation augmented signal increases compared to CD3 stimulation without affecting their kinetics. For LAT, analogous signals were observed for CD3 stimulation, suggesting fast pY-dependent complex-formation with PLCγ1 and corecruitment to the array. For SLP76, signal decreases on LATpY peptides were detected upon CD3 stimulation. Interestingly, this decrease was most pronounced after 10 min of stimulation, indicating that recruitment of SLP76 to the LAT complex occurred with a slower kinetics than the phosphorylation of LAT and recruitment of PLCγ1. In the presence of antiCD28, signals of murine detection antibodies could not be quantified because of high overall backgrounds, accounting for the data points missing for LAT and SLP. For PI3K, no systematic signal changes were observed upon stimulation with CD3 or CD28 alone, whereas costimulation led to a signal decrease. Pervanadate stimulation was conducted in parallel as a positive control, yielding signal changes consistent with the antibody effects. Pervanadate effects were weaker than in the experiments presented above (Fig. 7.3). Antibody stimulation required preincubation on ice, a condition that apparently also affected pervanadate-dependent cell activation.

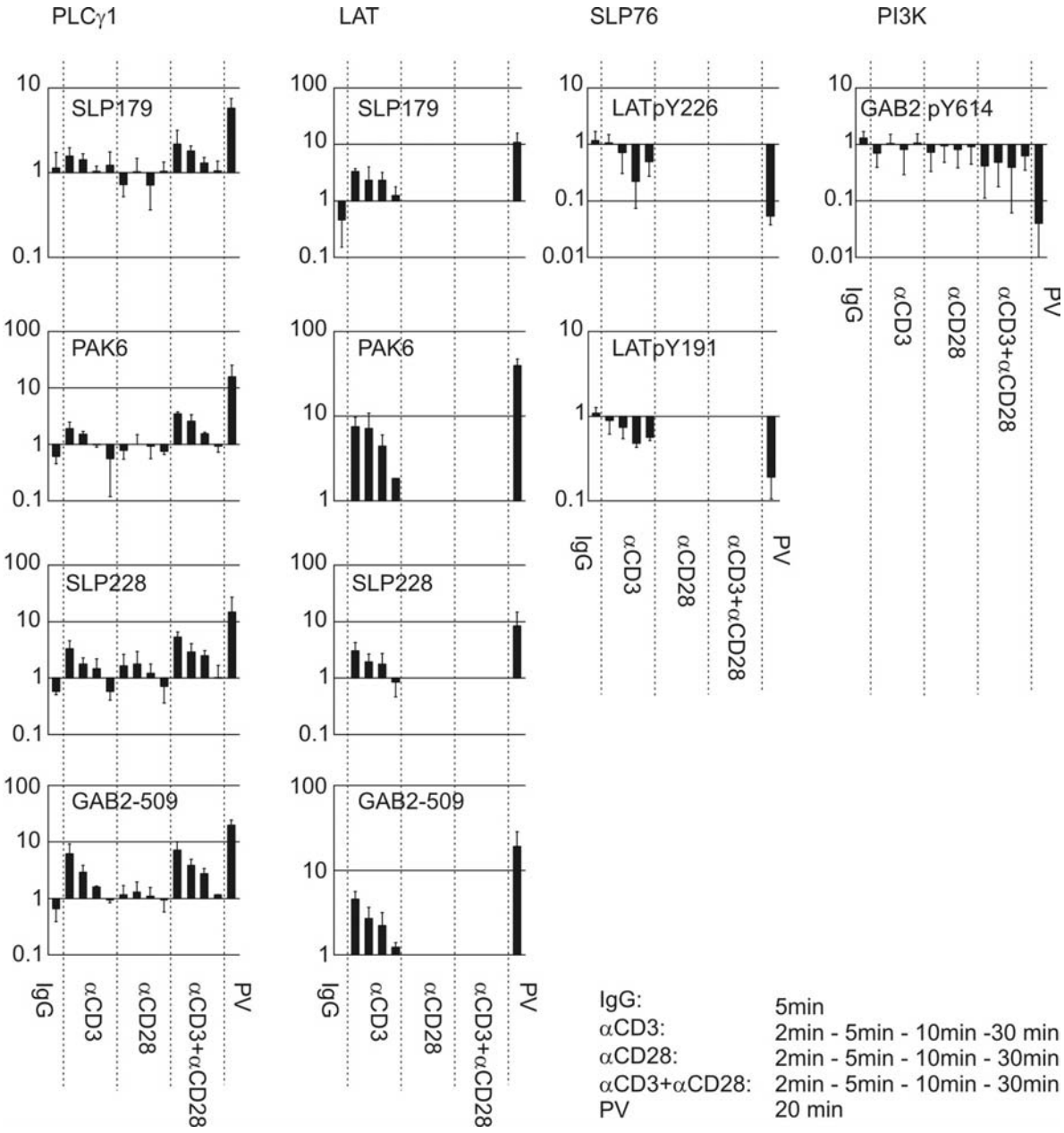

Figure 7.6 Signal changes on the peptide microarrays following treatment of Jurkat cells with stimulatory antibodies against the TCR/CD3-complex (αCD3) and the CD28 coreceptor (αCD28) for different time points. Ratios of stimulated versus resting cells. Negative control by mock-stimulation with an isotype antibody (IgG), positive control by incubation with 0.5 mM pervanadate (PV). Signals for the protein indicated on top of each column of graphs, derived from the peptide spot indicated in each graph. Means and mean deviations of the mean of 3 experiments.

7.4 Discussion

Signalling processes downstream of transmembrane receptors typically occur in a timeframe of minutes through rearrangement of a given repertoire of signalling components. While signal-induced fast degradation of single components may occur, the levels of most components remain unchanged and expression of further components is still far downstream. However, the molecular interactions of signalling components change significantly. We demonstrate how these changes in interaction can be detected in cell lysates using peptide microarrays.

We have shown previously that change in the availability of a protein domain involved in a signalling-dependent protein-protein interaction can be detected by a capture peptide probing for the availability of the binding domain [199]. This approach was now generalized for the parallel detection of different interactions. In addition, we exploit that proteins directly binding to capture peptides bring along their interaction partners, making microarrays a highly parallel variant of co-purification techniques. In a typical experiment (Fig. 7.6), proteins bound by 24 capture peptides were probed with 8 different antibodies under 16 different conditions, yielding 3072 data points for the analysis of interactions in T cell signalling using only 10^6 cells per array. In contrast to high throughput tag-based affinity purifications, the array-based approach does not require the introduction of recombinant components into the signalling network. Therefore, the molecular system under scrutiny is not already manipulated before the experiment begins.

On the molecular level, inducible tyrosine phosphorylations trigger the onset of complex formation. Therefore, additional pY sites generated through stimulation compete for SH2-proteins with the pY peptides on the array, while the total cellular level of polyP motifs is not changed through stimulation. This may explain a general trend we observed for stimulation-dependent signal changes on the arrays: On pY peptides, signal decreases were dominant, while on polyP peptides signal increases dominated.

Especially on polyP peptides, we detected proteins without a cognate binding motif. Indeed, we were able to dismantle supposed complexes on the arrays in a stepwise and dose dependent manner through competition and titration with peptides corresponding to binding motifs between the proteins in the complex. This finding demonstrates, that detected proteins need not interact directly with the peptide, but may instead be brought along by another protein directly binding the peptide.

In lysates of resting cells, we detected the presence of polyP-SH3 domain mediated preformed complex 'nuclei'. For example, on LATpY132, representing a direct binding motif for PLCγ1, we observed stimulation-dependent decreases to the binding of PLCγ1 and SLP76 in Jurkat lysates. In lysates of PLCγ1-deficient Jurkat cells, both proteins were not detectable on LATpY132, suggesting PLCγ1-dependent recruitment of SLP76. For LCK-defective cells, both proteins were detectable, but their signals did not decrease upon stimulation. On LATpY191, corresponding observations were made for the preformed complex of GADS and SLP76. Taken together, these observations suggest that upon stimulation, the preformed complexes contributed to the assembly of larger, phosphotyrosine-dependent signalling complexes.

We realized that complex architectures inferred from the peptide competition experiments were correlated to the different magnitudes of signalling-dependent signal changes for the different proteins detected on a given peptide. The more distant from the peptide, the more pronounced was the relative signal change for the protein (Fig. 7.4, Fig. 7.7). Assuming a linear chain of protein-protein interactions, this observation can be explained by the potentiation of changes from one level of protein binding to the next: If each of the interactions contributing to a linear complex on the immobilized peptide (peptide-A-B-C) occurred with a different probability after stimulation (peptide-A changing x-fold, A-B changing y-fold, B-C changing z-fold), then the chance to find the outermost protein C on the immobilized peptide would change x*y*z-fold. Per se, x, y, and z may each be larger or smaller that 1. While situations are conceivable where the increases and decreases balance, we found that the relative magnitude of signal changes as described above was a useful indicator of the interaction architectures.

For the interplay of stimulation of TCR/CD3 and CD28 by stimulatory antibodies, our peptide microarrays allowed the analysis of timecourses of protein complex formation in a parallel manner. We demonstrate that the recruitment of SLP to the LAT signalosome follows a different timecourse than the recruitment of PLCγ1. Recently, an analysis of phosphorylation kinetics in early T-cell signalling showed, that phosphorylation of LAT-residues Y132 and Y191 reaches maximum levels within two minutes [17].

Our data shows that the arrayed LATpY191 is maximally competed by its cellular counterpart after 10 minutes of stimulation, suggesting that LAT-phosphorylation is not the rate-limiting step for formation of the LAT-signalosome. Co-stimulation with anti-CD28 and anti-CD3 led to more distinct, and additional signal changes concerning PI3K,

compared to CD3 stimulation alone. This finding demonstrates the potential of the peptide microarrays for integrated network analysis in systems with multiple stimuli. Likewise, for the analysis of signalling systems missing single proteins, peptide arrays provide a means to uncover effects of molecular links on interaction subsystems.

In conclusion, peptide microarrays provide a tool for the highly parallel analysis of protein-protein interactions in cellular signal transduction, bridging the gap between binding studies with single proteins and complex interactomics experiments. Quantitative analysis of signal changes upon stimulation and competition experiments provide a wealth of information on the functional organisation of protein complexes. This approach will benefit from the use of arrayed peptide libraries derived from the literature as well as by motif prediction [202;203]. In combination with antibody libraries, the simultaneous probing for all potential molecular interactions in a molecular signalling network can deepen our understanding of signal transduction in a systems biological view.

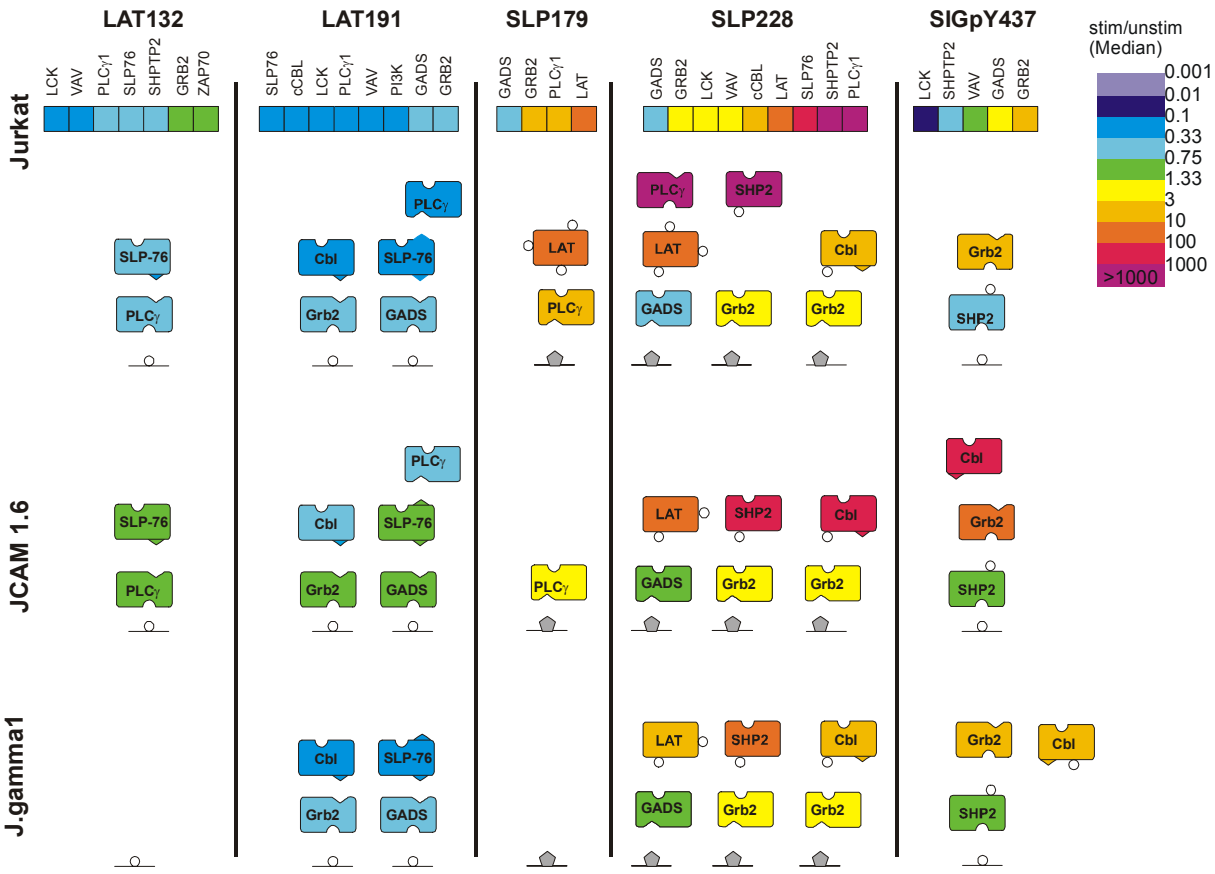

Figure 7.7 Schematic diagram for selected proteins detected on the arrays and their proposed hierarchy of binding based on the relative signal change upon pervanadate treatment of cells (represented by the colour of proteins, taken from Fig. 7.4). The immobilized peptides are depicted at the basis of the protein stacks. White circles depict a phosphorylation-dependent binding motif, grey pentangle a polyP motif.

8. Experimental procedures

8.1 General

8.1.1 Inhibitors. ML-3403 was supplied from Stefan Laufer (University of Tübingen). PP2 and piceatannol were from Calbiochem (Schwalbach, Germany), Cytochalasin D, Ro-31-8220, SB-203580, Alsterpaullone, PD98059 and LY-294002 from Sigma (Taufkirchen, Germany). FK506 was purchased from LC Laboratories, Woburn, MA, USA. All inhibitors were added as indicated from freshly prepared aqueous solutions prepared from DMSO stock solutions, and added to the cells 15 min before the initiation of stimulation, unless indicated otherwise. Common chemicals of analytical grade were purchased from Sigma-Aldrich and Merck, Darmstadt, Germany.

8.1.2 Stimulatory antibodies. The stimulatory anti-CD3 (clone OKT3) and anti-CD28 antibodies (clone 9.3) were purified by Protein A affinity chromatography (Pharmacia, Freiburg, Germany). rM28, a recombinant single chain FV bispecific antibody-fragment directed against CD28 and a melanoma-associated proteoglycan (MAPG) was purified from the supernatant of the stably transfected mouse myeloma cell line Sp2/0 by Protein L affinity chromatography (Perbio, Bonn, Germany). All antibody solutions were dialyzed against PBS and stored at 4°C after filter-sterilization (0.22 μm). All stimulatory antibodies against human epitopes used for this study were produced by Ludger-Grosse Hovest and Gundram Jung.

8.1.3 Cell culture. For the analysis of T cell activation, we used the Jurkat human T cell leukemia cell line[133]. Using random mutagenesis, various Jurkat-derived mutants deficient for key signalling molecules have been generated. Moreover, Jurkat cells are deficient for the phosphatases SHIP (SH2-domain-containing inositol polyphosphate 5' phosphatase) and PTEN ((phosphatase and tensin homologue), [204]. While the effect of SHIP deficiency on T cell signalling is still unclear, PTEN deficiency might induce a hyperactivity of the PI3K signalling pathway [205;206]. However, the function of PI3K in early T cell signalling is still poorly understood. Jurkat cells, the LCK-deficient derivative JCaM 1.6 [201] and the PLCγ-deficient derivative line J.gamma1 [200] (ATCC, Manassas, VA,

USA;were cultivated in RPMI 1640 (PAN, Aidenbach, Germany) supplemented with 10% fetal calf serum (FCS; PAN). at 37°C/5% CO_2 Expression of CD3 and CD28 surface antigens was validated using anti-CD3 (clone OKT3) and anti-CD28 (clone 9.3; both antibodies were kindly provided by G. Jung, Institute for Cell Biology, Tübingen, Germany) at a concentration of 2 μg/ml for 1 h at 4°C each.with subsequent detection by flow cytometry (BD FACSCalibur System, Becton Dickinson, Heidelberg, Germany) using an Alexa 488 goat anti-mouse secondary antibody (2 μg/ml). 3A9 hybridoma T cells and derivatives were cultured in Dulbecco's modified Eagle's medium (DMEM) supplement with 10% FCS (PAN, Aidenbach, Germany), 100 μM sodium pyruvate, non-essential amino acids, 45 nM β-mercaptoethanol, 200 μM L-glutamine, 100 U/ml penicillin, and 100 μg/ml streptomycin [207]. Plat-E packaging cells were cultured with the addition of 1 μg/ml puromycin and 10 μg/ml of blasticidin. Supplements were from Gibco BRC (Karlsruhe, Germany) and Sigma (Deisenhofen, Germany). Jurkat JCaM1.6 and derived cell lines were cultivated in RPMI 1640 (PAN) with 10 % FCS [208]. Cell vitality after inhibitor incubation was controlled using an MTT assay.

8.1.4 Generation and characterization of 3A9-fusion protein cell lines.

To insert EYFP into the retroviral expression vector pMFG, the *SacI- NotI* fragment from the EYFP-N1 vector (Clontech, Heidelberg, Germany) containing the EYFP coding region was ligated into the *SacI-NotI* site of pBluescript KS^+. The EYFP coding region was then recovered as a *NcoI-BamHI* fragment and cloned into the corresponding unique sites of the retroviral vector pMFG [209]. The murine ZAP-70 gene was amplified by PCR from murine thymic cDNA using the forward primer: `5'atacatgtccgatcccgcgg-cgca` containing an *AflIII* restriction site at its start codon. The reverse primer: `5'ccacatgttggccgatcccccaccgccagacccgccacatg cagcctcggccac` includes the last 6 codons of ZAP-70 fused to a linker sequence (GGSGGGGSAN) and an *AflIII* restriction site. The PCR product was purified, ligated into pGEM-TZ and sequenced (Genome Express, Grenoble, France). The ZAP-70 *AflIII* fragment was recovered from pGEM-TZ and cloned into the *NcoI* site of pMFG-YFP to give ZAP-70 with a C-terminal fusion of YFP (ZAP-70-YFP). The CD3ζ-CFP fusion was derived from a pMFG-CD3ζ-YFP (pAPVR1, M. Malissen, CIML) construct by exchanging YFP for CFP via unique *NcoI-NotI* sites. 3A9 hybridoma T cells were infected with retrovirus

generated with the pMFG vector via the Plat-E packaging cells as described by Morita [210]. YFP fusion protein expression was monitored by flow cytometry 48 h post infection. Cells were expanded, sorted by flow cytometry and sub-cloned by limiting dilution. For double labeling with CD3ζ-CFP, the wild type 3A9 cells were first infected with CD3ζ-CFP DNA, as described above. Immediately after infection, cells were cloned by limiting dilution. Clones expressing labeled CD3ζ-CFP at the plasma membrane were selected by visual inspection under an epifluorescence microscope. These clonal populations were then infected with pMFG-ZAP-70-YFP, sorted for YFP expression and subcloned. To verify the integrity of the YFP and CFP chimeras expressed in the 3A9 cells, post nuclear cell lysates were prepared, run on 10 % SDS-PAGE, transferred to PVDF membrane and probed for GFP expression using an anti-GFP mAb (Clontech) followed by using donkey anti-mouse HRP conjugate (Immunotech Beckman Coulter, Fullerton, USA) and ECL / autoradiography. Anti-phosphotyrosine mAb 4G10 was a kind gift of Dr. H.-T. He, CIML, Marseille, France.

8.1.5 Western Blots and coimmunoprecipitation. In order to analyze the cellular ZAP-70-YFP content at different time points of cell stimulation, $2.5*10^5$ cells per coverslip were stimulated as described above for a given time and lysed ($5*10^6$ cells/ml) in lysis buffer (1 % Triton X-100, 20 mM Tris, 1mM EDTA, 150 mM NaCl, 1 mM Na_3VO_4, protease inhibitor cocktail (Roche, Mannheim, Germany), pH 7.5) on ice for 30 min. The crude lysates were clarified by centrifugation at 20,000 x g for 15 min, separated by SDS-PAGE on a 10 % polyacrylamide gel [211] and transferred to a PVDF membrane. The blots were probed for ZAP-70 expression using a ZAP-70-YFP antibody (BD Transduction Labs, Franklin Lake, USA) in combination with a goat anti-mouse alkaline phosphatase conjugate for detection (Sigma). In order to analyze the activation-dependent recruitment of ZAP-70 to the CD3/TCR complex, cells were stimulated as described above. Anti-CD3ε antibodies (final concentration of 10 μg/ml) and μMACS-beads functionalized with protein G (Miltenyi Biotec, Bergisch Gladbach, Germany, dilution 1:20) were added to the lysates. Samples were incubated on ice for 20 h and precipitated by centrifugation. The pellets were washed twice with lysis buffer and once with PBS, and analyzed on a Western Blot as described above.

8.1.6 ELISA. For the quantitation of IL-2 expression under the influence of different inhibitors, 200 µl per well of Jurkat cell suspension ($6.25*10^5$/ml) was added to a freshly prepared aqueous antibody solution of the inhibitor and preincubated at 37°C for 15 min. For stimulation, a Falcon 3075 ELISA plate was coated for 2 h at 37°C with 5 µg/ml each of anti-CD3 (OKT3) and anti-CD28 (9.3), blocked with 1% BSA/PBS for 15 min, washed with PBS. Cells were stimulated for 16 h at 37°C. The anti-IL-2 ELISA was performed on a 96 well ELISA plate (Greiner, Frickenhausen, Germany), using a pair of capture/biotinylated detection antibodies from BD Pharmingen (San Diego, USA).

8.2 Imaging of cells in contact with immobilized stimuli

8.2.1 Production of surfaces for antibody immobilization. For functionalization of 12 mm coverslips (Fluka, Seelze, Germany) with 3-(glycidyloxypropyl)trimethoxysilane (GOPTS) enabling covalent binding of proteins, coverslips were cleaned with 1 M NaOH for 30 min. Then, the coverslips were treated with freshly prepared Piranha solution (mixture of 30 % hydrogen peroxide and concentrated sulphuric acid at a ratio of 2:3 (v/v); Caution: Highly aggressive!) for 30 min, washed with H_2O, and dried before being overlayed with GOPTS (100 %, or 2.5 % in ethanol) for 1 h. Then, coverslips were washed with ethanol and subsequently overlayed with the protein to be immobilized. In order to produce a hydrophobic surface for the noncovalent binding of antibodies, coverslips were silanizedwith trimethoxy-octadecylsilane in the same manner as described previously [212].

8.2.2 Antibody microarray procedures. Antibody microarrays were generated by pipetting (6 nL/spot) solutions of antibodies in 300 mM sodium phosphate buffer, pH 8.5 with 0.005% Tween-20 (Fluka) 0.01% BSA (Sigma, Steinheim, Germany) and 0.5% trehalose (Sigma) on hydrogel microarray substrates (Slide H, Schott, Jena, Germany) using a piezo-electric nanopipettor (NP2.0 GeSiM, Dresden, Germany) at dew point (16°C). As a negative control 100 µg/ml poly-L-lysine (MW 150,000-300,000; Sigma) was used. rM28 was spotted at a concentration of 50 µg/ml. Subsequently arrays were stored for 16 h at 4°C with 70% relative humidity. Afterwards, arrays were washed for 5 min with PBS containing 0.5% Tween-20, then for 2x5 min with PBS. Subsequently,

reactive groups were quenched with 50 mM ethanolamine (Sigma) in 50 mM borate buffer, pH 8 for 1 h. After three washes with PBS, the surface was blocked with 0.1% BSA for 15 min.

8.2.3 Cellular antibody stimulation experiments. For parallel processing of several microarrays, a 16-well superstructure (ProPlate Multiarray System, Grace Biolabs, Eugene, OR, USA) was clamped onto the hydrogel slide. Cells suspended in serum-free RPMI medium ($5x10^5$ cells/ml) were preincubated with inhibitor for 15 min at 37°C before being added into the well. After 60 min at 37°C/5% CO_2 the medium was removed, cells were fixed with 4% PFA in PBS, first for 10 min at 4 °C, then for 15 min at room temperature, and washed 3 x with PBS. In order to quantify the spreading of the cells on the surface, the surface not shielded by adherent cells was stained by incubation with an Alexa546-labeled anti-mouse antibody (Molecular Probes, Eugene, OR, USA) 4 μg/ml in PBS, 0.1% BSA) 30 min at room temperature. For visualization of NFAT translocation cells were then washed with PBS, permeabilized with saponin buffer (PBS, 0.1% saponin (Sigma), 0.1% BSA) and incubated with a FITC-labeled anti-NFAT IgG (BD Pharmingen, 1.25 μg/ml) in combination with the nuclear stain TOPRO (Molecular Probes, 100 nM) for 30 min in saponin buffer. After washing 3 x with saponin buffer, samples were fixed with 4% PFA for 15 min, and washed 3 x with PBS. Subsequently, the superstructure was removed and the arrays were embedded in anti-fading reagent (10% Mowiol, Aventis, Frankfurt, Germany, in 100 mM Tris-HCl, pH 8.5, and 25% glycerol [213]) and sealed with a coverslip.

8.2.4 PDMS stamps. Stamp masters were designed and produced by Günter Roth, and stamps manufactured by Günter Roth and Alexander Ganser. The procedures for the generation of the stamp master PDMS stamps are adapted from [214]. The production of the PDMS stamp (Fig. 8.1) started with the demolding of the stamp master by deposition of perfluorinated alkyl-trichlorosilane, such as (1-H, 1-H, 2-H, 2-H)-Perfluorodecyltrichlorsilane SIH5841.0 (ABCR). A few drops of the perfluorodecyltrichlorsilane were put in a small plastic container and put together with the stamp master into an exsiccator, which was subsequently evacuated under a hood, and left standing for 10 minutes. A 10:1 mixture of PDMS Sylgard 184 silicone elastomer and the respective curing agent (Dow Corning, Midland, MI, USA) was prepared, and degassed

in an exsiccator. The mixture was poured into a hydrophobic Petri dish containing the master up to the desired level, remaining in a horizontal position. After escape of the air bubbles, the PDMS was polymerized by incubation at 60°C for 20 h. After peeling the stamps off the master, the desired PDMS stamps were cut out and overlayed with stimulatory antibodies of a total concentration of 100 µg/ml, plus 15 µg/ml Alexa 546-labelled anti-mouse IgG (Molecular Probes) for 1 h to generate a protein monolayer on the surface. Then, supernatant was removed, stamps thoroughly washed with Millipore H_2O, and dried in an air-stream. Stamps were then placed on polished glass slides (Marienfeld, Lauda-Königshofen, Germany) that had been thoroughly cleaned by ethanol and aceton (p.a.). The stamp was softly pressed onto the slide so that adhesion was visible, and left there for 20 s. Then, stamps were removed, the printed area sealed with Gene Frames (Peqlab, Erlangen, Germany) and slides quickly overlayed with antibody solution or blocking buffer (1% BSA inPBS), each step for 30 min. 200 µl of cell suspension ($2*10^6$ cells/ml) was added to the arrays. The following steps of fixation and permeabilization were as described above. Cells were stained with 5 µg/ml anti-phosphotyrosine antibody (Cell Signalling, Danvers, MA, USA) for 1 h , which had previously been labelled according to the manufacturer's direction with Zenon-Alexa 633 (Molecular Probes), and surface-associated mouse IgG antibody detected by staining with Alexa 488-labelled goat anti-mouse IgG (2 µg/ml). Following permeabilization and fixation, slides were mounted with MOWIOL with a glass coverslip. Imaging was performed as described for protein clustering at a resolution of 1024 x 1024 pixels using a C-Apochromat 63 W x 1.2 NA water immersion objective.

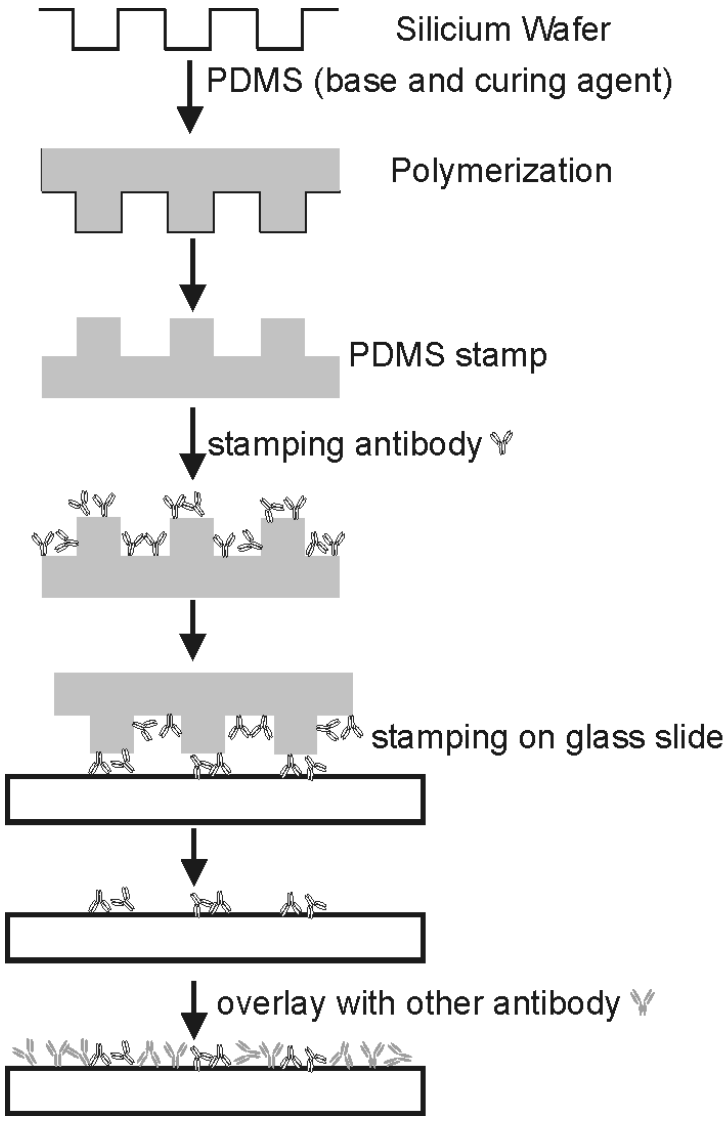

Figure 8.1 Schematic of the generation of microstructured surfaces.

8.2.5 Fluorescence microscopy of living cells. For live cell microscopy of 3A9 cells, silanized coverslips were coated with 200 µl 5 µg/ml anti-mouse CD3ε mAb (mAb145-2C11, BD Pharmingen) for 16 h at 4 °C. After coating, the surface was washed twice for 5 min with phosphate-buffered saline (PBS) followed by blocking with PBS containing 1 % bovine serum albumine (BSA) for 30 min at RT. Finally, coverslips were washed three times 5 min with PBS and stored at 4 °C until use. For control experiments, silanized slides were left uncoated, coated with BSA (Sigma) or with poly-L-lysine (Sigma). Confocal microscopy of living cells was performed on an inverted LSM 510 laser scanning microscope (Carl Zeiss, Göttingen, Germany) using a C-Apochromat 63 x 1.4 Oil lens (Carl Zeiss) in a custom-made chamber, using CO_2-independent serum-free DMEM (Gibco). YFP was imaged by excitation at 514 nm and detection with a BP 530-

600 nm band pass filter. For the parallel detection of CFP and YFP, the spectrally resolving META detector of the instrument was also used. CFP was excited at 458 nm and detected at 465-518 nm when using the META detector or with a BP 475-525 band pass filter. YFP was excited at 514 nm and detected at 518-604 nm when using the META detector or with a 530-600 band pass filter. For parallel detection of YFP and Cy5 the 514 nm line of the Argon ion laser and the light of the 633 nm HeNe laser were directed over an HFT 514/633 beam splitter in combination with an NFT 635vis beam splitter and a BP 530-600 band pass filter for YFP detection and an LP 650 long pass filter for detection of Cy5.

8.2.6 Immunofluorescence. After cell stimulation on the surfaces at 37 °C, cells were fixed with 3.7 % PFA in PBS first for 10 min at 4 °C, then for 15 min at RT, followed by washing and permeabilization with PBS containing 0.2 % saponin (Sigma) and 0.1 % BSA (saponin buffer). For the quantification of cell spreading on the surface, the surface not shaded by adherent cells was visualized using an Alexa546 labelled anti-mouse antibody (4 μg/ml in PBS, BSA (0.1 %), Molecular Probes) or Cy5 labelled anti-Armenian hamster antibody (3 μg/ml), Dianova) directed against the immobilized stimulatory anti-CD3 and anti-CD28 antibodies for 30 min before permeabilization. Incubations with antibodies were carried out for 1 h at RT in saponin buffer. Actin was detected using biotin-labelled phalloidin (50 μg/ml, Alexis, Grünberg, Germany) in in combination with 1:1500 Cy5-streptavidin (Dianova) or using Cy5-labelled phalloidin (5 U/sample, Molecular Probes) in saponin buffer. After washing with saponin buffer samples were fixed once more with PFA for 15-20 min, washed three times with PBS, and embedded in MOWIOL [213]. For the detection of intrinsic fusion protein fluorescence, remaining fixative was quenched by 3 washes with 100 mM Tris-acetate buffer (pH 8) for 5 min prior to mounting in Mowiol (Fluka).

8.2.7 Image acquisition and data analysis for cell spreading and NFAT translocation. Immunofluorescence microscopy performed on an inverted LSM 510 confocal laser scanning microscope (Carl Zeiss, Göttingen, Germany) using a Plan-Neofluar 40 x 0.75 NA lens for non confocal and a C-Apochromat 63 x 1.3 NA oil immersion objective or a C-Apochromat 63x water immersion objective for confocal imaging (both objectives from Carl Zeiss). Alexa 488/546 and Cy5/TOPRO fluorescence

were detected using a filter set consisting of an HFT UV/488/543/633 beam splitter in combination with an NFT 635 VIS beam splitter, a BP 560-615 detection filter for Alexa 546, a BP 505-550 detection filter for Alexa 488, and an LP650 long pass filter for Cy5. Image analysis of NFAT translocation was performed using Metamorph (Universal Imaging, Downingtown, PA, USA). For each cell, nuclear translocation of NFAT and cell attachment were quantified using a specially designed macro (Fig.8.2). Determination of NFAT translocation followed general protocols for the quantification of protein translocation [99]. A TOPRO-staining beyond an arbitrary threshold was used to generate a mask for the area of the nucleus. In order to get comparable nuclear masks between different images, it is necessary to adjust the intensities of the TOPRO fluorescence already during imaging. The nuclear mask shrunk with the erode command to generate a closed area representing the nucleus (mask N), but containing also small parts of the extranuclear area, since the Jurkat cell nucleus often is kidney-shaped. Also, the nuclear mask was dilated with the dilate command, and the resulting mask subtracted with the original nuclear mask, forming a ring beyond the nucleus, representing the cytoplasm (mask C). Masks N and C were combined with the NFAT staining and to generate the NFAT staining intensity for the nucleus and the cytoplasm. NFAT translocation was expressed as the ratio of NFAT fluorescence to extract from N and that of the cytoplasm concerning mask C. Cell spreading was evaluated by measuring the area of the surface shielded against staining with the secondary antibody, which was detectable as a dark patch.

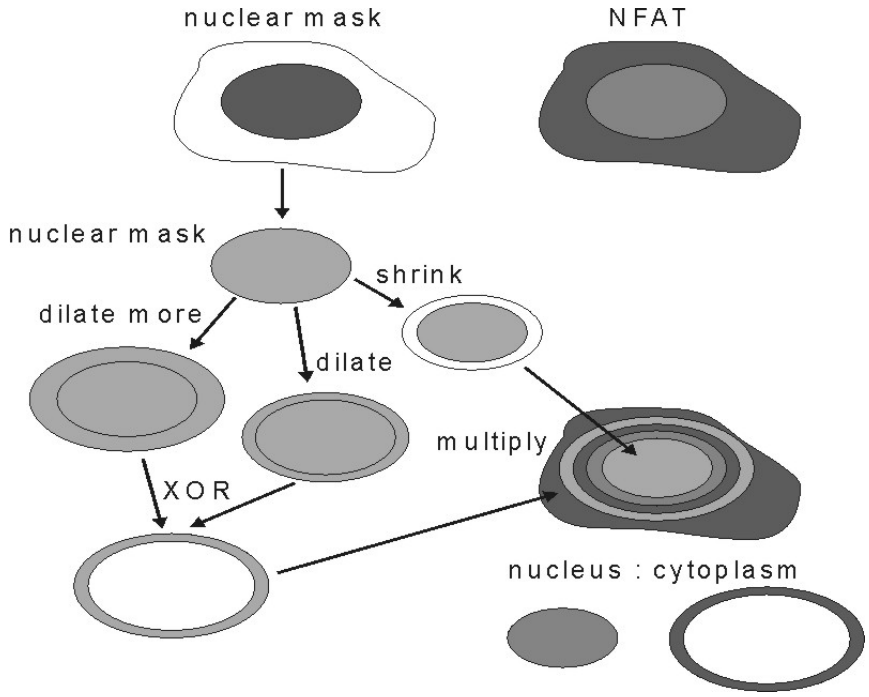

Figure 8.2 Overview of the macro for NFAT translocation. The fluorescence of the nuclear stain TOPRO was used to generate a nuclear mask. This mask was dilated for the generation of a mask around the nucleus, representing the cytoplasmic area, and shrunk, to generate an entirely nuclear area. Both masks were multiplied with the NFAT image to generate images representing the nuclear and cytoplasmic fluorescence. Relations were calculated by dividing the mean cytoplasmic NFAT staining by that in the nucleus. Figure c./o. by Roland Brock.

8.2.8 Imaging of stimulation-dependent protein clustering. For the parallel analysis of stimulatory antibody-induced protein clustering, cells were stimulated on slides with microstructured stimulatory antibody immobilization, or on hydrogels with stimulatory antibody microarrays. After fixation at the indicated time points, cells were permeabilized with saponin buffer (in the case of phosphotyrosine imaging supplemented with 1 mM Na_3VO_4) stained with the same rabbit antibodies as used for the detection of proteins on the peptide microarray with concentrations of 2 µg/ml each for 1 h (see the table in the peptide microarray section) For confocal imaging of PLCγpY783, the rabbit polyclonal antibody (Cell Signalling) was applied in an 1/50 dilution. For detection, Alexa 488 labelled anti-rabbit secondary antibody was incubated for 30 min, in some cases together with a TOPRO staining of the nucleus.

The quantitative image analysis of protein clustering was performed on Image Pro Plus 4.5 using the confocal slices representing the cell/stimulus contact surface. For the general analysis of protein phosphoryation, masks representing cells were generated by

filtering objects with an area larger than 200 pixels and a mean fluorescence staining higher than 20. For the analysis of PLCγ clustering in special, because of low signal intensity, the staining intensity was thresholded by a value of higher intensity, which was selected to represent only intense protein clusters. The generated masks were multiplied with the colour channel of the respective protein staining. For the generated image, the number of pixels and the total intensity was counted. The total pixel intensity, divided by the number of pixels, represents the mean protein intensity per area, while the number of pixels, divided by the number of cells, can be used to represent the area of protein clustering. In case of dissecting the influence of spatially distinct stimuli, multi-channel images were separated into the channels representing the areas with different types of stimulation, and that representing the protein of interest (Fig. 8.3). From the channel representing the immobilized antibody, a positive mask (representing the stamp) and negative mask (representing the anti-stamp) were generated by manually adjusting the threshold. The colour channel to be quantified was filtered by those masks using the AND function. For the quantification of clustering using micropatterned stimuli, the mean density per area, as depicted in the diagrams, was calculated by dividing the sum of the total intensity by area for each individual object by the total area covered by the cells.

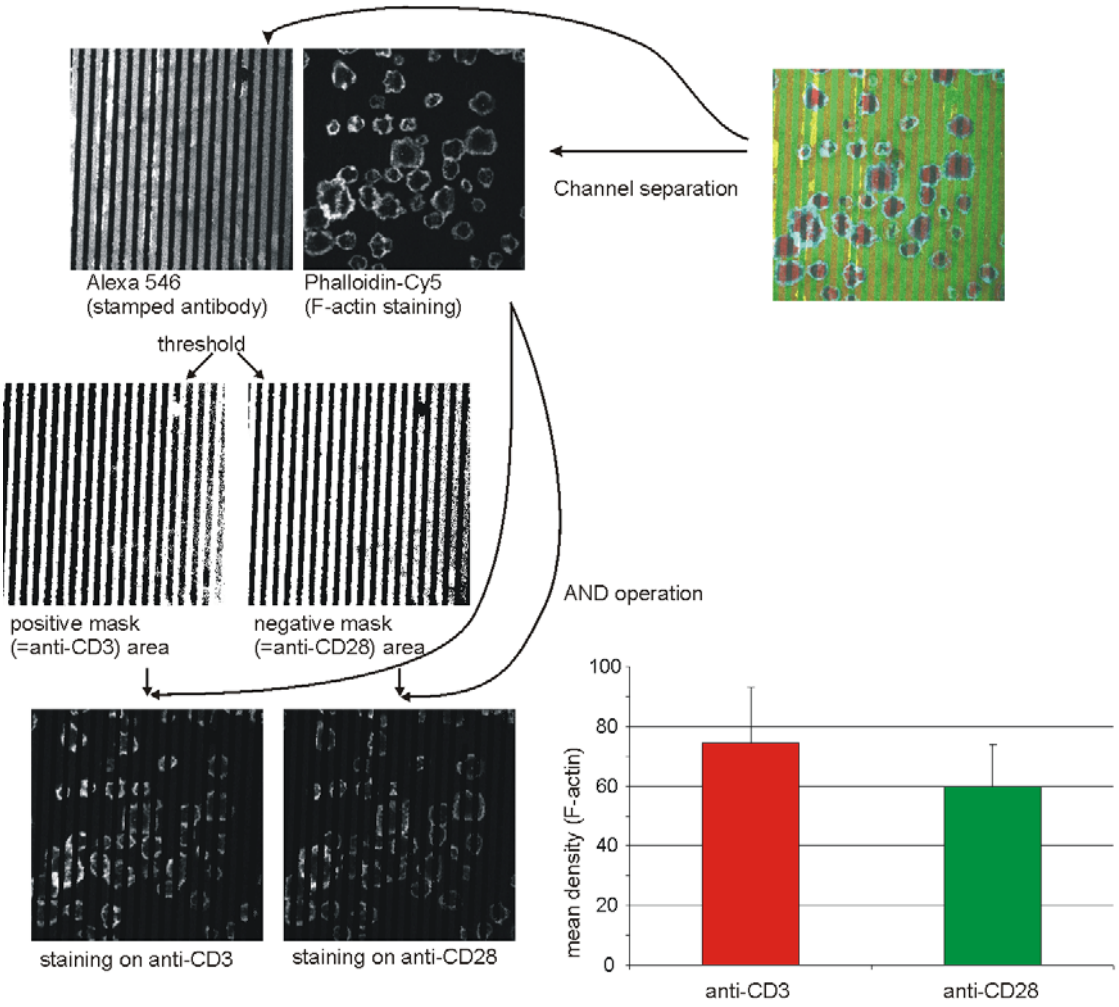

Figure 8.3 Scheme of the quantification of the effects of spatially distinct stimuli on cell activation. Here, Jurkat cells were stimulated for 10 min on microstructured antibody surfaces composed.from anti-CD3 + Alexa546 anti-mouse (stamped) and anti-CD28 (overlayed) antibodies. Distinct areas for CD3 and CD28-stimulation were created of masks representing areas below or above an arbitrary threshold for the Alexa 546 fluorescence. The positive and negative masks were multiplied with the channel representing the actin staining, and the fluorescence intensity quantified.

8.2.9 Reflectometric Interference Spectroscopy (RIFS). RIfS-transducer chips of 1 mm D 263 glass with layers of 10 nm Nb_2O_5 and 330 nm SiO_2 were purchased from Unaxis Balzers AG (Balzers, Liechtenstein). For functionalization, the RIfS-transducer chips were first cleaned in 1 M NaOH for 2 min, washed with tap water, followed by cleaning of the surfaces and mechanical drying with KIMTECH tissues (Kimberly-Clark, Reigate, UK). Then the transducer chips were treated with freshly prepared Piranha solution (mixture of 30 % hydrogen peroxide and concentrated sulphuric acid at a ratio of 2:3; Caution: Highly aggressive!) for 30 min in an ultrasonic bath to activate the silanol groups. After rinsing with Milli-Q water and drying in a nitrogen stream, the surface was immediately activated for protein binding by incubation with 3-(glycidyloxypropyl)trimethoxysilane (GOPTS), Fluka) for 1 h. Thereafter the surface was cleaned with water-free aceton and dried in a nitrogen stream. Solutions of anti-CD3 (OKT3) and anti-CD28 antibodies (9.3, 20 μg/ml in PBS) were added onto the activated transducer surface and incubated for 16 h at 4 °C. Before assembly into the flow cell the transducers were rinsed with Milli-Q water and thoroughly dried in a nitrogen stream. Samples were handled with an Automated Sample Injection Analyser - ASIA (Ismatec, Wertheim-Mondfeld, Germany). Samples were perfused over the transducer in a continuous flow of 20 μl/min. First, FCS-free RPMI 1640 medium was pumped over the transducer until the signal showed no further drift. Then the transducer was blocked by perfusion of a solution of 0.1 % BSA in PBS until again, the signal showed no further drift. The time for a complete measurement of cell adhesion and spreading was 2500 s. The first 120 s serum-free RPMI 1640 medium was pumped over the transducer. Then, for 1800 s the cell suspension with a density of $5*10^5$ cells/ml in serum-free medium in the absence or presence of inhibitor was pumped through the flow cell. Finally, RPMI 1640 medium was pumped through the flow cell for the remainder of the measurement interval. The initial slope of the RIFS curves corresponds to the average increase in optical thickness between the 250 s and 350 s time points. All RIfS experiments were performed by Bernd Möhrle.

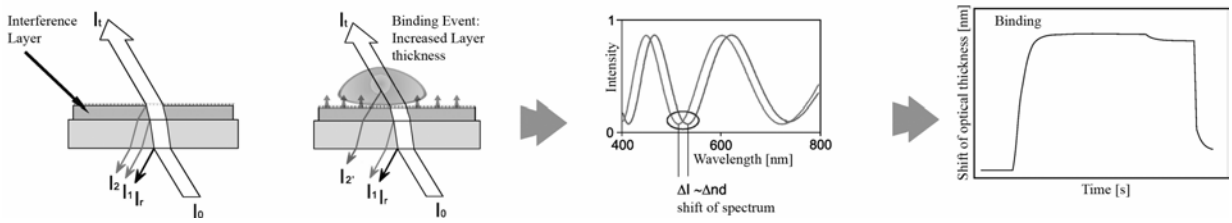

Figure 8.4 Scheme of the RIfS detection method. The left part of the scheme shows how the reflected beams superimpose and how the binding of cells on the surface changes the optical thickness of the transducer surface. The right part shows the change of the characteristic interference spectrum and how this shift is transformed into a binding curve. Figure by Bernd Möhrle.

For the comparison of cell spreading by fluorescence microscopy and RIfS measurements, the anti-CD3 and anti-CD28 antibodies were immobilized on glass slides functionalized with GOPTS in the same way as the RIfS transducers. Solutions of antibodies (20 μg/ml in PBS) were incubated on the coverslips for 16 h at 4 °C, followed by 3 washes with PBS, and blocked with 0.1% BSA for 1 h. Cells were added to antibody-functionalized coverslips at a density of $5*10^5$ cells/mL in serum-free RPMI at 37 °C. In order to assess the effect of the inhibition of actin polymerization on cell spreading, cells were preincubated for 15 min with 10 μM cytochalasin D.

8.3 Peptide microarrays

8.3.1 Peptide synthesis. All peptides carried an N-terminal Cys residue for immobilization to epoxy-activated surfaces. Peptide designations are composed from the name of the protein from which they were derived, and either the position of the pY residue in the whole protein (for pY-peptides) or the position of the first residue in the peptide (for polyP and other peptides). Standard chemicals for peptide chemistry were obtained from Fluka and Merck; solvents were p. a. grade. 9-fluorenylmethoxycarbonyl-(Fmoc-) protected amino acids were purchased from Novabiochem (Heidelberg, Germany), Senn Chemicals (Dielsdorf, Switzerland), and Orpegen Pharma (Heidelberg, Germany). Fmoc-Tyr(PO(OBzl)OH)-OH was purchased from Novabiochem. Automated synthesis of the bisphosphopeptide C-Ahx-NQL(pY)NELNLGRREE(pY)DVL-NH2 (pITAM; Ahx=6-aminohexanoic acid) on Rink amide resin (Rapp Polymere, Tübingen, Germany) was performed by solid-phase Fmoc/tert-butyl-chemistry in a 100 μmol scale using an automated peptide synthesizer (433 A, Applied Biosystems, Weiterstadt, Germany). Coupling of amino acids was carried out using a 10-fold excess of Fmoc-amino acids activated in situ using 2-(1H-benzotriazol-1-yl)-1,1,3,3-tetramethyluronium tetrafluoroborate (TBTU), 1-hydroxybenzotriazol (HOBt) and N,N'-diisopropylethylamine (DIPEA). The removal of the Fmoc-protecting group was performed by treatment with piperidine/DMF, and monitored using UV/Vis spectrometry. Synthesis of the other peptides and phosphopeptides was performed by standard multiple solid-phase peptide synthesis, partially by Echaz Microcollections, Tübingen, Germany [215]. N-terminal acetylation was performed by treating the resin-bound peptide with acetic anhydride/DIPEA/DMF (1:1:8, v/v/v) twice for 30 min. Peptides were cleaved off the resin by treatment with trifluoroacetic acid (TFA)/triisopropylsilane/ethanedithiole/H_2O (92.5:2.5:2.5:2.5, v/v/v/v) for 4 h. Crude peptides were precipitated by adding cold diethyl ether (-20 °C), collected by centrifugation and resuspended in cold diethyl ether. This procedure was repeated twice. Finally, peptides were dissolved in tert-butyl alcohol/H_2O (4:1, v/v), lyophilised and analyzed by reverse phase HPLC and MALDI-TOF mass [215]. The synthesis of the fluorescein-labelled control peptide Fluo-Ahx-KAA followed a procedure described in [216]. If prominent impurities were present, peptides were purified by RP-HPLC using optimised H_2O (0.1 % TFA)/acetonitrile (0.1 % TFA) gradients to > 90 % purity. After lyophilisation, peptides were dissolved to a concentration of 3 mM in DMF. Prior to spotting, peptides were freshly diluted from

DMF stock solutions to a spotting concentration of 100 μM in 0.1 M phosphate buffer (pH 8.0).

8.3.2 Generation of peptide microarrays. For parallel peptide microarrays arrays, epoxy-functionalized glass slides were applied(Nexterion Slide E, Schott, Jena), on which 16 identical arrays of up to 100 spots per array were spotted at 15°C at dew point (70% air humidity in the spotter casing), using a GeSiM NP2.0 nanopipettor (GeSiM, Dresden, Germany). Per spot, 1.2 nl was spotted in duplicate with a centre-to-centre spacing of 500 μm. For orientation, a fluorescein-labelled control peptide was spotted. After 60 min incubation at room temperature, the slides were incubated with 1 ml of O,O'-bis(2-aminopropyl) polyethylene glycol 800 (Fluka) at 70 °C for 16 h to quench the remaining reactive epoxy groups and block the surface. After cooling, the slides were rinsed with deionized water, dried under airstream, and stored at 4° C.

8.3.3 Readouts for peptide microarrays using microscopy and determination of protein concentration. Confocal laser scanning microscopy was performed using an inverted LSM510 confocal laser scanning microscope (Carl Zeiss, Göttingen, Germany). YFP was excited with the 514 nm line of an argon-ion laser and detected using a BP530-600 nm band pass filter, Cy5 was excited with the 633 nm line of a helium neon laser and detected using an LP650 nm long pass filter. Cell images were acquired at a resolution of 1024 x 1024 pixels using a C-Apochromat 63 x 1.2 NA water immersion objective. The coverslips with the arrayed peptides were mounted in a custom-made open measurement chamber with the coated surface up, allowing addition of solution to the microarray during observation. 100 μl of cell lysate or antibody solutions were used for incubation on each cover slip. After addition to the cover slip the solution was mixed by pipetting up and down several times. Incubation was carried out for 3 min for the lysates and for 15 min for antibodies. Antibodies were diluted to 5 μg/ml for anti-ZAP-70, and to 15 μg/ml for anti-phosphotyrosine (Cell Signalling) and to 2.8 μg/ml for Cy-5 labelled goat-anti-mouse-antibody (Dianova, Hamburg, Germany) in TPBS containing 0.5% BSA. Between each incubation step, arrays were washed twice with TPBS. Digital images were acquired at a resolution of 512 x 512 pixels using a Plan-Neofluar 10 x 0.3 NA objective. For data evaluation, the functionalised spots and the surrounding background were defined as separate areas-of-interest and the mean intensity within the respective area-of-interest

determined using Image Pro Plus 4.5 (Media Cybernetics Inc., Silver Spring, USA). The net fluorescence F was calculated by subtracting the mean intensity of the background from the mean intensity of the respective spot. The net fluorescence over equally functionalised spots was averaged. ZAP-YFP protein concentrations in the lysates were determined by Oda Stoevesandt on a Zeiss ConfoCor2 fluorescence correlation spectroscope as described in [199].

8.3.4 Parallelized peptide microarray incubation and analysis. For antibody stimulation, Jurkat cells and derivative cell lines (10^7/ml) were resuspended in ice-cold HEPES-buffered saline (HBS; 10 mM HEPES, 135 mM NaCl, 5 mM KCl, 1 mM MgCl2, 1.8 mM CaCl2, pH 7.4) supplemented with 0.1 % BSA and 5 mM glucose containing 10 µg/ml of the anti-CD3 clone OKT3) and/or anti CD28 antibody (clone 9.3) or the isotype control (mouse IgG2a, Sigma) and were incubated on ice for 10 min. Then, the crosslinking secondary antibody (goat anti-mouse Ig, Calbiochem), was added to a final concentration of 20 µg/ml and samples were immediately transferred to 37°C for the time indicated. For activation via broad-range phosphatase inhibition, cells were treated in the same medium for 20 min at 37 °C with 0.5 mM pervanadate, freshly diluted from a reaction between 5 mM Na_3VO_4 and 5 mM H_2O_2 in HBS for 15 min at room temperature.

Stimulation was stopped by placing the samples on ice, and washing the cells in ice-cold HBS. For lysis, $2*10^7$ cells/ml were resuspended in ice-cold lysis buffer (1 % Triton X-100, 50 mM n-octyl-β-D-glucopyranoside (Fluka), 20 mM Tris, 1 mM EDTA, 150 mM NaCl, 1 mM Na_3VO_4, pH 7.5, and protease inhibitor cocktail (Roche, Mannheim, Germany)), and incubated on ice for 60 min. For the assessment of peptide effects on molecular interactions, peptides were added to the lysis buffer prior to lysis in the following concentrations, unless indicated otherwise: LATpY191 (20 µM), LATpY132 (0.5 µM), SLP228 (20 µM) and SLP 179 (20 µM) to a maximal DMF concentration of 1 % in the lysate. Crude lysates were clarified by centrifugation at 20,000 x g for 15 min, total protein concentration determined by a standard protein assay (BioRad, Munich, Germany), and adjusted to the same concentration. Before incubation, slides carrying arrays were shortly washed with lysis buffer and dd H_2O and dried by air-stream. A 16-well clip-on frame was clamped onto the slide to create separate incubation chambers for

each of the 16 arrays. Arrays were blocked with 1% Top Block (Fluka) in PBS for 1 h. Afterwards, the arrays were washed with 100 µl/chamber TPBSB (PBS + 0.05% Tween + 0.05 % BSA), before being incubated with 50 µl/chamber of the cell lysates at 4°C for 1 h. Then, the arrays were washed with TPBSB, and incubated with 2 µg/ml of the primary antibody (Table 8.1) at room temperature for 15 min.

For each antibody, a negative staining control was taken into account by incubating the arrays with antibodies without prior lysate incubation. After washing with TPBSB, arrays were incubated with 1 µg/ml of the secondary antibody at room temperature for 10 min. Subsequently, arrays were washed with TPBSB, rinsed with dd H_2O, and dried in an air-stream. The slides were stored at 4°C previous to scanning. The specificity of detection antibodies was validated by Western Blotting. Slides were scanned at 10 µm resolution on a ScanArray array scanner (Perkin Elmer, Rodgau-Jügesheim, Germany) using lasers of 543 nm and 633 nm for excitation. Prior to applying the antibodies to the microarray, the binding specificity of the antibodies had been validated using a Western Blot of Jurkat cell lysates. However, in contrast to the Western blots, the antibodies on the microarray are expected to bind to the proteins under a nondenaturing condition, similar to that of immunoprecipitations. Correspondingly, not all antibodies that were suitable for Western Blot, were able to yield signals on the microarray, compared to all of the antibodies described as suitable for immune precipitation (data not shown).

Table 8.1 Antibodies used for the evaluation of the peptide microarrays

Primary antibodies	**Antigen**	**Type**	**Source**
	c-Cbl	mouse monocl. IgG1	BD Transduction Labs(Heidelberg)
	GADS	rabbit polycl. IgG	Upstate/Biomol (Hamburg)
	GRB2	rabbit polycl.	Santa Cruz
	LAT	mouse monocl. IgG1	Upstate/Biomol
	LCK	mouse monocl. IgG2bκ	Upstate/Biomol
	Nck	rabbit polycl. IgG	USBiological/Biomol (Hamburg)
	PI3K	rabbit polycl. IgG	BD Transduction Labs
	PLCγ1	rabbit polycl. IgG	Santa Cruz
	SHP2	rabbit polycl. IgG	Santa Cruz
	SLP76	mouse monocl. IgG2a	USBiological/Biomol (Hamburg)
	Vav	rabbit polycl.	Santa Cruz
	ZAP-70	mouse monocl. IgG2a	BD Transduction Labs
Secondary antibodies	anti-Rabbit IgG	Goat polycl. Alexa Fluor 633	Molecular Probes/Invitrogen
	anti-Mouse IgG	Goat polycl. Alexa Fluor 546	Molecular Probes/Invitrogen

8.3.5 Image analysis of peptide microarrays. Semiautomatic image analysis of microarrays was performed using Array Pro (Media Cybernetics, Silver Spring, USA). For each experiment, the image of the array was overlayed with a grid corresponding to the array layout. The net signal intensity of each spot was determined by subtracting the local background intensity, determined by a ring surrounding the spot, from the raw intensity. From signals of each peptide spot and incubation condition, the respective signal of the antibody control was subtracted. If a negative value was the result, it was set to 1, in order to enable further batch calculations. Corrected signal intensities of the stimulated conditions were divided by the corrected signal intensity of the unstimulated condition from respective peptide spots, if at least one of the values was above a certain threshold. Thresholds were established empirically. For PV-stimulation experiments, a threshold of 100 was used, while for antibody stimulation, a threshold of 50 was used. Thresholds were employed in order to filter out error-prone ratios resulting from division of one small values by another.

Reference List

1. 1984. IUPAC-IUB Joint Commission on Biochemical Nomenclature (JCBN). Nomenclature and symbolism for amino acids and peptides. Recommendations 1983. *Eur.J.Biochem.* 138:9-37.

2. van der Merwe,P.A. and S.J.Davis. 2003. Molecular interactions mediating T cell antigen recognition. *Annu.Rev.Immunol.* 21:659-684.

3. Healy,J.I. and C.C.Goodnow. 1998. Positive versus negative signaling by lymphocyte antigen receptors. *Annu.Rev.Immunol.* 16:645-670.

4. Dustin,M.L. and J.A.Cooper. 2000. The immunological synapse and the actin cytoskeleton: molecular hardware for T cell signaling. *Nat.Immunol.* 1:23-29.

5. Dustin,M.L., M.W.Olszowy, A.D.Holdorf, J.Li, S.Bromley, N.Desai, P.Widder, F.Rosenberger, P.A.van der Merwe, P.M.Allen, and A.S.Shaw. 1998. A novel adaptor protein orchestrates receptor patterning and cytoskeletal polarity in T-cell contacts. *Cell* 94:667-677.

6. Lee,K.H., A.D.Holdorf, M.L.Dustin, A.C.Chan, P.M.Allen, and A.S.Shaw. 2002. T cell receptor signaling precedes immunological synapse formation. *Science* 295:1539-1542.

7. Bunnell,S.C., D.I.Hong, J.R.Kardon, T.Yamazaki, C.J.McGlade, V.A.Barr, and L.E.Samelson. 2002. T cell receptor ligation induces the formation of dynamically regulated signaling assemblies. *J.Cell Biol.* 158:1263-1275.

8. Schmitt,H.M., A.Brecht, J.Piehler, and G.Gauglitz. 1997. An integrated system for optical biomolecular interaction analysis. *Biosensors & Bioelectronics* 12:809-816.

9. Möhrle,B.P., K.Köhler, J.Jaehrling, R.Brock, and G.Gauglitz. 2006. Label-free characterization of cell adhesion using reflectometric interference spectroscopy (RIfS). *Anal.Bioanal.Chem.* 384:407-413.

10. Stoevesandt,O., K.Köhler, R.Fischer, I.C.Johnston, and R.Brock. 2005. One-step analysis of protein complexes in microliters of cell lysate. *Nat.Methods* 2:833-835.

11. Varma,R. and S.Mayor. 1998. GPI-anchored proteins are organized in submicron domains at the cell surface. *Nature* 394:798-801.

12. Mustelin,T. and K.Tasken. 2003. Positive and negative regulation of T-cell activation through kinases and phosphatases. *Biochem.J.* 371:15-27.

13. Irles,C., A.Symons, F.Michel, T.R.Bakker, P.A.van der Merwe, and O.Acuto. 2003. CD45 ectodomain controls interaction with GEMs and Lck activity for optimal TCR signaling. *Nat.Immunol.* 4:189-197.

14. Johnson,K.G., S.K.Bromley, M.L.Dustin, and M.L.Thomas. 2000. A supramolecular basis for CD45 tyrosine phosphatase regulation in sustained T cell activation. *Proc.Natl.Acad.Sci.U.S A* 97:10138-10143.

15. Veillette,A., M.A.Bookman, E.M.Horak, and J.B.Bolen. 1988. The CD4 and CD8 T cell surface antigens are associated with the internal membrane tyrosine-protein kinase p56lck. *Cell* 55:301-308.

16. Bergman,M., T.Mustelin, C.Oetken, J.Partanen, N.A.Flint, K.E.Amrein, M.Autero, P.Burn, and K.Alitalo. 1992. The human p50csk tyrosine kinase phosphorylates p56lck at Tyr-505 and down regulates its catalytic activity. *EMBO J.* 11:2919-2924.

17. Houtman,J.C., R.A.Houghtling, M.Barda-Saad, Y.Toda, and L.E.Samelson. 2005. Early phosphorylation kinetics of proteins involved in proximal TCR-mediated signaling pathways. *J.Immunol.* 175:2449-2458.

18. Isakov,N., R.L.Wange, W.H.Burgess, J.D.Watts, R.Aebersold, and L.E.Samelson. 1995. ZAP-70 binding specificity to T cell receptor tyrosine-based activation motifs: the tandem SH2 domains of ZAP-70 bind distinct tyrosine-based activation motifs with varying affinity. *J.Exp.Med.* 181:375-380.

19. Iwashima,M., B.A.Irving, N.S.van Oers, A.C.Chan, and A.Weiss. 1994. Sequential interactions of the TCR with two distinct cytoplasmic tyrosine kinases. *Science* 263:1136-1139.

20. Di,B., V, M.Malissen, E.Dufour, E.Sechet, B.Malissen, and O.Acuto. 2002. Tyrosine 315 determines optimal recruitment of ZAP-70 to the T cell antigen receptor. *Eur.J.Immunol.* 32:568-575.

21. Lupher,M.L., Jr., Z.Songyang, S.E.Shoelson, L.C.Cantley, and H.Band. 1997. The Cbl phosphotyrosine-binding domain selects a D(N/D)XpY motif and binds to the Tyr292 negative regulatory phosphorylation site of ZAP-70. *J.Biol.Chem.* 272:33140-33144.

22. Zhang,W., J.Sloan-Lancaster, J.Kitchen, R.P.Trible, and L.E.Samelson. 1998. LAT: the ZAP-70 tyrosine kinase substrate that links T cell receptor to cellular activation. *Cell* 92:83-92.

23. Wardenburg,J.B., C.Fu, J.K.Jackman, H.Flotow, S.E.Wilkinson, D.H.Williams, R.Johnson, G.Kong, A.C.Chan, and P.R.Findell. 1996. Phosphorylation of SLP-76 by the ZAP-70 protein-tyrosine kinase is required for T-cell receptor function. *J.Biol Chem.* 271:19641-19644.

24. Yamasaki,S., K.Nishida, M.Hibi, M.Sakuma, R.Shiina, A.Takeuchi, H.Ohnishi, T.Hirano, and T.Saito. 2001. Docking protein Gab2 is phosphorylated by ZAP-70 and negatively regulates T cell receptor signaling by recruitment of inhibitory molecules. *J.Biol Chem.* 276:45175-45183.

25. Pawson,T. and P.Nash. 2003. Assembly of cell regulatory systems through protein interaction domains. *Science* 300:445-452.

26. Wange,R.L. 2000. LAT, the linker for activation of T cells: a bridge between T cell-specific and general signaling pathways. *Sci.STKE.* 2000:RE1.

27. Paz,P.E., S.Wang, H.Clarke, X.Lu, D.Stokoe, and A.Abo. 2001. Mapping the Zap-70 phosphorylation sites on LAT (linker for activation of T cells) required for recruitment and activation of signalling proteins in T cells. *Biochem.J.* 356:461-471.

28. Peterson,E.J., J.L.Clements, N.Fang, and G.A.Koretzky. 1998. Adaptor proteins in lymphocyte antigen-receptor signaling. *Curr.Opin.Immunol.* 10:337-344.

29. Bubeck,W.J., R.Pappu, J.Y.Bu, B.Mayer, J.Chernoff, D.Straus, and A.C.Chan. 1998. Regulation of PAK activation and the T cell cytoskeleton by the linker protein SLP-76. *Immunity* 9:607-616.

30. da Silva,A.J., Z.Li, C.de Vera, E.Canto, P.Findell, and C.E.Rudd. 1997. Cloning of a novel T-cell protein FYB that binds FYN and SH2-domain-containing leukocyte protein 76 and modulates interleukin 2 production. *Proc.Natl.Acad.Sci.U.S A* 94:7493-7498.

31. Su,Y.W., Y.Zhang, J.Schweikert, G.A.Koretzky, M.Reth, and J.Wienands. 1999. Interaction of SLP adaptors with the SH2 domain of Tec family kinases. *Eur.J.Immunol.* 29:3702-3711.

32. Clements,J.L., N.J.Boerth, J.R.Lee, and G.A.Koretzky. 1999. Integration of T cell receptor-dependent signaling pathways by adapter proteins. *Annu.Rev.Immunol.* 17:89-108.

33. Kimura,T., H.Kihara, S.Bhattacharyya, H.Sakamoto, E.Appella, and R.P.Siraganian. 1996. Downstream signaling molecules bind to different phosphorylated immunoreceptor tyrosine-based activation motif (ITAM) peptides of the high affinity IgE receptor. *J.Biol Chem.* 271:27962-27968.

34. Ravichandran,K.S., K.K.Lee, Z.Songyang, L.C.Cantley, P.Burn, and S.J.Burakoff. 1993. Interaction of Shc with the zeta chain of the T cell receptor upon T cell activation. *Science* 262:902-905.

35. Liu,S.K., N.Fang, G.A.Koretzky, and C.J.McGlade. 1999. The hematopoietic-specific adaptor protein gads functions in T-cell signaling via interactions with the SLP-76 and LAT adaptors. *Curr.Biol.* 9:67-75.

36. Lin,J. and A.Weiss. 2001. Identification of the minimal tyrosine residues required for linker for activation of T cell function. *J.Biol.Chem.* 276:29588-29595.

37. Kwon,J., C.K.Qu, J.S.Maeng, R.Falahati, C.Lee, and M.S.Williams. 2005. Receptor-stimulated oxidation of SHP-2 promotes T-cell adhesion through SLP-76-ADAP. *EMBO J.* 24:2331-2341.

38. Berry,D.M., S.J.Benn, A.M.Cheng, and C.J.McGlade. 2001. Caspase-dependent cleavage of the hematopoietic specific adaptor protein Gads alters signalling from the T cell receptor. *Oncogene* 20:1203-1211.

39. Griffiths,E.K. and J.M.Penninger. 2002. Communication between the TCR and integrins: role of the molecular adapter ADAP/Fyb/Slap. *Curr.Opin.Immunol.* 14:317-322.

40. Songyang,Z., S.E.Shoelson, J.McGlade, P.Olivier, T.Pawson, X.R.Bustelo, M.Barbacid, H.Sabe, H.Hanafusa, T.Yi, and . 1994. Specific motifs recognized by the SH2 domains of Csk, 3BP2, fps/fes, GRB-2, HCP, SHC, Syk, and Vav. *Mol.Cell Biol* 14:2777-2785.

41. Rivero-Lezcano,O.M., J.H.Sameshima, A.Marcilla, and K.C.Robbins. 1994. Physical association between Src homology 3 elements and the protein product of the c-cbl proto-oncogene. *J.Biol Chem.* 269:17363-17366.

42. She,H.Y., S.Rockow, J.Tang, R.Nishimura, E.Y.Skolnik, M.Chen, B.Margolis, and W.Li. 1997. Wiskott-Aldrich syndrome protein is associated with the adapter protein Grb2 and the epidermal growth factor receptor in living cells. *Mol.Biol.Cell* 8:1709-1721.

43. Bokoch,G.M., Y.Wang, B.P.Bohl, M.A.Sells, L.A.Quilliam, and U.G.Knaus. 1996. Interaction of the Nck adapter protein with p21-activated kinase (PAK1). *J.Biol.Chem.* 271:25746-25749.

44. Vojtek,A.B. and J.A.Cooper. 1995. Rho family members: activators of MAP kinase cascades. *Cell* 82:527-529.

45. Gil,D., W.W.Schamel, M.Montoya, F.Sanchez-Madrid, and B.Alarcon. 2002. Recruitment of Nck by CD3 epsilon reveals a ligand-induced conformational change essential for T cell receptor signaling and synapse formation. *Cell* 109:901-912.

46. Lee,K.M., E.Chuang, M.Griffin, R.Khattri, D.K.Hong, W.Zhang, D.Straus, L.E.Samelson, C.B.Thompson, and J.A.Bluestone. 1998. Molecular basis of T cell inactivation by CTLA-4. *Science* 282:2263-2266.

47. Schaeper,U., N.H.Gehring, K.P.Fuchs, M.Sachs, B.Kempkes, and W.Birchmeier. 2000. Coupling of Gab1 to c-Met, Grb2, and Shp2 mediates biological responses. *J.Cell Biol* 149:1419-1432.

48. Yasuda,K., M.Nagafuku, T.Shima, M.Okada, T.Yagi, T.Yamada, Y.Minaki, A.Kato, S.Tani-Ichi, T.Hamaoka, and A.Kosugi. 2002. Cutting edge: Fyn is essential for tyrosine phosphorylation of Csk-binding protein/phosphoprotein associated with glycolipid-enriched microdomains in lipid rafts in resting T cells. *J.Immunol.* 169:2813-2817.

49. Brdickova,N., T.Brdicka, L.Andera, J.Spicka, P.Angelisova, S.L.Milgram, and V.Horejsi. 2001. Interaction between two adapter proteins, PAG and EBP50: a possible link between membrane rafts and actin cytoskeleton. *FEBS Lett.* 507:133-136.

50. Saito,T. and S.Yamasaki. 2003. Negative feedback of T cell activation through inhibitory adapters and costimulatory receptors. *Immunol.Rev.* 192:143-160.

51. Wang,H.Y., Y.Altman, D.Fang, C.Elly, Y.Dai, Y.Shao, and Y.C.Liu. 2001. Cbl promotes ubiquitination of the T cell receptor zeta through an adaptor function of Zap-70. *J.Biol Chem.* 276:26004-26011.

52. Joazeiro,C.A., S.S.Wing, H.Huang, J.D.Leverson, T.Hunter, and Y.C.Liu. 1999. The tyrosine kinase negative regulator c-Cbl as a RING-type, E2-dependent ubiquitin-protein ligase. *Science* 286:309-312.

53. Lock,L.S., I.Royal, M.A.Naujokas, and M.Park. 2000. Identification of an atypical Grb2 carboxyl-terminal SH3 domain binding site in Gab docking proteins reveals Grb2-dependent and -independent recruitment of Gab1 to receptor tyrosine kinases. *J.Biol Chem.* 275:31536-31545.

54. Gu,H., J.C.Pratt, S.J.Burakoff, and B.G.Neel. 1998. Cloning of p97/Gab2, the major SHP2-binding protein in hematopoietic cells, reveals a novel pathway for cytokine-induced gene activation. *Mol.Cell* 2:729-740.

55. Pages,F., M.Ragueneau, R.Rottapel, A.Truneh, J.Nunes, J.Imbert, and D.Olive. 1994. Binding of phosphatidylinositol-3-OH kinase to CD28 is required for T-cell signalling. *Nature* 369:327-329.

56. Vanhaesebroeck,B. and D.R.Alessi. 2000. The PI3K-PDK1 connection: more than just a road to PKB. *Biochem.J.* 346 Pt 3:561-576.

57. Cross,D.A., D.R.Alessi, P.Cohen, M.Andjelkovich, and B.A.Hemmings. 1995. Inhibition of glycogen synthase kinase-3 by insulin mediated by protein kinase B. *Nature* 378:785-789.

58. Scharenberg,A.M., O.El Hillal, D.A.Fruman, L.O.Beitz, Z.Li, S.Lin, I.Gout, L.C.Cantley, D.J.Rawlings, and J.P.Kinet. 1998. Phosphatidylinositol-3,4,5-trisphosphate (PtdIns-3,4,5-P3)/Tec

kinase-dependent calcium signaling pathway: a target for SHIP-mediated inhibitory signals. *EMBO J.* 17:1961-1972.

59. Bunnell,S.C., M.Diehn, M.B.Yaffe, P.R.Findell, L.C.Cantley, and L.J.Berg. 2000. Biochemical interactions integrating Itk with the T cell receptor-initiated signaling cascade. *J.Biol Chem.* 275:2219-2230.

60. Li,Z., M.I.Wahl, A.Eguinoa, L.R.Stephens, P.T.Hawkins, and O.N.Witte. 1997. Phosphatidylinositol 3-kinase-gamma activates Bruton's tyrosine kinase in concert with Src family kinases. *Proc.Natl.Acad.Sci.U.S A* 94:13820-13825.

61. Reynolds,L.F., L.A.Smyth, T.Norton, N.Freshney, J.Downward, D.Kioussis, and V.L.Tybulewicz. 2002. Vav1 transduces T cell receptor signals to the activation of phospholipase C-gamma1 via phosphoinositide 3-kinase-dependent and -independent pathways. *J.Exp.Med.* 195:1103-1114.

62. Altman,A. and M.Villalba. 2003. Protein kinase C-theta (PKCtheta): it's all about location, location, location. *Immunol.Rev.* 192:53-63.

63. Liu,Y., S.Witte, Y.C.Liu, M.Doyle, C.Elly, and A.Altman. 2000. Regulation of protein kinase Ctheta function during T cell activation by Lck-mediated tyrosine phosphorylation. *J.Biol Chem.* 275:3603-3609.

64. Roose,J.P., M.Mollenauer, V.A.Gupta, J.Stone, and A.Weiss. 2005. A diacylglycerol-protein kinase C-RasGRP1 pathway directs Ras activation upon antigen receptor stimulation of T cells. *Mol.Cell Biol* 25:4426-4441.

65. Sun,Z., C.W.Arendt, W.Ellmeier, E.M.Schaeffer, M.J.Sunshine, L.Gandhi, J.Annes, D.Petrzilka, A.Kupfer, P.L.Schwartzberg, and D.R.Littman. 2000. PKC-theta is required for TCR-induced NF-kappaB activation in mature but not immature T lymphocytes. *Nature* 404:402-407.

66. Nobes,C.D. and A.Hall. 1999. Rho GTPases control polarity, protrusion, and adhesion during cell movement. *J.Cell Biol* 144:1235-1244.

67. Machesky,L.M. and R.H.Insall. 1998. Scar1 and the related Wiskott-Aldrich syndrome protein, WASP, regulate the actin cytoskeleton through the Arp2/3 complex. *Curr.Biol* 8:1347-1356.

68. Anton,I.M. and G.E.Jones. 2006. WIP: A multifunctional protein involved in actin cytoskeleton regulation. *Eur.J.Cell Biol* 85:295-304.

69. Tybulewicz,V.L. 2005. Vav-family proteins in T-cell signalling. *Curr.Opin.Immunol.* 17:267-274.

70. Reynolds,L.F., C.de Bettignies, T.Norton, A.Beeser, J.Chernoff, and V.L.Tybulewicz. 2004. Vav1 transduces T cell receptor signals to the activation of the Ras/ERK pathway via LAT, Sos, and RasGRP1. *J.Biol Chem.* 279:18239-18246.

71. Zeng,R., J.L.Cannon, R.T.Abraham, M.Way, D.D.Billadeau, J.Bubeck-Wardenberg, and J.K.Burkhardt. 2003. SLP-76 coordinates Nck-dependent Wiskott-Aldrich syndrome protein recruitment with Vav-1/Cdc42-dependent Wiskott-Aldrich syndrome protein activation at the T cell-APC contact site. *J.Immunol.* 171:1360-1368.

72. Faure,S., L.I.Salazar-Fontana, M.Semichon, V.L.Tybulewicz, G.Bismuth, A.Trautmann, R.N.Germain, and J.Delon. 2004. ERM proteins regulate cytoskeleton relaxation promoting T cell-APC conjugation. *Nat.Immunol.* 5:272-279.

73. Raab,M., S.Pfister, and C.E.Rudd. 2001. CD28 signaling via VAV/SLP-76 adaptors: regulation of cytokine transcription independent of TCR ligation. *Immunity* 15:921-933.

74. Marinari,B., A.Costanzo, A.Viola, F.Michel, G.Mangino, O.Acuto, M.Levrero, E.Piccolella, and L.Tuosto. 2002. Vav cooperates with CD28 to induce NF-kappaB activation via a pathway involving Rac-1 and mitogen-activated kinase kinase 1. *Eur.J.Immunol.* 32:447-456.

75. Acuto,O. and F.Michel. 2003. CD28-mediated co-stimulation: a quantitative support for TCR signalling. *Nat.Rev.Immunol.* 3:939-951.

76. Holdorf,A.D., J.M.Green, S.D.Levin, M.F.Denny, D.B.Straus, V.Link, P.S.Changelian, P.M.Allen, and A.S.Shaw. 1999. Proline residues in CD28 and the Src homology (SH)3 domain of Lck are required for T cell costimulation. *J.Exp.Med.* 190:375-384.

77. Michel,F., G.Attal-Bonnefoy, G.Mangino, S.Mise-Omata, and O.Acuto. 2001. CD28 as a molecular amplifier extending TCR ligation and signaling capabilities. *Immunity.* 15:935-945.

78. Schneider,H., Y.C.Cai, K.V.Prasad, S.E.Shoelson, and C.E.Rudd. 1995. T cell antigen CD28 binds to the GRB-2/SOS complex, regulators of p21ras. *Eur.J.Immunol.* 25:1044-1050.

79. Diehn,M., A.A.Alizadeh, O.J.Rando, C.L.Liu, K.Stankunas, D.Botstein, G.R.Crabtree, and P.O.Brown. 2002. Genomic expression programs and the integration of the CD28 costimulatory signal in T cell activation. *Proc.Natl.Acad.Sci.U.S.A* 99:11796-11801.

80. Kane,L.P. and A.Weiss. 2003. The PI-3 kinase/Akt pathway and T cell activation: pleiotropic pathways downstream of PIP3. *Immunol.Rev.* 192:7-20.

81. Beals,C.R., C.M.Sheridan, C.W.Turck, P.Gardner, and G.R.Crabtree. 1997. Nuclear export of NF-ATc enhanced by glycogen synthase kinase-3. *Science* 275:1930-1934.

82. Macian,F. 2005. NFAT proteins: key regulators of T-cell development and function. *Nat.Rev.Immunol.* 5:472-484.

83. Sanchez-Lockhart,M., E.Marin, B.Graf, R.Abe, Y.Harada, C.E.Sedwick, and J.Miller. 2004. Cutting edge: CD28-mediated transcriptional and posttranscriptional regulation of IL-2 expression are controlled through different signaling pathways. *J.Immunol.* 173:7120-7124.

84. Viola,A., S.Schroeder, Y.Sakakibara, and A.Lanzavecchia. 1999. T lymphocyte costimulation mediated by reorganization of membrane microdomains. *Science* 283:680-682.

85. Wesselborg,S., D.A.Fruman, J.K.Sagoo, B.E.Bierer, and S.J.Burakoff. 1996. Identification of a physical interaction between calcineurin and nuclear factor of activated T cells (NFATp). *J.Biol Chem.* 271:1274-1277.

86. Aramburu,J., F.Garcia-Cozar, A.Raghavan, H.Okamura, A.Rao, and P.G.Hogan. 1998. Selective inhibition of NFAT activation by a peptide spanning the calcineurin targeting site of NFAT. *Mol.Cell* 1:627-637.

87. Neal,J.W. and N.A.Clipstone. 2001. Glycogen synthase kinase-3 inhibits the DNA binding activity of NFATc. *J.Biol Chem.* 276:3666-3673.

88. Zhu,J., F.Shibasaki, R.Price, J.C.Guillemot, T.Yano, V.Dotsch, G.Wagner, P.Ferrara, and F.McKeon. 1998. Intramolecular masking of nuclear import signal on NF-AT4 by casein kinase I and MEKK1. *Cell* 93:851-861.

89. Gomez,d.A., S.Martinez-Martinez, J.L.Maldonado, I.Ortega-Perez, and J.M.Redondo. 2000. A role for the p38 MAP kinase pathway in the nuclear shuttling of NFATp. *J.Biol Chem.* 275:13872-13878.

90. Chow,C.W., M.Rincon, and R.J.Davis. 1999. Requirement for transcription factor NFAT in interleukin-2 expression. *Mol.Cell Biol.* 19:2300-2307.

91. Weil,R. and A.Israel. 2004. T-cell-receptor- and B-cell-receptor-mediated activation of NF-kappaB in lymphocytes. *Curr.Opin.Immunol.* 16:374-381.

92. Zhou,H., I.Wertz, K.O'Rourke, M.Ultsch, S.Seshagiri, M.Eby, W.Xiao, and V.M.Dixit. 2004. Bcl10 activates the NF-kappaB pathway through ubiquitination of NEMO. *Nature* 427:167-171.

93. Bromley,S.K., W.R.Burack, K.G.Johnson, K.Somersalo, T.N.Sims, C.Sumen, M.M.Davis, A.S.Shaw, P.M.Allen, and M.L.Dustin. 2001. The immunological synapse. *Annu.Rev.Immunol.* 19:375-396.

94. Grakoui,A., S.K.Bromley, C.Sumen, M.M.Davis, A.S.Shaw, P.M.Allen, and M.L.Dustin. 1999. The immunological synapse: a molecular machine controlling T cell activation. *Science* 285:221-227.

95. Monks,C.R., B.A.Freiberg, H.Kupfer, N.Sciaky, and A.Kupfer. 1998. Three-dimensional segregation of supramolecular activation clusters in T cells. *Nature* 395:82-86.

96. Schreiber,S.L. 1998. Chemical genetics resulting from a passion for synthetic organic chemistry. *Bioorg.Med.Chem.* 6:1127-1152.

97. Crews,C.M. and U.Splittgerber. 1999. Chemical genetics: exploring and controlling cellular processes with chemical probes. *Trends Biochem.Sci.* 24:317-320.

98. Peterson,R.T., B.A.Link, J.E.Dowling, and S.L.Schreiber. 2000. Small molecule developmental screens reveal the logic and timing of vertebrate development. *Proc.Natl.Acad.Sci.U.S A* 97:12965-12969.

99. Giuliano,K.A., R.L.Debiasio, R.T.Dunlay, A.Gough, J.M.Volosky, J.Zock, G.N.Pavlakis, and D.L.Taylor. 1997. High Content Screening - A New Approach to Easing Key Bottlenecks in the Drug Discovery Process. *J.Biomol.Screen.* 2:249-259.

100. Yarrow,J.C., G.Totsukawa, G.T.Charras, and T.J.Mitchison. 2005. Screening for cell migration inhibitors via automated microscopy reveals a Rho-kinase inhibitor. *Chem.Biol* 12:385-395.

101. Ziauddin,J. and D.M.Sabatini. 2001. Microarrays of cells expressing defined cDNAs. *Nature* 411:107-110.

102. Bailey,S.N., D.M.Sabatini, and B.R.Stockwell. 2004. Microarrays of small molecules embedded in biodegradable polymers for use in mammalian cell-based screens. *Proc.Natl.Acad.Sci.U.S A* 101:16144-16149.

103. Belov,L., l.de, V, C.G.dos Remedios, S.P.Mulligan, and R.I.Christopherson. 2001. Immunophenotyping of leukemias using a cluster of differentiation antibody microarray. *Cancer Res.* 61:4483-4489.

104. Soen,Y., D.S.Chen, D.L.Kraft, M.M.Davis, and P.O.Brown. 2003. Detection and characterization of cellular immune responses using peptide-MHC microarrays. *PLoS.Biol.* 1:E65.

105. Stone,J.D., W.E.Demkowicz, Jr., and L.J.Stern. 2005. HLA-restricted epitope identification and detection of functional T cell responses by using MHC-peptide and costimulatory microarrays. *Proc.Natl.Acad.Sci.U.S.A* 102:3744-3749.

106. Dustin,M.L. and A.C.Chan. 2000. Signaling takes shape in the immune system. *Cell* 103:283-294.

107. Barber,E.K., J.D.Dasgupta, S.F.Schlossman, J.M.Trevillyan, and C.E.Rudd. 1989. The CD4 and CD8 antigens are coupled to a protein-tyrosine kinase (p56lck) that phosphorylates the CD3 complex. *Proc.Natl.Acad.Sci.U.S.A* 86:3277-3281.

108. Huppa,J.B. and M.M.Davis. 2003. T-cell-antigen recognition and the immunological synapse. *Nat.Rev.Immunol.* 3:973-983.

109. Parsey,M.V. and G.K.Lewis. 1993. Actin polymerization and pseudopod reorganization accompany anti-CD3-induced growth arrest in Jurkat T cells. *J.Immunol.* 151:1881-1893.

110. Hanke,J.H., J.P.Gardner, R.L.Dow, P.S.Changelian, W.H.Brissette, E.J.Weringer, B.A.Pollok, and P.A.Connelly. 1996. Discovery of a novel, potent, and Src family-selective tyrosine kinase inhibitor. Study of Lck- and FynT-dependent T cell activation. *J.Biol.Chem.* 271:695-701.

111. Endo,A., K.Nagashima, H.Kurose, S.Mochizuki, M.Matsuda, and N.Mochizuki. 2002. Sphingosine 1-phosphate induces membrane ruffling and increases motility of human umbilical vein endothelial cells via vascular endothelial growth factor receptor and CrkII. *J.Biol Chem.* 277:23747-23754.

112. Bain,J., H.McLauchlan, M.Elliott, and P.Cohen. 2003. The specificities of protein kinase inhibitors: an update. *Biochem.J.* 371:199-204.

113. Zhen,X., J.Zhang, G.P.Johnson, and E.Friedman. 2001. D(4) dopamine receptor differentially regulates Akt/nuclear factor-kappa b and extracellular signal-regulated kinase pathways in D(4)MN9D cells. *Mol.Pharmacol.* 60:857-864.

114. Kandula,S. and C.Abraham. 2004. LFA-1 on CD4+ T cells is required for optimal antigen-dependent activation in vivo. *J.Immunol.* 173:4443-4451.

115. Cannon,J.L. and J.K.Burkhardt. 2002. The regulation of actin remodeling during T-cell-APC conjugate formation. *Immunol.Rev.* 186:90-99.

116. Morgan,M.M., C.M.Labno, G.A.Van Seventer, M.F.Denny, D.B.Straus, and J.K.Burkhardt. 2001. Superantigen-induced T cell:B cell conjugation is mediated by LFA-1 and requires signaling through Lck, but not ZAP-70. *J.Immunol.* 167:5708-5718.

117. Valensin,S., S.R.Paccani, C.Ulivieri, D.Mercati, S.Pacini, L.Patrussi, T.Hirst, P.Lupetti, and C.T.Baldari. 2002. F-actin dynamics control segregation of the TCR signaling cascade to clustered lipid rafts. *Eur.J.Immunol.* 32:435-446.

118. Bunnell,S.C., V.Kapoor, R.P.Trible, W.Zhang, and L.E.Samelson. 2001. Dynamic actin polymerization drives T cell receptor-induced spreading: a role for the signal transduction adaptor LAT. *Immunity.* 14:315-329.

119. Schade,A.E. and A.D.Levine. 2002. Signal transduction through the T cell receptor is dynamically regulated by balancing kinase and phosphatase activities. *Biochem.Biophys.Res.Commun.* 296:637-643.

120. Blake,R.A., M.A.Broome, X.Liu, J.Wu, M.Gishizky, L.Sun, and S.A.Courtneidge. 2000. SU6656, a selective src family kinase inhibitor, used to probe growth factor signaling. *Mol.Cell Biol.* 20:9018-9027.

121. Rozdzial,M.M., C.M.Pleiman, J.C.Cambier, and T.H.Finkel. 1998. pp56Lck mediates TCR zeta-chain binding to the microfilament cytoskeleton. *J.Immunol.* 161:5491-5499.

122. Carman,C.V. and T.A.Springer. 2003. Integrin avidity regulation: are changes in affinity and conformation underemphasized? *Curr.Opin.Cell Biol* 15:547-556.

123. Dustin,M.L., T.G.Bivona, and M.R.Philips. 2004. Membranes as messengers in T cell adhesion signaling. *Nat.Immunol.* 5:363-372.

124. Giannoni,E., P.Chiarugi, G.Cozzi, L.Magnelli, M.L.Taddei, T.Fiaschi, F.Buricchi, G.Raugei, and G.Ramponi. 2003. Lymphocyte function-associated antigen-1-mediated T cell adhesion is impaired by low molecular weight phosphotyrosine phosphatase-dependent inhibition of FAK activity. *J.Biol.Chem.* 278:36763-36776.

125. Schade,A.E. and A.D.Levine. 2003. Phosphatases in concert with kinases set the gain for signal transduction through the T cell receptor. *Mol.Immunol.* 40:531-537.

126. Stefanova,I., B.Hemmer, M.Vergelli, R.Martin, W.E.Biddison, and R.N.Germain. 2003. TCR ligand discrimination is enforced by competing ERK positive and SHP-1 negative feedback pathways. *Nat.Immunol.* 4:248-254.

127. Janes,K.A., J.G.Albeck, S.Gaudet, P.K.Sorger, D.A.Lauffenburger, and M.B.Yaffe. 2005. A systems model of signaling identifies a molecular basis set for cytokine-induced apoptosis. *Science* 310:1646-1653.

128. Chakraborty,A.K., M.L.Dustin, and A.S.Shaw. 2003. In silico models for cellular and molecular immunology: successes, promises and challenges. *Nat.Immunol.* 4:933-936.

129. Papin,J.A., T.Hunter, B.O.Palsson, and S.Subramaniam. 2005. Reconstruction of cellular signalling networks and analysis of their properties. *Nat.Rev.Mol.Cell Biol.* 6:99-111.

130. Slavik,J.M., D.G.Lim, S.J.Burakoff, and D.A.Hafler. 2001. Uncoupling p70(s6) kinase activation and proliferation: rapamycin-resistant proliferation of human CD8(+) T lymphocytes. *J.Immunol.* 166:3201-3209.

131. Neumeister,E.N., Y.Zhu, S.Richard, C.Terhorst, A.C.Chan, and A.S.Shaw. 1995. Binding of ZAP-70 to phosphorylated T-cell receptor zeta and eta enhances its autophosphorylation and generates specific binding sites for SH2 domain-containing proteins. *Mol.Cell Biol.* 15:3171-3178.

132. Gillis,S. and J.Watson. 1980. Biochemical and biological characterization of lymphocyte regulatory molecules. V. Identification of an interleukin 2-producing human leukemia T cell line. *J.Exp.Med.* 152:1709-1719.

133. Weiss,A., R.L.Wiskocil, and J.D.Stobo. 1984. The role of T3 surface molecules in the activation of human T cells: a two-stimulus requirement for IL 2 production reflects events occurring at a pre-translational level. *J.Immunol.* 133:123-128.

134. Abraham,R.T. and A.Weiss. 2004. Jurkat T cells and development of the T-cell receptor signalling paradigm. *Nat.Rev.Immunol.* 4:301-308.

135. Salazar-Fontana,L.I., V.Barr, L.E.Samelson, and B.E.Bierer. 2003. CD28 engagement promotes actin polymerization through the activation of the small Rho GTPase Cdc42 in human T cells. *J.Immunol.* 171:2225-2232.

136. Grosse-Hovest,L., I.Hartlapp, W.Marwan, G.Brem, H.G.Rammensee, and G.Jung. 2003. A recombinant bispecific single-chain antibody induces targeted, supra-agonistic CD28-stimulation and tumor cell killing. *Eur.J.Immunol.* 33:1334-1340.

137. Kusnezow,W., A.Jacob, A.Walijew, F.Diehl, and J.D.Hoheisel. 2003. Antibody microarrays: an evaluation of production parameters. *Proteomics.* 3:254-264.

138. Fabian,M.A., W.H.Biggs, III, D.K.Treiber, C.E.Atteridge, M.D.Azimioara, M.G.Benedetti, T.A.Carter, P.Ciceri, P.T.Edeen, M.Floyd, J.M.Ford, M.Galvin, J.L.Gerlach, R.M.Grotzfeld, S.Herrgard, D.E.Insko, M.A.Insko, A.G.Lai, J.M.Lelias, S.A.Mehta, Z.V.Milanov, A.M.Velasco, L.M.Wodicka, H.K.Patel, P.P.Zarrinkar, and D.J.Lockhart. 2005. A small molecule-kinase interaction map for clinical kinase inhibitors. *Nat.Biotechnol.* 23:329-336.

139. Katagiri,K. and S.Matsuura. 1971. Antitumor activity of cytochalasin D. *J.Antibiot.(Tokyo)* 24:722-723.

140. Oliver,J.M., D.L.Burg, B.S.Wilson, J.L.McLaughlin, and R.L.Geahlen. 1994. Inhibition of mast cell Fc epsilon R1-mediated signaling and effector function by the Syk-selective inhibitor, piceatannol. *J.Biol.Chem.* 269:29697-29703.

141. Wang,B.H., Z.X.Lu, and G.M.Polya. 1998. Inhibition of eukaryote serine/threonine-specific protein kinases by piceatannol. *Planta Med.* 64:195-199.

142. Hers,I., J.M.Tavare, and R.M.Denton. 1999. The protein kinase C inhibitors bisindolylmaleimide I (GF 109203x) and IX (Ro 31-8220) are potent inhibitors of glycogen synthase kinase-3 activity. *FEBS Lett.* 460:433-436.

143. Leost,M., C.Schultz, A.Link, Y.Z.Wu, J.Biernat, E.M.Mandelkow, J.A.Bibb, G.L.Snyder, P.Greengard, D.W.Zaharevitz, R.Gussio, A.M.Senderowicz, E.A.Sausville, C.Kunick, and L.Meijer. 2000. Paullones are potent inhibitors of glycogen synthase kinase-3beta and cyclin-dependent kinase 5/p25. *Eur.J.Biochem.* 267:5983-5994.

144. Davies,S.P., H.Reddy, M.Caivano, and P.Cohen. 2000. Specificity and mechanism of action of some commonly used protein kinase inhibitors. *Biochem.J.* 351:95-105.

145. Alessi,D.R., A.Cuenda, P.Cohen, D.T.Dudley, and A.R.Saltiel. 1995. PD 098059 is a specific inhibitor of the activation of mitogen-activated protein kinase kinase in vitro and in vivo. *J.Biol Chem.* 270:27489-27494.

146. Liu,J., J.D.Farmer, Jr., W.S.Lane, J.Friedman, I.Weissman, and S.L.Schreiber. 1991. Calcineurin is a common target of cyclophilin-cyclosporin A and FKBP-FK506 complexes. *Cell* 66:807-815.

147. Eder,A.M., L.Dominguez, T.F.Franke, and J.D.Ashwell. 1998. Phosphoinositide 3-kinase regulation of T cell receptor-mediated interleukin-2 gene expression in normal T cells. *J.Biol.Chem.* 273:28025-28031.

148. Laufer,S.A., G.K.Wagner, D.A.Kotschenreuther, and W.Albrecht. 2003. Novel substituted pyridinyl imidazoles as potent anticytokine agents with low activity against hepatic cytochrome P450 enzymes. *J.Med.Chem.* 46:3230-3244.

149. Cuenda,A., J.Rouse, Y.N.Doza, R.Meier, P.Cohen, T.F.Gallagher, P.R.Young, and J.C.Lee. 1995. SB 203580 is a specific inhibitor of a MAP kinase homologue which is stimulated by cellular stresses and interleukin-1. *FEBS Lett.* 364:229-233.

150. Wu,C.C., S.C.Hsu, H.M.Shih, and M.Z.Lai. 2003. Nuclear factor of activated T cells c is a target of p38 mitogen-activated protein kinase in T cells. *Mol.Cell Biol.* 23:6442-6454.

151. Schoeberl,B., C.Eichler-Jonsson, E.D.Gilles, and G.Muller. 2002. Computational modeling of the dynamics of the MAP kinase cascade activated by surface and internalized EGF receptors. *Nat.Biotechnol.* 20:370-375.

152. Seminario,M.C. and R.L.Wange. 2003. Lipid phosphatases in the regulation of T cell activation: living up to their PTEN-tial. *Immunol.Rev.* 192:80-97.

153. Rozdzial,M.M., B.Malissen, and T.H.Finkel. 1995. Tyrosine-phosphorylated T cell receptor zeta chain associates with the actin cytoskeleton upon activation of mature T lymphocytes. *Immunity* 3:623-633.

154. Anton,I.M., M.A.de la Fuente, T.N.Sims, S.Freeman, N.Ramesh, J.H.Hartwig, M.L.Dustin, and R.S.Geha. 2002. WIP deficiency reveals a differential role for WIP and the actin cytoskeleton in T and B cell activation. *Immunity* 16:193-204.

155. Perlman,Z.E., M.D.Slack, Y.Feng, T.J.Mitchison, L.F.Wu, and S.J.Altschuler. 2004. Multidimensional drug profiling by automated microscopy. *Science* 306:1194-1198.

156. Sachs,K., O.Perez, D.Pe'er, D.A.Lauffenburger, and G.P.Nolan. 2005. Causal protein-signaling networks derived from multiparameter single-cell data. *Science* 308:523-529.

157. Sadra,A., T.Cinek, J.L.Arellano, J.Shi, K.E.Truitt, and J.B.Imboden. 1999. Identification of tyrosine phosphorylation sites in the CD28 cytoplasmic domain and their role in the costimulation of Jurkat T cells. *J.Immunol.* 162:1966-1973.

158. Sanchez-Lockhart,M. and J.Miller. 2006. Engagement of CD28 outside of the immunological synapse results in up-regulation of IL-2 mRNA stability but not IL-2 transcription. *J.Immunol.* 176:4778-4784.

159. Piehler,J., A.Brecht, T.Giersch, B.Hock, and G.Gauglitz. 1997. Assessment of affinity constants by rapid solid phase detection of equilibrium binding in a flow system. *J.Immunol.Methods* 201:189-206.

160. Pröll,F., B.Mohrle, M.Kumpf, and G.Gauglitz. 2005. Label-free characterisation of oligonucleotide hybridisation using reflectometric interference spectroscopy. *Anal.Bioanal.Chem.* 382:1889-1894.

161. Hecht,E. 1987. Optics, 2nd edition. Addison Wesley, Boston.

162. Proll,G., M.Kumpf, M.Mehlmann, J.Tschmelak, H.Griffith, R.Abuknesha, and G.Gauglitz. 2004. Monitoring an antibody affinity chromatography with a label-free optical biosensor technique. *J.Immunol.Methods* 292:35-42.

163. Piehler,J., A.Brecht, and G.Gauglitz. 1996. Affinity detection of low molecular weight analytes. *Analytical Chemistry* 68:139-143.

164. Kröger,K., J.Bauer, B.Fleckenstein, J.Rademann, G.Jung, and G.Gauglitz. 2002. Epitope-mapping of transglutaminase with parallel label-free optical detection. *Biosensors & Bioelectronics* 17:937-944.

165. Pourshafie,M.R., B.I.Marklund, and S.Ohlson. 2004. Binding interactions of Escherichia coli with globotetraosylceramide (globoside) using a surface plasmon resonance biosensor. *Journal of Microbiological Methods* 58:313-320.

166. Jenkins,A.T., R.ffrench-constant, A.Buckling, D.J.Clarke, and K.Jarvis. 2004. Study of the attachment of Pseudomonas aeruginosa on gold and modified gold surfaces using surface plasmon resonance. *Biotechnol.Prog.* 20:1233-1236.

167. Quinn,J.G., S.O'Neill, A.Doyle, C.McAtamney, D.Diamond, B.D.MacCraith, and R.O'Kennedy. 2000. Development and application of surface plasmon resonance-based biosensors for the detection of cell-ligand interactions. *Anal.Biochem.* 281:135-143.

168. Mackay,C.R. 2001. Chemokines: immunology's high impact factors. *Nature Immunology* 2:95-101.

169. Engelhardt,B. and H.Wolburg. 2004. Mini-review: Transendothelial migration of leukocytes: through the front door or around the side of the house? *Eur.J.Immunol.* 34:2955-2963.

170. Köhler,K., A.C.Lellouch, S.Vollmer, O.Stoevesandt, A.Hoff, L.Peters, H.Rogl, B.Malissen, and R.Brock. 2005. Chemical inhibitors when timing is critical: a pharmacological concept for the maturation of T cell contacts. *Chembiochem.* 6:152-161.

171. Gonzalez,P.A., L.J.Carreno, D.Coombs, J.E.Mora, E.Palmieri, B.Goldstein, S.G.Nathenson, and A.M.Kalergis. 2005. T cell receptor binding kinetics required for T cell activation depend on the density of cognate ligand on the antigen-presenting cell. *Proc.Natl.Acad.Sci.U.S.A* 102:4824-4829.

172. Grolleau,A., J.Bowman, B.Pradet-Balade, E.Puravs, S.Hanash, J.A.Garcia-Sanz, and L.Beretta. 2002. Global and specific translational control by rapamycin in T cells uncovered by microarrays and proteomics. *J.Biol Chem.* 277:22175-22184.

173. Kim,J.E. and F.M.White. 2006. Quantitative analysis of phosphotyrosine signaling networks triggered by CD3 and CD28 costimulation in Jurkat cells. *J.Immunol.* 176:2833-2843.

174. Wange,R.L. and L.E.Samelson. 1996. Complex complexes: signaling at the TCR. *Immunity.* 5:197-205.

175. Zhang,W., R.P.Trible, M.Zhu, S.K.Liu, C.J.McGlade, and L.E.Samelson. 2000. Association of Grb2, Gads, and phospholipase C-gamma 1 with phosphorylated LAT tyrosine residues. Effect of LAT tyrosine mutations on T cell angigen receptor-mediated signaling. *J.Biol.Chem.* 275:23355-23361.

176. Zhu,M., E.Janssen, and W.Zhang. 2003. Minimal requirement of tyrosine residues of linker for activation of T cells in TCR signaling and thymocyte development. *J.Immunol.* 170:325-333.

177. Yablonski,D., T.Kadlecek, and A.Weiss. 2001. Identification of a phospholipase C-gamma1 (PLC-gamma1) SH3 domain-binding site in SLP-76 required for T-cell receptor-mediated activation of PLC-gamma1 and NFAT. *Mol.Cell Biol.* 21:4208-4218.

178. Anderson,S.M., E.A.Burton, and B.L.Koch. 1997. Phosphorylation of Cbl following stimulation with interleukin-3 and its association with Grb2, Fyn, and phosphatidylinositol 3-kinase. *J.Biol.Chem.* 272:739-745.

179. Barda-Saad,M., A.Braiman, R.Titerence, S.C.Bunnell, V.A.Barr, and L.E.Samelson. 2005. Dynamic molecular interactions linking the T cell antigen receptor to the actin cytoskeleton. *Nat.Immunol.* 6:80-89.

180. Duan,L., A.L.Reddi, A.Ghosh, M.Dimri, and H.Band. 2004. The Cbl family and other ubiquitin ligases: destructive forces in control of antigen receptor signaling. *Immunity.* 21:7-17.

181. Kusnezow,W., Y.V.Syagailo, S.Ruffer, K.Klenin, W.Sebald, J.D.Hoheisel, C.Gauer, and I.Goychuk. 2006. Kinetics of antigen binding to antibody microspots: strong limitation by mass transport to the surface. *Proteomics* 6:794-803.

182. Harkiolaki,M., M.Lewitzky, R.J.Gilbert, E.Y.Jones, R.P.Bourette, G.Mouchiroud, H.Sondermann, I.Moarefi, and S.M.Feller. 2003. Structural basis for SH3 domain-mediated high-affinity binding between Mona/Gads and SLP-76. *EMBO J.* 22:2571-2582.

183. Itoh,K., M.Sakakibara, S.Yamasaki, A.Takeuchi, H.Arase, M.Miyazaki, N.Nakajima, M.Okada, and T.Saito. 2002. Cutting edge: negative regulation of immune synapse formation by anchoring lipid raft to cytoskeleton through Cbp-EBP50-ERM assembly. *J.Immunol.* 168:541-544.

184. Cuevas,B., Y.Lu, S.Watt, R.Kumar, J.Zhang, K.A.Siminovitch, and G.B.Mills. 1999. SHP-1 regulates Lck-induced phosphatidylinositol 3-kinase phosphorylation and activity. *J.Biol.Chem.* 274:27583-27589.

185. Pelosi,M., B.Di, V, V.Mounier, D.Mege, J.M.Pascussi, E.Dufour, A.Blondel, and O.Acuto. 1999. Tyrosine 319 in the interdomain B of ZAP-70 is a binding site for the Src homology 2 domain of Lck. *J.Biol.Chem.* 274:14229-14237.

186. Goda,S., A.C.Quale, M.L.Woods, A.Felthauser, and Y.Shimizu. 2004. Control of TCR-mediated activation of beta 1 integrins by the ZAP-70 tyrosine kinase interdomain B region and the linker for activation of T Cells adapter protein. *J.Immunol.* 172:5379-5387.

187. Poulin,B., F.Sekiya, and S.G.Rhee. 2005. Intramolecular interaction between phosphorylated tyrosine-783 and the C-terminal Src homology 2 domain activates phospholipase C-gamma1. *Proc.Natl.Acad.Sci.U.S A* 102:4276-4281.

188. Geng,L. and C.Rudd. 2001. Adaptor ADAP (adhesion- and degranulation-promoting adaptor protein) regulates beta1 integrin clustering on mast cells. *Biochem.Biophys.Res.Commun.* 289:1135-1140.

189. Yamaguchi,H. and W.A.Hendrickson. 1996. Structural basis for activation of human lymphocyte kinase Lck upon tyrosine phosphorylation. *Nature* 384:484-489.

190. Nicoll,G., J.Ni, D.Liu, P.Klenerman, J.Munday, S.Dubock, M.G.Mattei, and P.R.Crocker. 1999. Identification and characterization of a novel siglec, siglec-7, expressed by human natural killer cells and monocytes. *J.Biol.Chem.* 274:34089-34095.

191. Arnaud,M., R.Mzali, F.Gesbert, C.Crouin, C.Guenzi, C.Vermot-Desroches, J.Wijdenes, G.Courtois, O.Bernard, and J.Bertoglio. 2004. Interaction of the tyrosine phosphatase SHP-2 with Gab2 regulates Rho-dependent activation of the c-fos serum response element by interleukin-2. *Biochem.J.* 382:545-556.

192. Okkenhaug,K. and R.Rottapel. 1998. Grb2 forms an inducible protein complex with CD28 through a Src homology 3 domain-proline interaction. *J.Biol.Chem.* 273:21194-21202.

193. Marengere,L.E., K.Okkenhaug, A.Clavreul, D.Couez, S.Gibson, G.B.Mills, T.W.Mak, and R.Rottapel. 1997. The SH3 domain of Itk/Emt binds to proline-rich sequences in the cytoplasmic domain of the T cell costimulatory receptor CD28. *J.Immunol.* 159:3220-3229.

194. Mak,P., Z.He, and T.Kurosaki. 1996. Identification of amino acid residues required for a specific interaction between Src-tyrosine kinase and proline-rich region of phosphatidylinositol-3' kinase. *FEBS Lett.* 397:183-185.

195. Deng,L., C.A.Velikovsky, C.P.Swaminathan, S.Cho, and R.A.Mariuzza. 2005. Structural basis for recognition of the T cell adaptor protein SLP-76 by the SH3 domain of phospholipase Cgamma1. *J.Mol.Biol* 352:1-10.

196. Kato,M., K.Miyazawa, and N.Kitamura. 2000. A deubiquitinating enzyme UBPY interacts with the Src homology 3 domain of Hrs-binding protein via a novel binding motif PX(V/I)(D/N)RXXKP. *J.Biol Chem.* 275:37481-37487.

197. Zettl,M. and M.Way. 2002. The WH1 and EVH1 domains of WASP and Ena/VASP family members bind distinct sequence motifs. *Curr.Biol.* 12:1617-1622.

198. Secrist,J.P., L.A.Burns, L.Karnitz, G.A.Koretzky, and R.T.Abraham. 1993. Stimulatory effects of the protein tyrosine phosphatase inhibitor, pervanadate, on T-cell activation events. *J.Biol Chem.* 268:5886-5893.

199. Stoevesandt,O., M.Elbs, K.Köhler, A.C.Lellouch, R.Fischer, T.Andre, and R.Brock. 2005. Peptide microarrays for the detection of molecular interactions in cellular signal transduction. *Proteomics.* 5:2010-2017.

200. Irvin,B.J., B.L.Williams, A.E.Nilson, H.O.Maynor, and R.T.Abraham. 2000. Pleiotropic contributions of phospholipase C-gamma1 (PLC-gamma1) to T-cell antigen receptor-mediated signaling: reconstitution studies of a PLC-gamma1-deficient Jurkat T-cell line. *Mol.Cell Biol* 20:9149-9161.

201. Straus,D.B. and A.Weiss. 1992. Genetic evidence for the involvement of the lck tyrosine kinase in signal transduction through the T cell antigen receptor. *Cell* 70:585-593.

202. Puntervoll,P., R.Linding, C.Gemund, S.Chabanis-Davidson, M.Mattingsdal, S.Cameron, D.M.Martin, G.Ausiello, B.Brannetti, A.Costantini, F.Ferre, V.Maselli, A.Via, G.Cesareni, F.Diella, G.Superti-Furga, L.Wyrwicz, C.Ramu, C.McGuigan, R.Gudavalli, I.Letunic, P.Bork, L.Rychlewski, B.Kuster, M.Helmer-Citterich, W.N.Hunter, R.Aasland, and T.J.Gibson. 2003. ELM server: A new resource for investigating short functional sites in modular eukaryotic proteins. *Nucleic Acids Res.* 31:3625-3630.

203. Neduva,V., R.Linding, I.Su-Angrand, A.Stark, F.de Masi, T.J.Gibson, J.Lewis, L.Serrano, and R.B.Russell. 2005. Systematic discovery of new recognition peptides mediating protein interaction networks. *PLoS.Biol* 3:e405.

204. Shan,X., M.J.Czar, S.C.Bunnell, P.Liu, Y.Liu, P.L.Schwartzberg, and R.L.Wange. 2000. Deficiency of PTEN in Jurkat T cells causes constitutive localization of Itk to the plasma membrane and hyperresponsiveness to CD3 stimulation. *Mol.Cell Biol* 20:6945-6957.

205. Seminario,M.C. and R.L.Wange. 2002. Signaling pathways of D3-phosphoinositide-binding kinases in T cells and their regulation by PTEN. *Semin.Immunol.* 14:27-36.

206. Astoul,E., C.Edmunds, D.A.Cantrell, and S.G.Ward. 2001. PI 3-K and T-cell activation: limitations of T-leukemic cell lines as signaling models. *Trends Immunol.* 22:490-496.

207. Allen,P.M. and E.R.Unanue. 1984. Differential requirements for antigen processing by macrophages for lysozyme-specific T cell hybridomas. *J.Immunol.* 132:1077-1079.

208. Goldsmith,M.A. and A.Weiss. 1987. Isolation and characterization of a T-lymphocyte somatic mutant with altered signal transduction by the antigen receptor. *Proc.Natl.Acad.Sci.U.S A* 84:6879-6883.

209. Riviere,I., K.Brose, and R.C.Mulligan. 1995. Effects of retroviral vector design on expression of human adenosine deaminase in murine bone marrow transplant recipients engrafted with genetically modified cells. *Proc.Natl.Acad.Sci.U.S.A* 92:6733-6737.

210. Morita,S., T.Kojima, and T.Kitamura. 2000. Plat-E: an efficient and stable system for transient packaging of retroviruses. *Gene Ther.* 7:1063-1066.

211. Laemmli,U.K. 1970. Cleavage of structural proteins during the assembly of the head of bacteriophage T4. *Nature* 227:680-685.

212. Hoff,A., T.Andre, T.E.Schaffer, G.Jung, K.H.Wiesmuller, and R.Brock. 2002. Lipoconjugates for the noncovalent generation of microarrays in biochemical and cellular assays. *Chembiochem.* 3:1183-1191.

213. Osborn,M. and K.Weber. 1982. Immunofluorescence and immunocytochemical procedures with affinity purified antibodies: tubulin-containing structures. *Methods Cell Biol.* 24:97-132.

214. Delamarche,E., A.Bernard, H.Schmid, B.Michel, and H.Biebuyck. 1997. Patterned delivery of immunoglobulins to surfaces using microfluidic networks. *Science* 276:779-781.

215. Fischer,R., O.Mader, G.Jung, and R.Brock. 2003. Extending the applicability of carboxyfluorescein in solid-phase synthesis. *Bioconjug.Chem.* 14:653-660.

216. Elbs,M. and R.Brock. 2003. Determination of binding constants on microarrays with confocal fluorescence detection. *Anal.Chem.* 75:4793-4800.

10. Publications and Presentations

10.1 Original Publications

Fischer, R., Waizenegger, T., **Köhler, K**., Brock, R. (2002): A quantitative validation of fluorophore-labelled cell-permeable peptide conjugates: fluorophore and cargo dependence of Import. *Biochem. Biophys. Acta* 1564 (2): 365-374

Fischer, R., **Köhler, K**., Fotin-Mleczek, M., Brock, R. (2004): A stepwise dissection of the intracellular fate of cationic cell-penetrating peptides. *J. Biol. Chem.* 26; 279(13):12625-35

Stoevesandt, O., Elbs, M., **Köhler, K**., Lellouch, A.C., Fischer, R., André, T., Brock, R. (2005): Peptide microarrays for the detection of molecular interactions in cellular signal transduction. *Proteomics* 5 (8):2010-2017

Köhler, K., Lellouch, A.C., Vollmer, S., Hoff, A., Peters, L., Rogl, H., Malissen, B., Stoevesandt, O., Brock, R. (2005): Chemical genetics when timing is critical: A pharmacological concept for the maturation of T cell contacts. *Chembiochem* 6(1):152-61

Stoevesandt, O., **Köhler, K.,** Fischer, R., Johnston, I., Brock, R. (2005): One-step detection of protein complexes in microliters of cell lysate. *Nature Methods* 2 (11): 833-835

Möhrle, B., **Köhler, K**., Jaehrling, J., Brock, R., Gauglitz, G. (2006): Label-free characterisation of T cell adhesion using reflectometric interference spectroscopy. *Anal. Bioanal. Chem.* 384 (2):407-13

Köhler, K., André, T., Grosse-Hovest, L., Jung, G., Brock, R. : Functional profiling of chemical inhibitors and therapeutic antibodies using cellular antibody microarrays. Manuscript submitted

Köhler, K., Stoevesandt, O., Wolff, S., Hummel, W., André, T., Brock, R.: Dissection of T cell-activation dependent protein complex formation using peptide microarrays. Manuscript in preparation

10.2 Presentations

Supper, J., Schröder, A., **Köhler, K**., Spieth, C., Brock, R., Zell, A.: Dynamic Modelling of the T Cell Signalling Network activated by TCR/CD3 stimulation and CD28 costimulation. Poster presentation at the Conference of Systems Biology of Mammalian Cells, Heidelberg, July 2006

Köhler, K., André, T., Grosse-Hovest, L., Jung, G., Brock, R.: Functional profiling of chemical inhibitors and therapeutic antibodies using cellular antibody microarray. Poster presentation at the conference of the *German Signal Transduction Society*, Weimar, November 2005; *Signal Transduction*, Vol. 6, Nr.1, Suppl. p.47

Ganser, A., Roth, G., **Köhler, K.**, André, T., Heeren, A., Henschel, W., Kern, D., Wiesmüller, K.-H., Brock, R.: Microsystems for the analysis of cellular signal transduction. Poster presentation at the NanoBio Euro Conference, Münster, September 2005; *Nanobiotechnology*, Vol.1, Nr.3, pp 277-278

Köhler, K., André, T., Grosse-Hovest, L., Jung, G., Brock, R.: Analysis of T cell activation using stimulatory antibody microarrays. Lecture at the public annual seminar of the Graduiertenkolleg 794 "Zellbiologische Mechanismen immunassoziierter Prozesse", July 2005

Köhler, K., Vollmer,S., Lellouch, A.M., Malissen, B., Brock, R.: CD3 engagement by immobilized antibodies is sensitive to Src-family kinase inhibition in the early phase of contact formation only. Poster presentation at the EMBO YIP Symposium "Chemistry meets Biology", Heidelberg, June 2005

Köhler, K., André, T., Stoevesandt, O. Brock, R.: Cellular antibody microarrays and chemical inhibitors for the analysis of signalling networks. Poster presentation at the German Society for Biochemistry and Molecular Biology (GBM), Berlin, September 2005

Köhler, K., André, T., Grosse-Hovest, L., Jung, G., Brock, R.: Combinatorial antibody microarrays as tools for the analysis of T cell activation. Poster presentation at the Dechema status seminar "Chip technologies", Frankfurt, February 2005

Roth, G., Stoevesandt, O., **Köhler, K.**, Kern, D., Brock, R., Wiesmüller, K.-H.: A device for the generation of 2D-antibody gradients by microstructured stamping. Poster presentation at the Dechema status seminar "Chip technologies", Frankfurt, February 2005

Köhler, K., Grosse-Hovest, L., André, Th., Jung, G., Brock, R.: Analysis of T cell signal transduction using combinatorial stimulatory antibody microarrays. Poster presentation at the conference of the *German Signal Transduction Society*, Weimar, November 2004; *Signal Transduction*, Vol.4, Nr.3-4, p. 145

Köhler, K., Brock, R., Lellouch, A.M., Malissen, B., Vollmer, S.: In the early phase of T cell receptor engagement continuous Src kinase activity is required for the maintenance of receptor-ligand contacts. Poster presentation at the Aventis ILAB Workshop, Kloster Eberbach, January 2004

Köhler, K., Lellouch, A., Vollmer, S., Malissen, B., Brock, R.: In the early phase of T cell receptor engagement continuous Src kinase activity is required for the maintenance of receptor-ligand contacts. Poster presentation at the 34th annual conference of the "German Society for Immunology", Berlin, September 2003; *Immunobiology*, Vol.208, Nr.1-3, p. 68

Köhler, K., Fischer, R., Waizenegger, T., Wiendl, H., Brock, R.: Pharmacokinetics and intracellular proteolytic breakdown as parameters for the biological activity of cell permeable inhibitor peptides. Poster presentation at the *Cell Target Workshop*, Budapest, Hungary, March 2003

Köhler, K., Fischer. R., Waizenegger, T., Wiendl, H., Brock, R.: Adding content to cell-permeable peptide-inhibitor constructs in intracellular target validation: Descriptors of pharmacokinectics and intracellular proteolytic break-down. Poster presentation at the "*8th Annual Conference of the Society for Biomolecular Screening*", Den Haag, the Netherlands, September 2002

Köhler, K., Fischer, R., Waizenegger, T., Brock, R.: Inhibition of cellular signal transduction with cell permeable peptides: Correlation of inhibitory activity with intracellular proteolytic stability. Poster presentation at the "*27th European Peptide Symposium"*, Sorrento, Italy, September 2002; *Journal of Peptide Science*, Supplement to Vol. 8, p. 202

11. Akademische Lehrer

Meine Akademischen Lehrer waren:

Prof. Albert, Prof. Bisswanger, Prof. Bock, Prof. Bohley, Prof. Braun, Prof. Breyer-Pfaff, PD Dr. Brock, Dr. Buchmann, Prof. Duszenko, Prof. Eckstein, Prof. Eisele, Prof. Fitzgerald-Hayes, Prof. Fröhlich, Prof. Gauglitz, Prof. Grabmayr, Prof. Götz, PD Dr. Gückel, Dr. Günzl, Prof. Häfelinger, Prof. Hagenmaier, Prof. Hamprecht, Prof. Hanack, Dr. Hartmann, Prof. Jung, Prof. Jung, Prof. Jürgens, Prof. Lindner, Dr. Kalbacher, PD Dr. Kapurniotu, Prof. Kohler, Prof. Madeo, Dr. Maier, PD Dr. Maier, Prof. Maier, Prof. Margulis, Prof. Martz, Prof. Mecke, Prof. Nakel, Prof. Ninnemann, Prof. Nordheim, Prof. Oberhammer, Prof. Pfeiffer, PD Dr. Pommer, Prof. Poralla, Prof. Probst, Prof. Rammensee, Prof. Reutter, Dr. Rziha, Dr. Schilde, Prof. Schott, Prof. Schwarz, Prof. Stevanovic, PD Dr. Stoeva, Prof. Strähle, Prof. Voelter, PD Dr. Voigt, Prof. Wadsworth, Prof. Weber, Prof. Wegmann, Prof. Weser, Prof. Wiesmüller, Prof. Wohlleben, Prof. Wolburg, Prof. Zell, Prof. Zimmermann

AUSBILDUNG

DOKTORARBEIT

September 2002 – Mai 2006	Anfertigung der Doktorarbeit *„Analyse von T-Zell Stimulation und Costimulation mit Zellulären Mikrosystemen (vorläufiger Titel)“* - betreut von Prof. Dr. H.-G. Rammensee, Institut für Zellbiologie, Abteilung Immunologie, Universität Tübingen - durchgeführt am Interfakultären Institut für Zellbiologie, Universität Tübingen, Arbeitsgruppe “Zelluläre Signaltransduktion“, Laborleiter Dr. R. Brock
Mai 2003 – Mai 2006	Kollegiat (assoziiert) des Graduiertenkollegs 794 „Zellbiologische Mechanismen Immunassoziierter Prozesse“

STUDIUM - BIOCHEMIE

Juli 2002	Diplom Biochemie, “sehr gut” (1,0)
November 2001 – Juli 2002	Anfertigung der Diplomarbeit „*Import, Prozessierung und Biologischer Effekt von Zellpermeablen Peptiden als Parameter für die Entwicklung von Peptid-Vakzinen und Inhibitoren der T-Zell-Aktivierung”*“ am Institut für Organische Chemie, Arbeitsgruppe von Prof. Dr. Günther Jung, Universität Tübingen, Laborleiter Dr. R. Brock
Oktober 2001	Mündliche Diplomprüfung (Biochemie, Organische Chemie, Pharmakologie/Toxikologie)
August – September 2000	Praktikum an der Bundesanstalt für Viruskrankheiten der Tiere, Tübingen, Arbeitsgruppe von Dr. Rziha
August 1999 – August 2000	Studium an der *University of Massachusetts*, Amherst, USA
März 1999	Diplomvorprüfung
Oktober 1996 – Juli 2002	Studium der Biochemie an der Universität Tübingen

SCHULBILDUNG

Mai 1995	Abitur (Gesamtnote: 1,1)
September 1987 – Juni 1995	Gymnasium der Kooperativen Gesamtschule Weyhe, Niedersachsen